



Photogrammetrie Fernerkundung Geoinformation

Journal for Photogrammetry, Remote Sensing
and Geoinformation Science

Organ der Deutschen Gesellschaft für Photogrammetrie,
Fernerkundung und Geoinformation (DGPF) e. V.

Jahrgang 2014, Heft 6

Hauptschriftleiter:
Prof. Dr.-Ing. Wolfgang Kresse

Schriftleiter:
Prof. Dr.-Ing. Stefan Hinz, Prof. Dr. techn. Franz Rottensteiner,
Prof. Dr. rer.nat. Ulrich Michel, Prof. Dr. rer.nat. Lars Bernard
und Dr.-Ing. Eckhardt Seyfert

Redaktionsbeirat (Editorial Board): Clement Atzberger, Andrew Frank,
Christian Heipke, Joachim Hill, Patrick Hostert, Hans-Gerd Maas, Wolfgang
Reinhardt, Camillo Ressl, Jochen Schiewe



E. Schweizerbart'sche Verlagsbuchhandlung
(Nägele u. Obermiller) Stuttgart 2014



Deutsche Gesellschaft für Photogrammetrie, Fernerkundung
und Geoinformation (DGPF) e.V.
Gegründet 1909

Die *Deutsche Gesellschaft für Photogrammetrie, Fernerkundung und Geoinformation* (DGPF) e.V. unterstützt als Mitglieds- bzw. Trägergesellschaft die folgenden Dachverbände:



International Society
for Photogrammetry
and Remote Sensing

DAGM

Deutsche Arbeits-
gemeinschaft für
Mustererkennung e.V.



GeoUnion
Alfred-Wegener-Stiftung

Herausgeber:

© 2014 Deutsche Gesellschaft für Photogrammetrie, Fernerkundung und Geoinformation (DGPF) e.V.
Präsident: Prof. Dr. Thomas Kolbe, Technische Universität München, Institut für Geodäsie, GIS und Landmanagement, Lehrstuhl für Geoinformatik, Arcisstraße 21, 80333 München, Germany, Tel. +49-89-289-23888
Geschäftsstelle: Tanja Nyc, c/o Technische Universität München, Institut für Geodäsie, GIS und Landmanagement, Lehrstuhl für Geoinformatik, Arcisstraße 21, 80333 München, Germany, Tel.: +49-89-289-22578, e-mail: geschaeftsstelle@dgpf.de, Gläubiger-Identifikationsnummer DE54 ZZZ0 0000 8351 37
Published by: E. Schweizerbart'sche Verlagsbuchhandlung (Nägele u. Obermiller), Johannesstraße 3A, 70176 Stuttgart, Germany, Tel.: +49-711 351456-0, Fax: +49-711 351456-99, e-mail: mail@schweizerbart.de
Internet: <http://www.schweizerbart.de>

⊗ Gedruckt auf alterungsbeständigem Papier nach ISO 9706-1994

All rights reserved including translation into foreign languages. This journal or parts thereof may not be reproduced in any form without permission from the publishers.

Die Wiedergabe von Gebrauchsnamen, Handelsnamen, Warenbezeichnungen usw. in dieser Zeitschrift berechtigt auch ohne besondere Kennzeichnung nicht zu der Annahme, dass solche Namen im Sinne der Warenzeichen- und Markenschutz-Gesetzgebung als frei zu betrachten wären und daher von jedermann benutzt werden dürften.

Verantwortlich für den Inhalt der Beiträge sind die Autoren.

ISSN 1432-8364 / e-ISSN 2363-7145

Science Citation Index Expanded (also known as SciSearch®) Journal Citation Reports/Science Edition
Hauptgeschäftsführer: Prof. Dr.-Ing. Wolfgang Kresse, Hochschule Neubrandenburg, Fachbereich Landschaftswissenschaften und Geomatik, Brodaer Straße 2, 17033 Neubrandenburg, Germany, e-mail: kresse@hs-nb.de
Schriftleiter: Prof. Dr.-Ing. Stefan Hinz, Karlsruher Institut für Technologie – KIT, Institut für Photogrammetrie und Fernerkundung, Englerstraße 7, 76131 Karlsruhe, Germany, e-mail: stefan.hinz@ipf.uni-karlsruhe.de, Prof. Dr. techn. Franz Rottensteiner, Leibniz Universität Hannover, Institut für Photogrammetrie und GeoInformation, Nienburger Straße 1, 30167 Hannover, Germany, e-mail: rotteneiner@ipi.uni-hannover.de, Prof. Dr. rer. nat. Ulrich Michel, Pädagogische Hochschule Heidelberg, Czernyring 22/11-12, 69115 Heidelberg, Germany, e-mail: michel@ph-heidelberg.de, Prof. Dr. rer. nat. Lars Bernard, Technische Universität Dresden, Fachrichtung Geowissenschaften, Helmholtzstraße 10, 01062 Dresden, Germany, e-mail: lars.bernard@tu-dresden.de, und Dr.-Ing. Eckhardt Seyfert, Landesvermessung und Geobasisinformation Brandenburg, Heinrich-Mann-Allee 103, 14473 Potsdam, Germany, e-mail: eckhardt.seyfert@geobasis-bb.de

Erscheinungsweise: 6 Hefte pro Jahrgang.

Bezugspreis im Abonnement: € 239,- pro Jahrgang. Mitglieder der DGPF erhalten die Zeitschrift kostenlos. Der Online-Zugang ist im regulären Subskriptionspreis enthalten.

Anzeigenverwaltung: E. Schweizerbart'sche Verlagsbuchhandlung (Nägele u. Obermiller), Johannesstraße 3A, 70176 Stuttgart, Germany, Tel.: +49-711 351456-0; Fax: +49-711 351456-99.

e-mail: mail@schweizerbart.de, Internet: <http://www.schweizerbart.de>

Bernhard Harzer Verlag GmbH, Westmarkstraße 59/59a, 76227 Karlsruhe, Germany, Tel.: +49-721 944020, Fax: +49-721 9440230, e-mail: Info@harzer.de, Internet: www.harzer.de

Printed in Germany by Tutte Druckerei & Verlagsservice GmbH, 94121 Salzwedel, Germany.

PFG – Jahrgang 2014, Heft 6

Inhaltsverzeichnis

Originalbeiträge

ASHRAFIANFAR, N., BUSCH, W., DEHGHANI, M., KNOSPE, S. & REZAPOUR TABARI, M.M.: DInSAR Time Series of ALOS PALSAR and ENVISAT ASAR Data for Monitoring Hashtgerd Land Subsidence due to Overexploitation of Groundwater	497
---	-----

Beiträge aus Wissenschaft und Praxis

JUNG, A. & VOHLAND, M.: Snapshot Hyperspectral Imaging for Soil Diagnostics – Results of a Case Study in the Spectral Laboratory	511
SIEGMANN, B., GLÄSSER, C., ITZEROTT, S. & NEUMANN, C.: An Enhanced Classification Approach using Hyperspectral Image Data in Combination with in situ Spectral Measurements for the Mapping of Vegetation Communities	523
LI, C., THINH, N.X. & ZHAO, J.: Spatiotemporally Varying Relationships between Urban Growth Patterns and Driving Factors in Xuzhou City, China	535

Mitteilungen

Berichte von Veranstaltungen 13. Internationales 3D-Forum, 6.–7. Mai 2014, Lindau	549
Hochschulnachrichten Karlsruher Institut für Technologie, Dissertation Nawras Shatnawi..... Technische Universität München, Dissertation Michael Schmitt	551
Technische Universität Dresden, Dissertation Stefan Hahmann	552
Technische Universität Dresden, Dissertation Thomas Schulz	553
Technische Universität Berlin, Dissertation Ronny Hänsch	554
Veranstaltungskalender	556
Korporative Mitglieder	558
Jahresinhaltsverzeichnis	559
	561

Zusammenfassungen der „Originalbeiträge“ und der „Beiträge aus Wissenschaft und Praxis“
(deutsch und englisch) sind auch verfügbar unter www.dgpf.de/neu/pfg/ausgaben.htm





DInSAR Time Series of ALOS PALSAR and ENVISAT ASAR Data for Monitoring Hashtgerd Land Subsidence due to Overexploitation of Groundwater

NAZEMEH ASHRAFIANFAR, WOLFGANG BUSCH, Clausthal-Zellerfeld, Germany,
MARYAM DEHGHANI, Shiraz, Iran, STEFFEN KNOSPE, Clausthal-Zellerfeld, Germany
& MAHMUD MOHAMMAD REZAPOUR TABARI, Shahrekord, Iran

Keywords: DInSAR, time series, land subsidence, groundwater overexploitation, Hashtgerd

Summary: Differential SAR Interferometry (DInSAR) is able to monitor land deformation at sub-millimetre as an areal measurement. DInSAR time series calculates land deformation on every radar acquisition date from all individual interferograms in relation to the first/arbitrary date. These calculations help to monitor long term (trend) as much as short terms (seasonal) variations of the land deformation. This research endeavours to investigate the feasibility of a time series algorithm by use of no consecutive radar data in a case study. The Hashtgerd area of north-western Iran is subject to land subsidence resulting from the overexploitation of groundwater. The only tool for areal monitoring subsidence in this area was the DInSAR method. SAR data covering the Hashtgerd Plain include ENVISAT ASAR and ALOS PALSAR data. The interferograms were calculated by ENVISAT ASAR and ALOS PALSAR raw data. For this calculation, the two-pass DInSAR method was applied. Time series algorithm was worked out in three main steps by use of calculated differential interferograms containing less decorrelation, atmospheric effects, topographic and unwrapping error and other noise sources. Firstly, residual orbital tilts and linear atmospheric effects were reduced from all interferograms by use of a least-squares plane fitting approach. Secondly, all interferograms were corrected in relation to one reference point. Finally, DInSAR time series was elaborated by a least-squares-based method integrated with a finite difference approximation approach. This algorithm was successful to link separate groups of interferograms by use of a proper weighting factor, and reduced a nonlinear part of atmospheric effects. The results of Hashtgerd time series calculations showed a relatively constant long term variation of subsidence about 14 cm/yr, in spite of seasonal variations of subsidence. The time series results of

Zusammenfassung: Monitoring von Bodensenkungen durch Grundwasserentnahme in Hashtgerd basierend auf DInSAR-Zeitreihen der Sensoren ALOS-PALSAR und ENVISAT-ASAR. Die Differentielle SAR-Interferometrie (DInSAR) ist eine flächenhaft arbeitende Messmethode, mit der Bodenbewegungen im Millimeter-Bereich bestimmt werden können. Mit DInSAR-Zeitreihen lassen sich Bodenbewegungen überwachen, wobei zu jedem Datum einer Radarmessung die Line-of-Sight (LOS) Entfernungsänderung in Bezug auf ein gewähltes (beliebiges Referenz-) Datum bestimmt wird. Diese Berechnungen helfen, sowohl langfristige Trends als auch kurzzeitige, z.B. saisonale, Variationen der Bodenbewegung abzuleiten. In diesem Beitrag wird die Anwendbarkeit eines Algorithmus zur Zeitreihenauswertung untersucht, wobei für das Untersuchungsgebiet nur unterbrochene Zeitreihen aufeinanderfolgender Radardaten zur Verfügung standen.

Die Hashtgerd Ebene im Nordwesten des Iran unterliegt Bodensenkungen, die durch ein übermäßiges Abpumpen des Grundwassers hervorgerufen werden. Die einzige anwendbare Messmethode für eine flächenhafte Überwachung der Bodensenkungen in diesem Bereich ist das DInSAR-Verfahren. Für das Untersuchungsgebiet sind SAR-Daten (ENVISAT-ASAR und ALOS-PALSAR) verfügbar. Die Interferogramme wurden aus den Rohdaten mit der GAMMA Software berechnet. Bei dieser Berechnung wurde das two-pass-DInSAR Verfahren und ein SRTM-Höhenmodell verwendet. Der Zeitreihenalgorithmus gliedert sich in drei Hauptschritte, wobei nur Interferogramme mit hoher Kohärenz und deutlichem Bodenbewegungs signal benutzt werden. Im ersten Schritt werden residuale (Orbit-) Trends und großräumige atmosphärische Effekte reduziert, indem in allen Interferogrammen eine mit einer Kleinstes Quadrate

ENVISAT ASAR were compared with the ALOS PALSAR time series results and by GPS data. The DInSAR time series results demonstrated the ability of the time series algorithm applied and the accuracy of the optimal weighting factor determined.

Schätzung angepasste Trendebene abgezogen wurde. Zweitens wurden alle Interferogramme in Bezug auf einen identischen Referenzpunkt außerhalb des durch Bodenbewegungen beeinflussten Gebietes reduziert. Im dritten Schritt wurde die eigentliche Berechnung der Zeitreihen mit einer Ausgleichsrechnung auf der Basis einer Finite-Differenzen-Approximation durchgeführt.

Die Ergebnisse der Zeitreihenberechnungen zeigten eine relativ konstante langfristige Bodensenkung von etwa 14 cm/Jahr sowie deutliche saisonale Schwankungen der Bodenbewegungen. Die Ergebnisse der ENVISAT-ASAR-Daten-Auswertung wurden den Ergebnissen aus ALOS-PALSAR-Daten sowie GPS-Daten gegenübergestellt. Mit dem vorgestellten Algorithmus konnten auch zeitlich getrennte Blöcke von Interferogrammen durch die Verwendung eines geeigneten Gewichtungsfaktors verbunden sowie ein nichtlinearer Störgrößenanteil (Trend) und atmosphärische Effekte reduziert werden. Die Ergebnisse der DInSAR-Zeitreihenberechnungen belegen die Nutzbarkeit des hier vorgestellten Algorithmus und die Adäquatheit des abgeleiteten Gewichtungsfaktors.

1 Introduction

In most big cities in Iran today progressive land subsidence due to the overexploitation of groundwater is creating some unrecoverable geo-environmental hazards (MOTAGH et al. 2008). The Hashtgerd area of north-western Iran is subject to land subsidence resulting from the overexploitation of groundwater. The first statement prohibiting the development of groundwater exploitation by drilling new wells in Hashtgerd was made by Iran's Ministry of Water and Energy in 1986 (formal declaration no. 1323, 3236/250), extended and is currently in force (ARASTEH 2005). Even after the prohibition of groundwater exploitation, progressive land subsidence in Hashtgerd is still damaging buildings, water and soil quality and is the motive for study of the subsidence in Hashtgerd. The only tool for monitoring subsidence in Hashtgerd is Interferometric Synthetic Aperture Radar (InSAR). InSAR uses radar signals with high spatio-temporal resolutions to measure deformation of the earth's surface (MASSONNET & FEIGL 1998).

Land subsidence in Hashtgerd was monitored for the first time by DEHGHANI et al.

(2008) applying InSAR technique and with four ENVISAT ASAR scenes, over part of summer and autumn 2008. The progressive land subsidence of this area was monitored using 21 ENVISAT ASAR scenes between 2003 and 2008 by ASHRAFIANFAR et al. (2009). However, owing to the gap in consecutive radar data, the time series calculations were done for two separate time series of 2003 – 2004 and 2007 – 2008 (ASHRAFIANFAR et al. 2009). Because of the importance of investigation of long term behaviour of subsidence in this area, this research undertakes to substantiate the feasibility of a time series algorithm by use of the existing no consecutive radar data. To this end, the ENVISAT ASAR and ALOS PALSAR data were ordered by ESA and processed by the DInSAR algorithm. Selection and implementation an effective method of time series calculation returns to the quality and quantity of calculated interferograms. Owing to incomplete consecutive radar data and the properties of the spatio-temporal baselines of the existing radar data, time series calculation was done using a least-squares-based method (BERARDINO et al. 2002), integrated with a finite difference approximation

approach (SCHMIDT & BÜRGMANN 2003). This approach and the process of removing residual orbital tilts of interferograms (e.g. FUNNING et al. 2005, HOFFMANN 2003) are termed as LSFD algorithm in this research. The acronym LSFD refers to the DInSAR time series algorithm of this research, which was developed in MATLAB environment. This algorithm is completed by three steps (see section 3.2). The two main steps of those three are as following: A “Least Squares plane fitting” and a “Least-squares inversion approach” integrated with a “Finite Difference Approximation”. The LSFD algorithm used a weighted factor in order to connect separate chains of interferograms. The resulting ENVISAT ASAR time series were corroborated by the results of ALOS PALSAR time series and by GPS data available. The DInSAR time series results demonstrated the accuracy of the DInSAR processing, applied time series algorithm and the ability of the optimum weighting factor used in this algorithm. The results of this research were applied to investigate the linear and nonlinear correlation and relationship between land subsidence and groundwater level data as the main indicator of aquifer compaction (ASHRAFIANFAR & BUSCH 2012). Moreover,

these results are usable to develop the linear and nonlinear simulation models of land deformation (ASHRAFIANFAR et al. 2011, 2013, ASHRAFIANFAR 2013).

This paper presents five sections of the research: Section 2 presents the hydro-geological background and existing radar datasets, section 3 discusses the applied algorithms of DInSAR and LSFD, section 4 presents the results of the time series of ENVISAT ASAR and ALOS PALSAR data and compares these results with GPS data, and section 5 presents the conclusions of the research.

2 Background and Datasets

2.1 Hydro-geological Properties of the Case Study

The city of Hashtgerd is the capital of Savojbolagh County, Alborz province in Iran. The Hashtgerd region is located to the west of Karaj and northwest of Tehran (Fig. 1). This area of 1282 km² is situated between geographical longitudes of 50° 20' and 51° 10' and latitudes of 35° 27' and 36° 07'. Hashtgerd Plain is located in the Kordan-River ba-

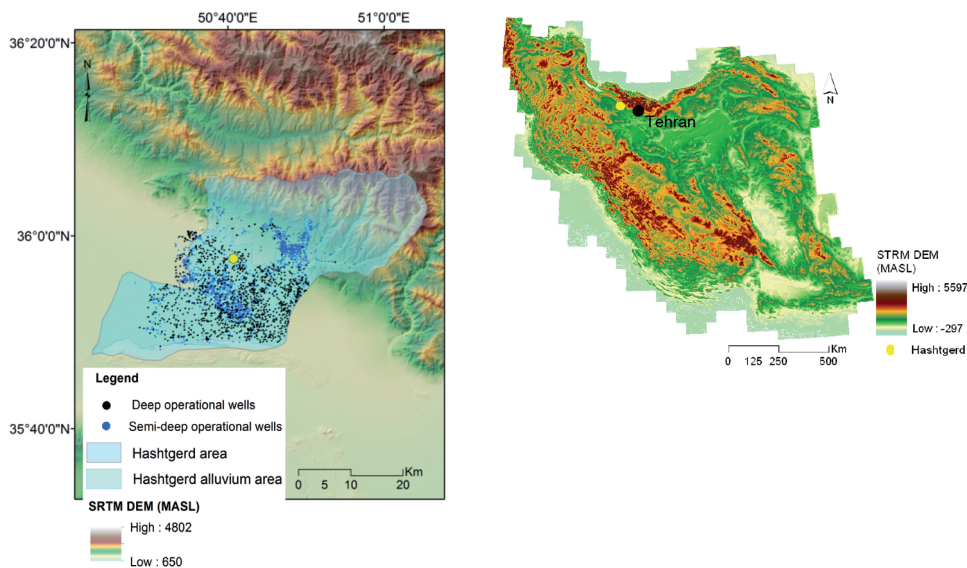


Fig. 1: Situation of the city of Hashtgerd in north-western Iran superimposed on the SRTM digital elevation model of Iran (from DLR) (right). The location of the operational wells over Hashtgerd Plain superimposed on the SRTM DEM (left).

sin of the alluvial area to the south of the Alborz range between Kordan and Abyek. The general slope of the plain is from north-north-east toward the south-west. The study area is mainly located in the part of the Quaternary sediment. With a mild climate and situated near Tehran, the area is consequently highly populated. The growth in population means increased demand for water. The area is mainly farm land and most of the water required for agriculture is provided by 4094 pumping wells. In the Hashtgerd Plain there are 21 piezometric wells with available monthly information for the years between 2003 and 2010. By interpolation of these data the unit hydrograph¹ (MOHAMMAD REZAPOUR TABARI 2009, ZAND & SAHRAEI 2014) of this area was calculated.

This unit hydrograph (Fig. 2) shows a decline of nearly 10 m especially between the

years 1996 and 2001 caused by an excessive pumping out of groundwater (ARASTEH 2005, MOHAMMAD REZAPOUR TABARI 2009) (Fig. 2).

2.2 Radar Data

Radar data covering the Hashtgerd Plain include ENVISAT ASAR and ALOS PALSAR data (Tab. 1). These data were ordered from the European Space Agency (ESA). At some locations ENVISAT ASAR data is available every 35 days and ALOS PALSAR data every 46 days. However, there is no such consecutive radar data for the Hashtgerd area. This absence of data aggravates decorrelation arising from vegetation and construction activity as well as provoking additional problems for DInSAR processing.

The ENVISAT ASAR data (45 radar images) include a total of 27 scenes from track 149 between July 2003 and April 2010 and a total of 18 scenes from track 421 between March 2004 and May 2006. All the 45 Level 0 ENVISAT ASAR images, in the descending mode and incidence angle 22.9 degrees, were converted into single look complex (SLC) format using orbital data of the Delft Institute for Earth-Oriented Space Research (by use of GAMMA software). The SLC data were used to calculate interferograms.

ALOS PALSAR data include a total of 14 scenes from track 572 in the ascending mode and incidence angle 38.7 degrees. These scenes cover the time span from June 2007 to November 2010. All the ALOS PALSAR im-

¹ The Unit hydrograph of this research was calculated by following steps: 1. Collecting the monthly groundwater level information of the existing piezometric wells, 2. Calculation of the Thiessen area of every piezometric well, 3. Calculation of the mean of groundwater level of all piezometric wells in the area with using of following equation: $h = \left(\sum_{i=1}^n A_i \cdot h_i \right) / A$, where, A_i = Area of the Thiessen polygons of piezometer i (in cubic metre), h_i = Groundwater level of piezometer i (in metre), and A = Total area of Thiessen polygons of all piezometers (in cubic metre), 4. The calculations of step 3 were done for every month and with using of these results of several months during 19 years, the unit hydrograph of Fig. 2 was constructed.

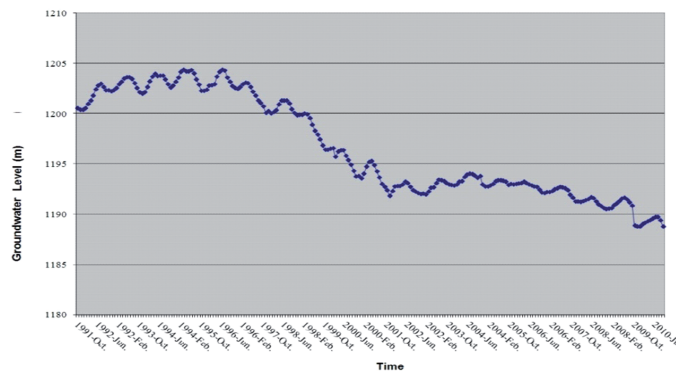


Fig. 2: The unit hydrograph of the Hashtgerd Plain between the years 1991 and 2010 (provided by Groundwater resource management, Ministry of Water and Energy of Iran, 2011).

Tab. 1: Radar acquisition dates and the calculated interferograms as solid lines between two radar dates: ENVISAT ASAR data and the 76 calculated interferograms (left). ALOS PALSAR data and the 18 calculated interferograms (right).

No.	Radar data	Track	Interferograms
1	20030718	149	
2	20030822	149	
3	20030926	149	
4	20031205	149	
5	20040109	149	
6	20040213	149	
7	20040303	421	
8	20040319	421	
9	20040423	421	
10	20040512	421	
11	20040528	149	
12	20040616	421	
13	20040702	149	
14	20040721	421	
15	20040806	149	
16	20040929	421	
17	20040910	149	
18	20041015	149	
19	20041119	149	
20	20041224	149	
21	20050427	421	
22	20050513	149	
23	20050810	421	
24	20050826	149	
25	20050914	421	
26	20051123	421	
27	20060217	149	
28	20060308	421	
29	20060428	149	
30	20071109	149	
31	20080502	149	
32	20080711	149	
33	20080815	149	
34	20080919	149	
35	20081024	149	

No.	RADAR data	Track	Interferograms
1	20070613	527	
2	20080430	527	
3	20080915	527	
4	20080618	527	
5	20090618	527	
6	20090918	527	
7	20100506	527	
8	20101106	527	

ages were converted into single look complex (SLC) format using orbital data of the Delft Institute for Earth-Oriented Space Research (by use of GAMMA software). The SLC data were used to calculate interferograms. A short overview of applied DInSAR procedures is presented in the next section.

3 Methods

3.1 Differential SAR Interferometry (DInSAR)

In order to calculate the interferograms, the procedures of the differential SAR interferometry were followed, thus enabling us to attain the differential interferometric phase by combining every two complex SAR images by the following steps (using the GAMMA software):

a. Multilooking was done for the radar images and they were co-registered in order to

eliminate some of the noise and to reduce geometrical and atmospheric errors and squint angles.

- b. The interferograms were calculated.
- c. The SRTM digital elevation model (C band) was used to remove the topographic phase of the interferograms (the last step) and calculation of differential interferograms. Selection of a small perpendicular baseline between every two radar data reduces the topographic error.
- d. An adaptive filter, originally by GOLDSTEIN & WERNER (1998), was used on the interferograms to reduce noise contribution in the interferometric phase. In this step, the degree of coherency of interferogram was defined. Higher coherency value shows less decorrelation between two radar images. The interferograms with high coherency value were selected for the next step (unwrapping step).
- e. The selected interferograms of the last step were unwrapped by minimum cost flow

(MCF) algorithm. In order to reduce unwrapping error, only a subset of the original interferograms was selected. This subset contained patterns of land deformation in most of the differential interferograms in the Hashtgerd area.

- f. The calculated interferograms were projected to the UTM coordinate reference system by geocoding.

Every individual interferogram records the difference phase between two radar acquisition dates, which is in fact an indication of the land deformation between these two dates. The Hashtgerd Plain is mostly a rural area and owing to the changes in the vegetation it produced high decorrelation during the radar observation period. This decorrelation and the existing temporal gap between radar data (Tab. 1) resulted in only a few of the interferograms being usable for time series calculations. A total of 487 interferograms were calculated using the ENVISAR ASAR (SLC) data of both tracks. However, only 76 interferograms used in the time series algorithm were containing less decorrelation, atmospheric effects, unwrapping error, topographic error and spatially constant patterns of land deformation (Tab. 1, left). The temporal difference between the interferograms calculated by ENVISAT ASAR data is between 35 days and 350 days. A short temporal baseline reduces decorrelation of interferograms. The minimum and maximum perpendicular baselines of the calculated interferograms are 8 m and 860 m, respectively. In addition, a small spatial baseline reduces topographic errors as well as decorrelation of the interferograms. After visual inspection of interferograms, the atmospheric effect of every interferogram was calculated and those interferograms containing less atmospheric effects were selected for time series calculations. This reduces nonlinear atmospheric artifacts on time series calculations.

A total of 28 interferograms were calculated using the ALOS PALSAR (SLC) data. However, considering those parameters of interferograms explained above, only 18 interferograms were used in the time series algorithm (Tab. 1, right). The temporal difference for the calculation of interferograms by ALOS ASAR data is a minimum of 46 days and a

maximum of 1242 days. The minimum and maximum perpendicular baselines of the calculated interferograms are 133 m and 4914 m, respectively. In Tab. 1 every interferogram is shown as a line between every two radar acquisition dates. These interferograms were used in the time series calculations of both data types, which is explained in next section.

3.2 DInSAR Time Series Algorithm

The calculated interferograms of Tab. 1 were used in the time series algorithm LSFD developed in MATLAB software by the following steps:

a. Removing residual orbital tilts of differential interferograms

A significant component of the atmosphere is linear and acts as an orbital ramp. This part of the atmosphere and the orbital ramp can be reduced by fitting a plane to the points far away from the deformation area (e.g. FUNNING et al. 2005, HOFFMANN 2003, DEHGHANI et al. 2008). According to FUNNING et al. (2005), this simple but effective method reduced a part of the linear atmospheric effects of the interferograms.

It should be noted that for reducing the nonlinear atmospheric effects (turbulence effects) those interferograms with high atmospheric effects were not used in the time series calculations (discussed in section 3.1). Also, a weighting factor (W) in step "c" of time series calculations was applied, which reduced a part of the nonlinear atmospheric effects of the time series (SCHMIDT & BÜRGmann 2003, BIGGS & WRIGHT 2004).

In this step of the research, the residual orbital tilts of the interferograms were corrected. This step was completed by subtracting a surface fitted to some of the points distributed over parts of the plain which showed no significant subsidence signals (e.g. FUNNING et al. 2005, HOFFMANN 2003, DEHGHANI et al. 2008, DEHGHANI 2010). For this aim, a least-squares plane fitting was performed. It is supposed that a plane is definable as (1).

$$ax + by + c = z \quad (1)$$

We considered that every plane is at least constructed using three points. These three points should not be located along one line, or in an area affected by atmospheric or phase unwrapping errors. The least-squares solution for the calculation of residual orbital tilts in the selected points far-off from the deformation area is expressed as (2).

$$z = In \cdot Flt \quad (2)$$

Where at the selected points: z is the calculated differential phase by every interferogram ($INT = 1, \dots, k$); In is the index matrix of the least-squares solution including indices of the plane (1); and Flt is the residual orbital tilt.

The algebraic solution of (2) is expressed as (3) for calculation of Flt .

$$Flt = (In^T \cdot In)^{-1} (In^T \cdot z) \quad (3)$$

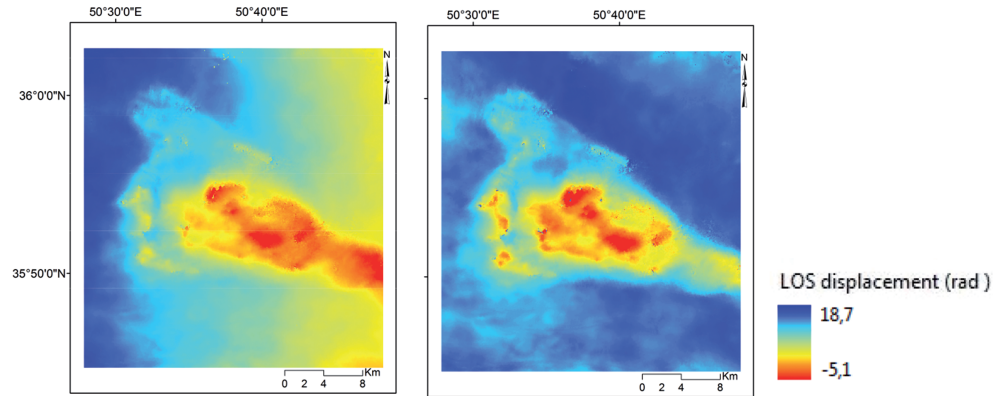


Fig. 3: An Interferogram calculated by ENVISAT ASAR data before (left), and after (right) removal residual orbital tilts. The positive values show subsidence in the line-of-sight (LOS) direction and in radian (15. 8. 2008 – 19. 9. 2008: temporal baseline (Δt) = 35 days, perpendicular baseline (B_{\perp}) = -390.05 m, RMSE = 0.0339 m).

Tab. 2: The maximum and minimum RMSE value of the least-squares plane fitting in order to remove residual the orbital tilts of the interferograms. This value shows the uncertainty of interferograms due to residual orbital tilts and linear atmospheric effects.

Interferogram		Track	Δt (day)	B_{\perp} (m)	RMSE (m)
ENVISAT ASAR	min. RMSE: 26.9.2003 – 6.8.2004	149	315	166.6	0.0002
	max. RMSE: 13.2.2004 – 2.7.2004	149	140	-443.5	0.0872
	min. RMSE: 10.8.2005 – 8.3.2006	421	210	337.6	0.0027
	max. RMSE: 10.8.2005 – 23.11.2005	421	105	618.1	0.0071
ALOS PALSAR	min. RMSE: 18.9.2009 – 6.11.2010	527	414	1925.7	0.00001
	max. RMSE: 15.9.2008 – 6.5.2010	527	598	3588.7	0.0569

Using (3) we fitted a plain to the selected points far-off from deformation area of every interferogram as (4).

$$Flt_{(i,j,k)} = Flt_{(n_1)} \cdot i + Flt_{(n_2)} \cdot j + Flt_{(n_3)} \quad (4)$$

Where i and j are rows and columns of the raster data of every interferogram, respectively; k is the number of the calculated interferograms; n_1 , n_2 and n_3 are the selected points in far-fields from deformation area.

The plane (4) is removed from all interferograms according to (5).

$$INT_Flt_{(i,j,k)} = z_{(i,j,k)} - Flt_{(i,j,k)} \quad (5)$$

Where $INT_Flt_{(i,j,k)}$ are the flattened interferograms. Now, all interferograms have the same scale in order to use them in the next

step of the algorithm. An example is given in Fig. 3, which presents an interferogram before and after removal of the residual orbital tilts.

All interferograms of Tab. 1 were processed by this method. The RMSE between the interferograms and the fitted plain in the far-off points is calculated for all interferograms. Tab. 2 presents the minimum and maximum values of the RMSE of the least-squares plane fitting for every radar type. The RMSE shows the uncertainty of interferograms due to residual orbital tilts and linear atmospheric effects.

b. Correction of differential interferograms to zero level

After step a, all interferograms were corrected related to a reference point, located in an area without land deformation. This correction of the interferograms is expressed as (6).

$$\text{INT_Flt_ref}_{(i,j,k)} = \text{INT_Flt}_{(i,j,k)} - \text{INT_Flt}_{(\text{ref}Y, \text{ref}X, k)} \quad (6)$$

Where $\text{INT_Flt_ref}_{(i,j,k)}$ are the corrected interferograms with relation to the reference point ($\text{ref}Y, \text{ref}X$).

The interferograms resulted by step b are expressed as INT in the following equations of time series algorithm for simplification of writing.

c. Calculation of land deformation in every radar acquisition date by use of the differential interferograms

DInSAR time series monitors land deformation on each radar acquisition date, beginning at the first date and using all calculated individual interferograms. We applied a least-squares-based method (LS) for the InSAR time series calculations. The main principle of the LS method is as follows: If there are at least as many independent interferograms as acquisition dates, and if the chain of interferograms is not broken at any point, it is possible to perform a least-squares inversion method in order to calculate land deformation on each radar acquisition date (BIGGS & WRIGHT 2004).

Accordingly, the relation of the calculated interferograms and deformation on every radar acquisition date $t = [t_1, t_2, t_3, \dots, t_n]$ is ex-

pressed as (7) (BERARDINO et al. 2001, SCHMIDT & BÜRGMANN 2003, BIGGS & WRIGHT 2004):

$$\text{For } \forall(i, j) \rightarrow \text{INT} = g \cdot \phi \quad (7)$$

Where $\text{INT} = [\phi_{12}, \phi_{23}, \dots]$ are the calculated interferograms (the observed land deformation between every two radar acquisition dates); $\phi = [\phi_1, \phi_2, \dots]$ is the unknown phase of land deformation in every radar acquisition date relating to the first date, the deformation in the first date is assumed to be zero ($\phi = 0$); g is the design matrix of LS solution, which links unknown and known values. The rows of the design matrix g is equal to the calculated interferograms (INT) and its columns are as much as the radar acquisition dates minus one (because we assumed the deformation in the first date is equal to zero).

The algebraic solution of (7) is expressed as (8) for the calculation of the land deformation in every radar acquisition date (ϕ).

$$\phi = (g^T \cdot g)^{-1} (g^T \cdot \text{INT}) \quad (8)$$

As mentioned before, if $\text{INT} \geq \phi$ and the chain of differential interferograms is continuous, the deformation phase in every acquisition date is calculated according to (8). Due to several error sources in the original interferograms (atmospheric, orbital, unwrapping etc.) this calculated time series is not very precise. However, land deformation as a natural phenomenon is considered as a smooth parameter of time (BIGGS & WRIGHT 2004). Therefore, in order to remove the noise partly, other methods are integrated with the LS method described above (BIGGS & WRIGHT 2004). We combined a finite difference approximation with the LS method (SCHMIDT & BÜRGMANN 2003). This integration of methods partially reduces temporal noises of time series as nonlinear atmospheric effects and connects separate groups of differential interferograms of the research. In order to link independent datasets of radar data and mitigate several error types, a finite difference approximation for the second order derivatives of the time series was used as a weighting factor added to (7). The application of this weighting factor (w) presupposes that the velocity of phase of deformation during two sequential time peri-

ods is relatively constant and there are no unexpected significant variations of subsidence (SCHMIDT & BÜRGMANN 2003). To apply this weighting factor (7) is written as (9):

$$\begin{pmatrix} INT \\ 0 \end{pmatrix} = \begin{pmatrix} g \\ w \cdot \frac{\partial^2}{\partial t^2} \end{pmatrix} \cdot \phi \quad (9)$$

Where w is the weighted factor of the LSFD algorithm. The weighting factor (w) was determined optimally by the common method of "trial and error" (e.g. BIGGS & WRIGHT 2004, GAMMA SOFTWARE DOCUMENTATION 2013). An appropriate value of the weighting factor can smooth a noisy time series preserving those nonlinear (seasonal) signals of land deformation (SCHMIDT & BÜRGMANN 2003, BIGGS & WRIGHT 2004). The plot of the root-mean-square error (RMSE) of the LS against various corresponding weighting factors is used in this research (Fig. 4). The RMSE is calculated as (10).

$$RMSE = \sqrt{\frac{1}{k} \left(\sum_{INT=1}^k \hat{R}_{INT} \right)^2} \quad (10)$$

Where k is the number of the differential interferograms; $\hat{R}_{INT} = (g \cdot \hat{\phi}) - INT$ according to (7), where $\hat{\phi}$ is the estimated phase by the least-squares solution.

We tested several values of W ranging from 0 to 0.15 (Fig. 4) in order to calculate the time

series of land deformation. The results of every time series with a specified W were compared to the results of the time series with a very small W ($W \sim 0$). The subtraction of the time series with a very small W (nearly zero) and a time series with a specified W , e.g. $W = 0.02$, should show only noise over the whole study area and no significant values of land deformation. This means, only high frequency components of the time series (noises) have been reduced. Finally, the results of the time series with the selected W were compared with the GPS information (see section 4).

Fig. 4 presents the plot of RMSE against different values of weighting factor of the ENVISAT ASAR time series calculations. The overall RMSE by use of weighting factor 0.02 is equal to 1.5 rad (0.0067 m).

The entire time series calculations are repeated using the optimally selected weighting factor for ALOS PALSAR ($w = 0.005$) and ENVISAT ASAR ($w = 0.02$) time series, which eliminates noisy fluctuations from the time series, but preserves the nonlinear (seasonal) signals of deformation. The results of time series calculations are interferometric phases (in radian). These values were converted to deformation along the line-of-sight (LOS) in metre by multiplying $-\lambda / 4\pi$, where λ is the wavelength of the radar data. The LOS displacements were converted to vertical displacement by dividing them by the cosine of incidence angle (θ) of the ENVISAT ASAR ($\theta = 22.9^\circ$) and ALOS PALSAR data ($\theta =$

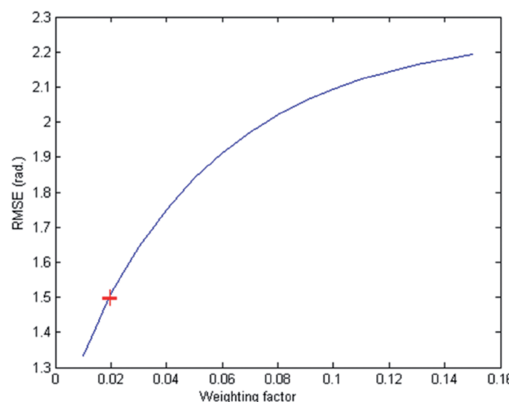


Fig. 4: The optimum weighting factor of the LSFD method used in the ENVISAT ASAR time series calculation at 0.02 rad (0.0067 m) (red cross).

38.7°). The time series results are presented and discussed in the next section.

4 Results and Discussions

The results of ENVISAR ASAR time series showed seasonal variations as uplift and subsidence signals in recharge and discharge periods of Hashtgerd area, respectively. In this area, the discharge drawdown season typically occurs during the period of May to November and the recharge recovery season from December to March (MOHAMMAD REZAPOUR TABARI 2009). The individual results of every discharge period showed that the areas with high subsidence are smaller in the discharge period of 2008 compared with that of 2003. Fig. 5 (left) shows the ENVISAT ASAR annual mean displacement map of the Hashtgerd Plain (between 18.7.2003 and 24.10.2008). The maximum annual rate of subsidence in every year was calculated at 0.142 m.

The time series of ALOS data also showed the seasonal variations of the subsidence. The area with the maximum subsidence has occurred particularly in the centre of the subsidence bowl, and in summer 2010, it seems to extend more toward the east of the area. Fig. 5

(right) represents the ALOS annual displacement map. The maximum annual rate of subsidence was calculated at 0.163 m.

In order to evaluate the results of the InSAR processing and time series calculation, the results of the ENVISAT ASAR and the ALOS PALSAR time series calculation in part of the recharge period of 2008 were compared with each other. Fig. 6 represents the displacement map of the ENVISAT (left: 2.5.2008 – 19.9.2008) and the ALOS time series calculation (right: 30.4.2008 – 15.9.2008). Fig. 7 represents the histogram of the difference between ALOS and ENVISAT displacement maps (mean deviation = ALOS minus ENVISAT). This histogram shows the distribution of the mean deviation of -0.0054 m around zero. This difference of 5 mm stems from several sources, such as different radar data types with various properties, errors contributed in InSAR processing and also the time series calculations. The ALOS PALSAR data with L-band tends to less temporal decorrelation, also less unwrapping errors compared with ENVISAT ASAR data (C-band). The interferograms calculated using ALOS PALSAR data contain smaller numbers of phase jumps and consequently, less unwrapping error. Accordingly, the time series results of ENVI-

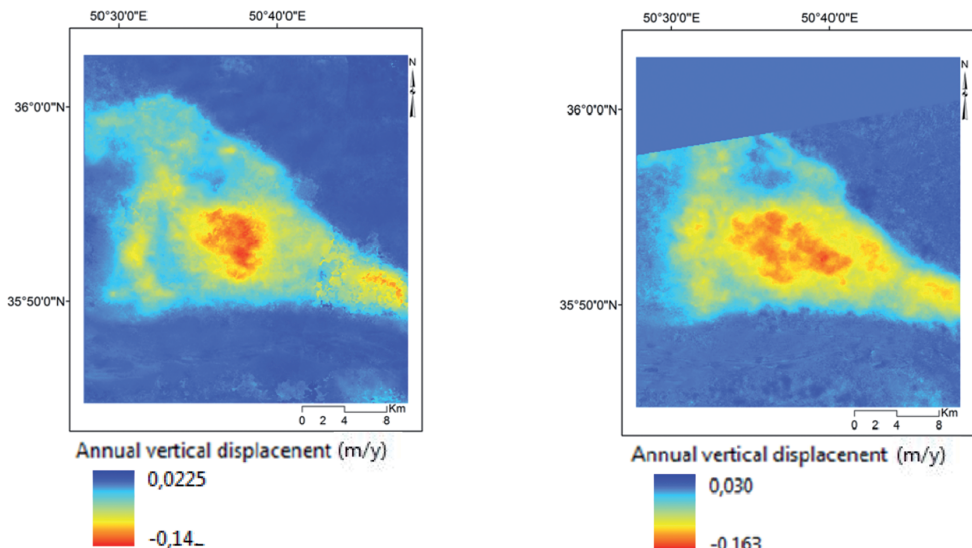


Fig. 5: ENVISAT ASAR annual deformation rate (from 18.7.2003 to 24.10.2008, left), and ALOS PALSAR annual vertical displacement map (from 15.9.2008 to 6.11.2010, right).

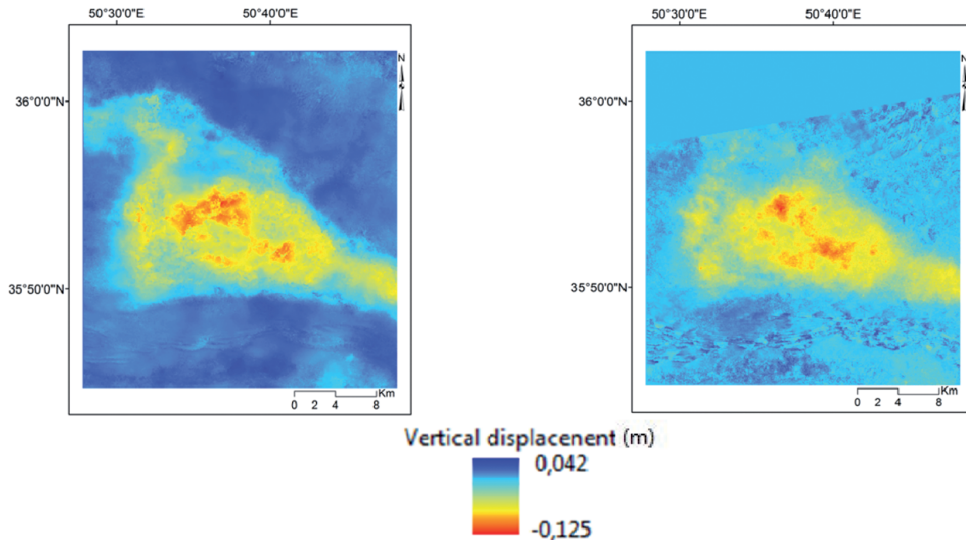


Fig. 6: Comparing the displacement maps of ENVISAT ASAR (left: 2.5.2008 – 19.9.2008) and ALOS PALSAR (right: 30.4.2008 – 15.9.2008).

SAT ASAR data showed an underestimation of vertical displacement in comparison with those of ALOS PALSAR data. The negative value of the mean deviation (-0.0054) is related to this fact.

The GPS information of Hashtgerd was compared with the results of the DInSAR time series of both data types. In the area there is one GPS continuous monitoring station (Najmabad Station) and some GPS periodic monitoring stations. The periodic GPS information was collected by the Geodynamics Group

of the Geological Survey of Iran (GSI) from July to December 2008. The location of periodic GPS stations in the Hashtgerd subsidence area is represented in Fig. 8. The differ-

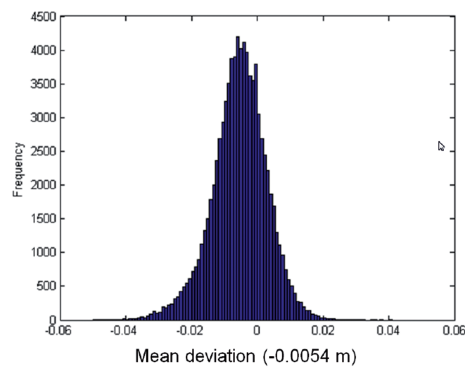


Fig. 7: Histogram of the mean deviation between displacement maps of the ALOS PALSAR and ENVISAT ASAR data (mean deviation = ALOS minus ENVISAT = -0.0054 m).

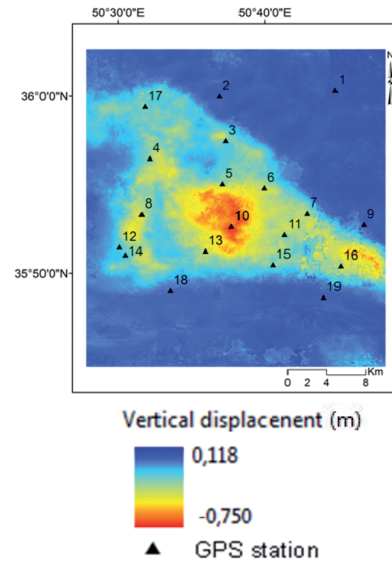


Fig. 8: The location of the GPS periodic monitoring stations in the Hashtgerd subsidence area superimposed on the vertical displacement map of ENVISAT (from 18.7.2003 to 24.10.2008).

ence between discontinuous GPS information and time series of ENVISAT and ALOS was calculated at 0.02 m and 0.005 m, respectively (mean deviation = GPS minus ENVISAT/ALOS) (Fig. 9). In accordance with these diagrams, DInSAR measurements show fewer values of the land displacements than those measured by the GPS. This discrepancy can be explained by the differences between the two techniques of subsidence monitoring. The results of the time series of the InSAR-derived subsidence and information of the continuous GPS continuous monitoring station (Fig. 10 left) showed good agreement (Fig. 10 right).

5 Conclusions

The performance of a developed time series algorithm for monitoring long term variation of land subsidence was demonstrated in spite of the incomplete radar data for the case study. This algorithm consists of three steps. Firstly, the residual orbital tilts of interferograms were removed by a least-squares plane fitting approach. Secondly, the interferograms were corrected to zero level. Finally, the land deformation in every radar acquisition date was calculated applying a least-squares inversion approach integrated with a finite difference approximation. The finite difference approxi-

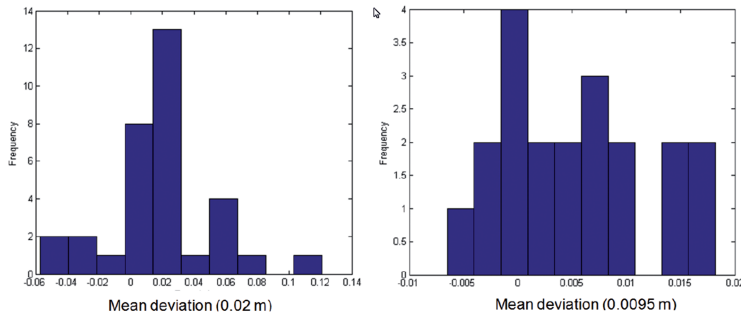


Fig. 9: Histograms of the difference between GPS information and time series calculation results of ENVISAT at 0.0235 m (left) and ALOS PALSAR time series at 0.0095 (right) (mean deviation = GPS-ENVISAT/ALOS).

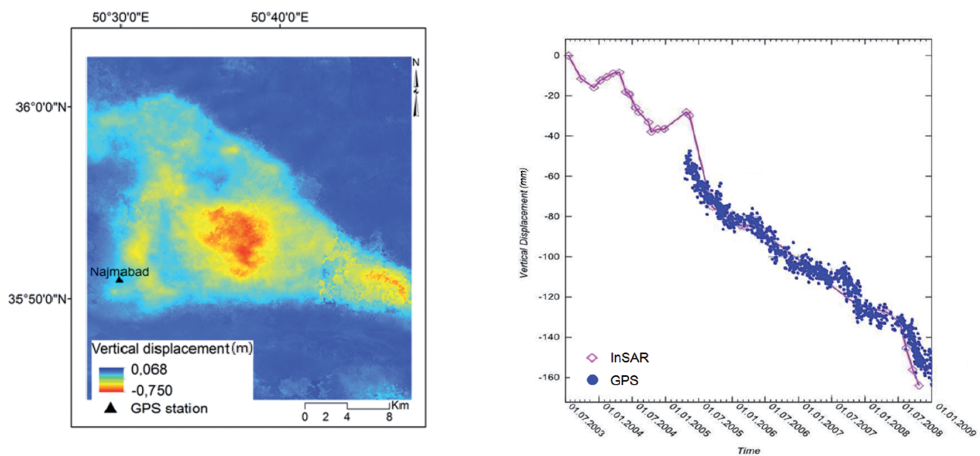


Fig. 10: The location of the GPS continuous monitoring station (Najmabad station) superimposed on the vertical displacement map of ENVISAT ASAR (from 18.7.2003 to 24.10.2008) (left), comparing the information of this station with the ENVISAT ASAR time series (right).

mation for the second order derivatives of the time series was applied as a weighting factor. The weighting factor was determined optimally by the common method of “trial and error”. An appropriate value of the weighting factor can smooth a noisy time series, preserving short-term temporal (seasonal) variations of land deformation. The time series results of ENVISAT ASAR with ALOS PALSAR data for a part of the discharge period of the year 2008 and with GPS data showed a good agreement. The results of the Hashtgerd time series calculations showed a relatively constant long term variation of subsidence about 14 cm/yr between years 2003 and 2008.

The DInSAR time series results confirmed the performance of the developed Hashtgerd time series algorithm and demonstrated the ability of the defined weighting factor. These results can be applied for the prediction and assessment of the land deformation in the Hashtgerd area and in order to prevent and/or mitigate subsidence hazards. The long term and seasonal variations of subsidence are both important in groundwater management programmes. Also, the results of the time series are applicable in the linear and nonlinear simulation models of land subsidence and aquifer parameters estimations.

Acknowledgements

This research was supported by the Institute of Geotechnical Engineering and Mine Surveying (IGMC), Clausthal University of Technology, Germany. The radar images used in the research were ordered from ESA (the project PI: C1P.9240). The groundwater data were provided by the Reyab Consulting Engineers of Iran. The GPS information was collected by geodynamic group of geomatics management, Geological Survey of Iran (GSI). Our appreciation we owe to Dr.-Ing. DIANA WALTER for the scientific comments and Dipl. Inform. TILMAN BROCK-HESSE for his support during DInSAR processing of ALOS PALSAR data.

References

- ARASTEH, M., 2005: Report on the continuing prohibition of groundwater exploitation programmes in the Hashtgerd area. – Department of Tehran Water Resources, Ministry of Water and Energy, Iran (Farsi, see below for access).
- ASHRAFIANFAR, N., BUSCH, W., DEHGHANI, M. & HAGHIGHATMEHR, P., 2009: Differential SAR Interferometric technique for land subsidence monitoring due to groundwater over-exploitation in the Hashtgerd. – Fringe 2009, Frascati, Italy.
- ASHRAFIANFAR, N., BUSCH, W., DEHGHANI, M. & MOHAMMAD REZAPOUR TABARI, M., 2011: Application of Differential SAR Interferometry technique in a Dynamic Neural Network-based simulation-optimization model for subsidence prediction. – Fringe 2011, 8th International Workshop on “Advances in the Science and Applications of SAR Interferometry”, 19–23 September 2011, Frascati, Italy, <http://earth.eo.esa.int/workshops/fringe2011/index.php?page=214&type=s> (31.7.2014).
- ASHRAFIANFAR, N. & BUSCH, W., 2012: The application of InSAR to monitor pumping induced-land subsidence and its relation with aquifer properties. – GeoHannover 2012, GeoRohstoffe für das 21. Jahrhundert. – Schriftenreihe der Deutschen Gesellschaft für Geowissenschaften (SDGG) **80**: 230.
- ASHRAFIANFAR, N., BUSCH, W., DEHGHANI, M. & MOHAMMAD REZAPOUR TABARI, M., 2013: Simulation of Land Subsidence Using InSAR Time Series and Aquifer Parameters in a Neurocomputational Approach. – Living planet symposium, Edinburgh, UK, <http://www.livingplanet2013.org/abstracts/850066.htm> (31.7.2014).
- ASHRAFIANFAR, N., 2013: The Application of Satellite Radar Interferometry in the Development of a Dynamic Neural Model of Land Subsidence Induced by Overexploitation of Groundwater. – Dissertation, Institut für Geotechnik und Markscheidewesen der Technischen Universität Clausthal.
- BERARDINO, P., FORNAR, G., LANARI, R. & SANSOTTI, E., 2002: A new algorithm for surface deformation monitoring based on small baseline differential SAR interferograms. – IEEE Transactions on Geoscience and Remote Sensing **40**: 2375–2383.
- BIGGS, J. & WRIGHT, T., 2004: Creating a time series of ground deformation using InSAR. – Center of observation and modelling of earthquakes and tectonics, unpublished paper, University of Oxford, UK.

- DEHGHANI, M., VALADAN ZOEJ, M.J., BOLOURCHI, M.J. & SHEMSHAKI, A. & SAATCHI, S., 2008: Monitoring of Hashtgerd Land Subsidence Induced by Overexploitation of Groundwater Using SAR Interferometry. – XXIst ISPRS Congress, Technical Commission **VIII**: 365–368.
- DEHGHANI, M., 2010: Estimation of deformation rate and modelling of land subsidence induced by groundwater exploitation using interferometry. – Dissertation, K.N.Toosi University of Technology, Iran (Farsi, see below for access).
- FUNNING, G.J., PARSONS, B., WRIGHT, T.J., JACKSON, J.A. & FIELDING, E.J., 2005: Surface displacements and source parameters of the 2003 Bam (Iran) earthquake from Envisat advanced synthetic aperture radar imagery. – Journal of Geophysical Research **110**: B09406.
- GAMMA SOFTWARE DOCUMENTATION, 2013: GAMMA Interferometric Point Target Analysis Software (IPTA), Reference Manual. – GAMMA Remote Sensing Research and Consulting AG, Gümligen, Switzerland.
- GOLDSTEIN, R.M. & WERNER, C.L., 1998: Radar Interferogram Filtering for Geophysical Applications. – Geophysical Research Letters **25** (21): 4035–4038.
- HOFFMANN, J., 2003: The application of satellite radar interferometry to the study of land subsidence over developed aquifer systems. – Dissertation, 211 p., Department of Geophysics, Stanford University, CA, USA.
- MASSONNET, D. & FEIGL, K.L., 1998: Radar interferometry and its application to changes in the Earth's surface. – Reviews of Geophysics **36** (4): 441–500.
- MOTAGH, M., WALTER, T.R., SHARIFI, M.A., FIELDING, E., SCHENK, A., ANDERSOHN, J. & ZSCHAU, J., 2008: Land subsidence in Iran caused by widespread water reservoir overexploitation. – Geophysical Research Letters **35** (16): L16403.
- MOHAMMAD REZAPOUR TABARI, M., 2009: The first step in the Karaj water resources preservation project, Hashtgerd area. – A long-term pro-
- gramme, Reyab Consulting Engineers of Iran (Farsi, see below for access).
- SCHMIDT, D.A. & BÜRGMANN, R., 2003: Time-dependent land uplift and subsidence in the Santa Clara Valley, California, from a large interferometric, synthetic aperture radar dataset. – Journal of Geophysical Research **108**: 8534–8543.
- ZAND, F. & SAHRAEI, A., 2014: Examining Issues of Groundwater Resources Exploitation in Malayer plain, Iran. – International Journal of Scientific Research in Knowledge **2** (3): 124–133, ISSN: 2322-4541.
- For access to the articles in Farsi please contact Mrs. NAZEMEH ASHRAFIANFAR at: nazemeh.ashraianfar@tu-clausthal.de
- Addresses of the Authors:
- Dr.-Ing. NAZEMEH ASHRAFIANFAR, Prof. Dr.-Ing. WOLFGANG BUSCH & Dr. rer. nat STEFFEN KNOSPE, Institute of Geotechnical Engineering and Mine Surveying, Clausthal University of Technology, Erzstraße 18, D-38678 Clausthal-Zellerfeld, Tel.: +49-5323-72-2666, Fax: +49-5323-72-2492, e-mail: {nazemeh.ashraianfar}{wolfgang.busch}{steffen.knospe}@tu-clausthal.de
- Dr. MARYAM DEHGHANI, Assistant Professor, Dep. of Civil and Environmental Engineering, School of Engineering, Shiraz University, Zand St., Shiraz, Iran, Tel.: +98-711-6133162, Fax: +98-711-6473161, e-mail: dehghani_rsgsi@yahoo.com
- Dr. MAHMOUD MOHAMMAD REZAPOUR TABARI, Assistant Professor, Institute of Geotechnical Engineering, Shahrood University, Km 2 Saman Road, Post code: 115, Shahrood, Iran. , Tel.: +98-381-4424401-6, e-mail: mrtabari@eng.sku.ac.ir

Manuskript eingereicht: März 2014
Angenommen: August 2014



Snapshot Hyperspectral Imaging for Soil Diagnostics – Results of a Case Study in the Spectral Laboratory

ANDRÁS JUNG & MICHAEL VOHLAND, Leipzig

Keywords: hyperspectral camera, proximal soil sensing, multivariate calibration, spectral variable selection, partial least squares regression

Summary: Field reflectance spectroscopy has been widely used in proximal soil sensing. Results of spectroscopic approaches depend, inter alia, from the experimental setup and the applied spectroradiometric instrumentation. Beyond the traditional instrument concepts (acquisition of ground truth data with field spectroradiometers, air- and space-borne scanners), there are currently alternative developments in the ground-based or near-ground spectroscopy: The hand-held and thus mobile non-scanning hyperspectral imaging technique might be one previously missing part in the operational spectral data chain to be used for down- and up-scaling purposes. It should effectively bridge the gap between point and image data as it enables a very rapid data acquisition.

This study describes how readings of a hyperspectral frame camera (in the nominal spectral range from 450 nm to 950 nm) could be utilised for soil detection and analysis. The proximally sensed hyperspectral images were compared to 1D spectroradiometric data, both acquired in the lab using raw, sieved and grinded soil samples. Measured spectral datasets were then used to define multivariate calibration models, i.e., the spectra were analysed to extract quantitative models between spectral data and soil constituents of interest determined by wet chemical analysis. We used partial least squares regression (PLS) as statistical calibration method to estimate soil organic carbon (OC), hot-water extractable carbon (HWE-C) and nitrogen (N). The results that we obtained from the camera data were satisfactory (with coefficients of determination (R^2) between 0.62 and 0.84 in the cross-validation), but only with crushed samples and when combining PLS with CARS (competitive adaptive reweighted sampling), an effective spectral variable selection technique. For in-field studies without any sample preparation, stratified approaches considering soil surface roughness and/or the elimination of shadow pixels from the acquired images might both be promising to improve the accuracy of obtainable estimates.

Zusammenfassung: Einblick in die hyperspektrale Abbildung zur Untersuchung von Böden – Ergebnisse einer Laboruntersuchung. Anwendungen der Feldspektroskopie zur Charakterisierung von Böden sind in zahlreichen Studien aufgezeigt worden. Erzielte Ergebnisse sind unter anderem von den eingesetzten Spektroradiometern und der gewählten Messkonfiguration abhängig. Neben klassischen Instrumentierungskonzepten (Erhebung von Referenzdaten mit Feldspektroradiometern, Scanner auf Flugzeug- und Satellitenplattformen) gibt es aktuell in der bodengestützten bzw. -nahen Spektroskopie eine Reihe von Neuentwicklungen. So könnte sich eine handgeholtene und somit mobil einsetzbare bildgebende (nicht-scannende) Hyperspektralkamera als ein bislang fehlendes Element in der operationellen Spektraldatenkette erweisen, nutzbar sowohl zum Up- als auch zum Downscaling. Diese Technik sollte die Lücke zwischen Punktmessung und Bilddaten effektiv schließen können, da sie eine sehr schnelle Datenaufnahme möglich macht.

Eine Vollformat-Hyperspektralkamera (nominaler Spektralbereich 450 nm bis 950 nm) wurde in der vorliegenden Studie zur spektralen Erfassung von Böden eingesetzt. Bodennah aufgenommene Hyperspektralbilder wurden dazu mit 1D Spektroradiometerdaten verglichen. Beide Datensätze wurden im Labor für jeweils unaufbereitete, gesiebte und fein gemahlene Bodenproben aufgenommen. Die gemessenen Spektren wurden genutzt, um multivariate Kalibrierungen aufzustellen, d.h. den Zusammenhang zwischen Spektraldaten (nach adäquater Transformation) und nasschemisch gemessen Bodenparametern zu modellieren. Als Methode zur Kalibrierung wurde die „partial least squares“-Regression (PLS) genutzt, um die Gehalte an organischem Kohlenstoff (OC), heißwasserlöslichem C (HWE-C) und Stickstoff (N) abzuschätzen. Die aus den Kameradaten abgeleiteten Schätzergebnisse waren zufriedenstellend. Die Bestimmtheitsmaße (R^2) der Schätzmodelle lagen zwischen 0.62 und 0.84 in der Kreuzvalidierung.

Diese Resultate konnten aber nur erzielt werden, wenn die Bodenproben vor der spektralen Messung zerkleinert und die PLS mit einer effektiven Spektralvariablenelektion (CARS, „competitive adaptive reweighted sampling“) kombiniert wurden. Für Feldstudien ohne mögliche Probenaufberei-

tung erscheinen Submodelle für aus den Bildern geschätzte unterschiedliche Bodenrauigkeiten und/oder die Beseitigung von Schattenpixeln als aussichtsreiche Möglichkeiten, um die Schätzergebnisse verbessern zu können.

1 Introduction

Spectroscopy in the visible and near-infrared (VNIR) has been widely used in soil sensing, either in the laboratory (e.g. BEN-DOR & BANIN 1995, SUDDUTH et al. 1989, VISCARRA ROSSEL & McBRATNEY 1998) or for in-situ soil monitoring (e.g. KOOISTRA et al. 2003, UDELHOVEN et al. 2003). Typically, field reflectance spectra are collected by portable field spectrometers (1D high-resolution spectra), which are often complemented by 2D data of air- or spaceborne imaging spectrometers with a more limited spatial resolution. Compared to portable field spectroscopy, airborne imaging spectroscopy has a greater potential to cover large areas during a single flight campaign, but accuracies of estimated soil properties are usually lower due to a lower signal-to-noise ratio and disturbing atmospheric influences, for example. Variable soil and surface properties (moisture content, roughness, crusting) induce spectral variability that is critical for large area approaches and may be accounted for by using stratified (local) calibrations (STEVENS et al. 2008, 2010, HILL et al. 2010).

With traditional instrument concepts, i.e., ground truthing with field spectrometers to link ground spectra with data of air- and spaceborne scanners, there is a gap in the “point-pixel-image”-upscaling approach as proximally sensed hyperspectral image data are missing. However, ground-based imaging line-scanners are currently less widespread in ground truthing than portable field spectrometers. One reason for this is the time factor as operating a field line scanner on a tripod set-up is very time consuming compared to the use of a 1D-field spectrometer. One of the concepts to overcome this limitation and to bridge the gap in the hyperspectral data chain is non-scanning snapshot hyperspectral imaging, which enables rapid (1 ms) data acquisition in a hand-held mode (JUNG et al. 2013).

Due to the novelty of this technique there are no available references for non-scanning hyperspectral cameras used in proximal soil sensing. However, there is a comprehensive list of studies and works conducted with line-scanners. Recently, STEFFENS & BUDDENBAUM (2013) utilised a hyperspectral scanner from 400 nm to 1000 nm to determine the concentrations of carbon, nitrogen, aluminium, iron and manganese of a stagnic Luvisol profile under laboratory conditions. For air- and spaceborne scanners e.g. STEVENS et al. (2010) provide an overview of available soil studies. In addition, numerous studies exist dealing with ground-based imaging spectroscopy using the line-by-line-scanning principle for applications in geology and vegetation analysis (KURZ et al. 2013, VIGNEAU et al. 2011, YE et al. 2008).

Irrespective of the instrumentation, hyperspectral measurements provide large sets of spectral variables which are strongly correlated and often contain noise. These data have to be processed to model the relationship between spectral values and soil constituents, which can make use of a simple spectral index, for example, or a number of factors or components extracted after data projection; these factors/components should ideally represent the underlying structure and contain the most relevant information of the data. In the calibration approach, the statistical components are then modelled against the constituents determined by wet chemical analysis. After its validation, either internal with e.g. leave-one-out cross-validation or – more appropriate – external with an additional dataset, this model may be applied to unknown samples.

The statistical method that is used in the calibration process should reflect the inherent structure of the hyperspectral data and be able to handle correlated and noisy data. In chemometrics, partial least squares regression (PLS) has firmly established as a robust multivariate

calibration tool. However, improvements of accuracy are usually achieved by selecting the most informative spectral variables instead of using the full spectrum. The selection of spectral variables also tends to reduce the complexity of the multivariate model that is finally retrieved for quantification purposes (XIAOBO et al. 2010).

This paper focuses on the use of the recently available non-scanning UHD 285 hyperspectral frame camera (Cubert GmbH, Ulm, Germany) for VNIR soil sensing in a laboratory experiment. The studied sample set consisted of 40 soil samples, which were analysed for their contents of organic carbon (OC), hot-water extractable carbon (HWE-C) and nitrogen (N); spectral readings were taken with the UHD 285 and an ASD (Analytical Spectral Devices, Boulder, Colorado, USA) full range spectroradiometer for three different

states of crushing (raw, sieved, grinded). For multivariate calibration, we applied both full spectrum-PLS and PLS combined with a key wavelengths selection procedure, the CARS method (competitive adaptive reweighted sampling; LI et al. 2009). The workflow followed in this study is illustrated in Fig. 1.

2 Data Acquisition

2.1 Study Site, Sampling and Soil Wet-Chemical Analysis

The soil sampling area was situated in the Northwest Saxon Basin (Geopark Muldenland), which is characterised by Permian bedrock geology (rhyolites and ignimbrites), Cretaceous-Tertiary weathering products (like Kaolin) and quaternary sediments (loess, Pleistocene terrace gravel).

Within the study area 40 randomly selected soil samples were taken on different agricultural fields from the very top layer (Ap, 0–10 cm depth). For further wet-chemical analysis, soil samples were air-dried, sieved ≤ 2 mm, and subsequently homogenised by grinding using an agate mortar. Soil texture was determined with the Köhn sieve-pipette method (E DIN ISO 11277:1994-06 1994) and ranged from loamy sand ($n = 2$), sandy loam (11), loam (4), silt loam (22) to silt clay loam (1) (after FAO classification; FAO 2006) (Tab. 1).

The total contents of OC and N were measured by gas chromatography after dry combustion at 1100°C with an EuroEA elemental analyser (HekaTech, Wegberg, Germany), all soil samples were free of carbonate-C. Determination of HWE-C followed the method of

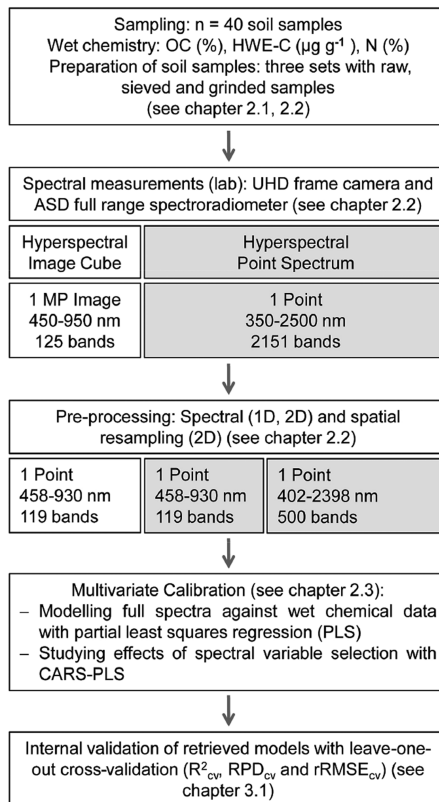


Fig. 1: Workflow to assess soil constituents from spectral data.

Tab. 1: Soil texture of three selected soil samples (from loess and sandy moraine material).

	Sand (%)	Silt (%)	Clay (%)
Soil from loess (silt loam)	5	79	16
Soil from sandy loess (sandy loam)	31	56	13
Soil over sandy moraine (loamy sand)	82	9	6

Tab. 2: Wet-chemical parameters of the studied soil samples.

	Mean	Min	Max	Std
OC (%)	1.54	0.62	4.31	0.74
HWE-C ($\mu\text{g g}^{-1}$)	652	306	1568	265
N (%)	0.145	0.048	0.377	0.068
Quotient C \times N ⁻¹	10.9	8.5	18.0	2.2

KÖRSCHENS et al. (1998) and was examined by an one hour extraction of 10 g soil with distilled water (50 ml) at 100 °C using a Gerhardt Turbotherm TT 125 (Gerhardt, Bonn, Germany). After the extraction, cooling, adding of MgSO₄ and centrifugation at 2600 rpm for 10 minutes, the dissolved organic carbon of the supernatant was analysed with a TOC-V_{CPN}-analyzer (Shimadzu, Duisburg, Germany). Tab. 2 illustrates mean, minimum, maximum, and standard deviation (std) of the analysed soil properties. In total, soil parameters given in Tab. 2 cover the values that are typical for agricultural soils.

2.2 1D and 2D Spectral Data Acquisition and Pre-Processing

For the acquisition of image data we used the UHD 285 hyperspectral frame camera. A silicon CCD chip with a sensor resolution of 970 \times 970 pixel captures the full frame images. The dynamic image resolution is 14 bit. At normal sun light illumination, the integration time of taking one hyperspectral data cube is 1 ms. The camera is able to capture more than 15 spectral data cubes per second, which facilitates hyperspectral video recording. The high-resolution imaging spectrometer coupled with the camera chip was designed and developed by ILM (Institute of Laser Technologies in Medicine and Metrology) at the University of Ulm and the Cubert GmbH. For our analysis, we used the spectral range from 450 nm to 950 nm that is covered by 125 channels. The hyperspectral data cube has a spectral resolution of 4 nm.

1D measurements were performed with an ASD FieldSpec 4 Wide-Res spectroradiometer with an available spectral range from

350 nm to 2500 nm. The spectral resolution of this instrument is 3 nm at 700 nm and 30 nm at 1400/2100 nm. The sampling interval is 1.4 nm in the VNIR range from 350 nm to 1050 nm and 2 nm in the SWIR range; spectra are provided with 1 nm increments (2151 channels).

For the data collection both instruments were mounted on a single tripod (Fig. 2). As illumination source we used an ASD Pro-Lamp model, which is also tripod-mountable for indoor laboratory diffuse reflectance measurements. The size of the calibrated reference panel (Zenith Polymer®) was 30 cm \times 30 cm. For imaging and non-imaging measurements, the same white reference panel was used to keep the referencing standardised.

The air-dried soil samples were prepared at three different degrees of fineness (raw, sieved \leq 2 mm and grinded, Fig. 3) in order to vary micro-shadowing and to possibly maximise the spectral significance of the chemical soil components. The distance between sensor and soil sample was set to 35 cm in the nadir position, the illumination zenith angle was 45°. All samples were prepared on a reflection neutral plate (spectrally tested before) and covered, prior to the spectroscopic measurement, by a black passepartout (reflectance under 5% over the entire spectral range from 400 nm to 2500 nm) with a window of 20 cm \times 20 cm. After each measurement, the soil sample was rotated by 90°, so that each sample was archived with 4 spectra. The spectra of the ASD instrument were pre-processed by ViewSpec (ASD software) and exported as mean spectra for the subsequent statistical analysis. The same measurement scheme was followed for

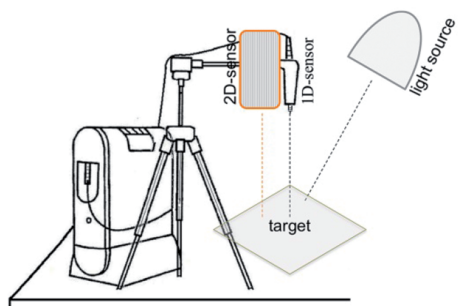


Fig. 2: Experimental set-up for 1D and 2D spectral measurements in the laboratory.

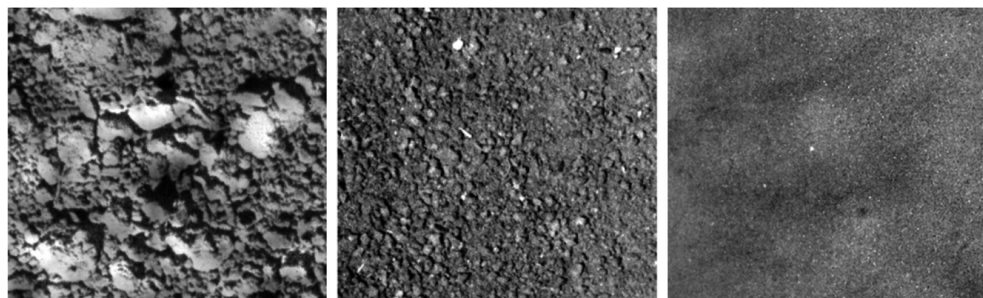


Fig. 3: Examples of the differently prepared soil samples (raw, sieved and grinded) with typical micro-structures and micro-shadowing due to surface roughness.

the 2D reflectance measurements. The native hyperspectral data cubes were converted into .bsq (band sequential) format and processed by the image analysis software ENVI (Exelis Visual Information Solutions).

The spectral resolution of both datasets was adjusted prior to the multivariate calibration procedure. In detail, both sets were reduced to 458 nm – 930 nm and spectrally resampled to the 4 nm resolution of the native image spectra. The camera's first spectral bands below 458 nm showed non-correctable artefacts and were removed. The spectral region over 930 nm suffered from a distinct Si-induced loss of sensitivity. Therefore, the last spectral band was set to 930 nm. It is a general and known phenomenon in CCD imaging technology that the light efficiency of a silicon

detector decreases from around 800 nm up to the response limit of the detector (MAGNAN 2003), which can to some extent be observed for the now reduced image spectra in Fig. 4 too. Based on the described pre-processing, 119 spectral dimensions (458 nm – 930 nm, see Fig. 4) were used for both the 1D reflectance vectors and the 2D image pixels. To enable a direct comparison to the 1D spectra, the 2D reflectance data (hyperspectral data cubes) were converted to virtual 1D measurements by averaging the entire image of each sample. Additionally, spectra were transformed by converting reflectances to absorbances with $\log(\text{reflectance}^{-1})$ and by applying the standard normal variate approach, that is assumed to partly remove the multiplicative interferences of scatter and particle size. Fig. 4 shows also the known effect of soil particle size on reflectance level, i.e., a general decrease with increasing particle size, which has often been described in soil spectroscopic studies (e.g. BOWERS & HANKS 1965).

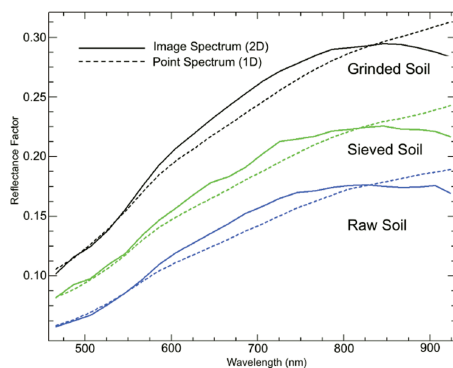


Fig. 4: 1D and 2D reflectance curves after spectral resampling for raw, sieved and grinded soil samples captured by the hyperspectral camera (2D) and the ASD field spectrometer (1D).

2.3 Statistical Methods

PLS has established as multivariate standard tool in the field of chemometrics. PLS is similar to principal component regression (PCR), as both employ statistical rotations to overcome the problems of high-dimensionality and multicollinearity. Different from PCR, PLS maximises the covariance between the spectral matrix (X) and the chemical concentration matrix (Y) to maximise the predictive power of the resulting model (WOLD et al.

2001). To calibrate a PLS model for each constituent, the optimum number of latent variables was identified by performing a leave-one-out cross-validation; the minimum root-mean-squared error (RMSE) in the cross-validation was used as decision criterion (with a predefined maximum of ten latent variables). For an overall description of the PLS method, please refer to ABDI (2003).

Many studies have shown that more accurate calibration models may be achieved by selecting the most informative spectral variables instead of using the full spectrum. For this purpose, we used the CARS approach, which was combined with PLS to CARS-PLS. For a detailed description of the CARS procedure, please refer to LI et al. (2009). Briefly, it uses two successive steps of wavelengths selection in a series of Monte Carlo sampling runs: In a first step, an exponentially decreasing function is used for an enforced removal of wavelengths with relatively small PLS regression coefficients. In a second step, an adaptive reweighted sampling of variables is employed to further eliminate wavelengths in a competitive way. In this step, random numbers are generated to pick variables; the probability of each spectral variable to be kept depends on its weight (calculated from the respective PLS regression coefficient). For our data, 50 successive sampling runs with both steps described above were performed; at the end, the optimal subset of variables with the lowest RMSE in the cross-validated PLS model is kept.

Due to the Monte Carlo strategy and the generation of random numbers in the second step, CARS does not provide a unique solution. Thus, CARS was rerun 50 times to generate 50 estimates for each sample and each constituent; these 50 solutions were averaged to obtain the final estimates.

To assess the accuracy of the multivariate calibrations, we used as measures the residual prediction deviation (RPD, defined as the ratio of standard deviation of the reference values to standard error of the cross-validated estimates), the RMSE, the relative RMSE ($rRMSE = RMSE \times \text{measured arithmetic mean}^{-1}$) and R^2 . Obtained accuracies (cross-validated (cv) values) were evaluated following the guideline of SAEYS et al. (2005): RPD_{cv} and R^2_{cv} values greater than 3.0 or 0.90, respectively, are

considered to indicate excellent predictions, whereas values from 2.5 to 3.0 (RPD_{cv}) and 0.82 to 0.90 (R^2_{cv}) denote a good prediction. Approximate quantitative predictions are indicated by RPD_{cv} values between 2.0 and 2.5 and R^2_{cv} values in the range from 0.66 to 0.81. The possibility to distinguish between high and low values is shown by values between 1.5 and 2.0 (RPD_{cv}) and 0.50 and 0.65 (R^2_{cv}). Unsuccessful predictions have RPD_{cv} or R^2_{cv} values lower than 1.5 or 0.50, respectively.

3 Results and Discussion

3.1 Estimates from Full Range and VNIR Spectra (Spectroradiometer and Image Data)

Estimates from full range spectroradiometer data (cross-validated results) obtained with both approaches, PLS and CARS-PLS, are summarised in Tab. 3. Excellent results were obtained with CARS-PLS for OC (raw samples) and N (raw and grinded samples); for HWE-C, results were slightly worse (good predictions using raw or grinded samples). As HWE-C represents a comparatively small carbon pool (as a measure of labile C), indirect correlations to the spectral data triggered by OC may be of relevance. High correlations between OC and HWE-C (Persons's $r = 0.93$, $p < 0.01$) also support the assumption of such an indirect correlation (see also VOHLAND et al. 2011). CARS-PLS outperformed PLS (without variable selection) in all cases and resulted in at least "approximate quantitative predictions". Due to the selection procedure, CARS-PLS models were – as a general rule – more parsimonious than PLS models. With the exception of sieved samples (OC and N), the number of latent variables reduced slightly; the number of spectral variables that were integrated in CARS-PLS models ranged between 13.9 (HWE-C, sieved samples – averaged from 50 runs) and 23.5 (N, sieved samples) and was thus distinctly lower than the original number of $n = 500$ spectral variables. With respect to the preparation level, worst results were obtained with the use of sieved samples.

Tab.3: Cross-validated results from field spectrometer data (1D) and image mean spectra (2D) for raw, sieved and grinded soils ($n = 40$, l.v.: number of latent variables (for CARS-PLS averaged from 50 runs); cv: leave-one-out cross-validation).

Spectral Range	Soil Preparation Level	Model	OC			N			HWE-C					
			l.v.	R ² _{cv}	RPD _{cv}	rRMSE _{cv}	l.v.	R ² _{cv}	RPD _{cv}	rRMSE _{cv}	l.v.	R ² _{cv}	RPD _{cv}	rRMSE _{cv}
ID 402 nm - 2398 nm 500 variables	raw	PLS	9	0.73	1.94	0.25	9	0.72	1.89	0.26	8	0.61	1.58	0.26
		CARS-PLS	8.2	0.93	3.85	0.13	8.0	0.91	3.30	0.15	7.2	0.86	2.73	0.15
	sieved	PLS	6	0.65	1.66	0.29	6	0.64	1.66	0.29	7	0.51	1.37	0.30
		CARS-PLS	6.0	0.84	2.49	0.19	6.0	0.84	2.49	0.19	6.0	0.72	1.91	0.21
	grinded	PLS	9	0.73	1.90	0.25	9	0.75	2.02	0.24	10	0.63	1.58	0.26
		CARS-PLS	6.7	0.88	2.93	0.16	7.3	0.92	3.53	0.14	8.2	0.88	2.86	0.14
ID 458 nm - 930 nm 119 variables	raw	PLS	7	0.41	1.28	0.37	10	0.34	1.19	0.41	7	0.43	1.28	0.32
		CARS-PLS	6.2	0.77	2.08	0.23	8.0	0.78	2.09	0.23	5.6	0.70	1.84	0.22
	sieved	PLS	9	0.63	1.64	0.29	8	0.45	1.34	0.36	9	0.64	1.64	0.25
		CARS-PLS	8.4	0.82	2.37	0.20	8.0	0.77	2.09	0.23	7.8	0.77	2.14	0.19
	grinded	PLS	10	0.66	1.73	0.28	10	0.49	1.38	0.35	9	0.56	1.49	0.27
		CARS-PLS	9.2	0.85	2.61	0.18	8.5	0.79	2.17	0.22	7.5	0.71	1.88	0.22
2D 458 nm - 930 nm 119 variables	raw	PLS	3	0.38	1.27	0.38	4	0.30	1.19	0.40	6	0.39	1.27	0.32
		CARS-PLS	3.5	0.49	1.42	0.34	3.0	0.42	1.33	0.36	4.1	0.58	1.56	0.26
	sieved	PLS	7	0.59	1.57	0.31	7	0.54	1.47	0.33	7	0.54	1.45	0.28
		CARS-PLS	6.5	0.72	1.89	0.25	6.7	0.70	1.83	0.26	5.6	0.62	1.63	0.25
	grinded	PLS	10	0.65	1.70	0.28	8	0.60	1.58	0.30	10	0.65	1.67	0.24
		CARS-PLS	8.4	0.84	2.49	0.19	7.1	0.75	2.01	0.24	8.9	0.83	2.45	0.17

excellent

good

Fig. 5 illustrates the selection frequencies of spectral variables for assessing OC, which were obtained in 50 runs of CARS-PLS with the full spectra of raw and sieved samples. Selection frequencies of grinded samples (not illustrated) showed peaks partly similar to raw and partly similar to sieved samples. Some regions in the visible were rather frequently selected for all preparation levels (e.g. 406 nm – 418 nm, 662 nm – 674 nm and – for sieved and grinded samples – 526 nm – 538 nm), whereas selection frequencies in the very near IR (a region covered by the UHD camera) were very low (Fig. 5). In the NIR range up to 1300 nm, selection peaks were found only at about 1100 nm (raw and grinded samples)

and at 1140 nm (sieved samples). Compared to the visible and the NIR domain, the shortwave IR (SWIR) region was distinctly more relevant for the CARS approach with markedly higher peaks of selection frequencies at 1374 nm – 1394 nm (raw and grinded samples), 1850 nm – 1902 nm (raw, grinded), 2078 nm – 2194 nm (all preparation levels) and some wavelengths beyond 2300 nm (e.g. 2306, 2334/2338 nm) (Fig. 5). In the wavelength range between 1406 nm and 1798 nm, selection frequencies were low in all cases.

The found selection peaks indicate some wavelength regions (VIS range, prominent water bands, hydroxyl band, C-H absorption bands) that were already identified in other

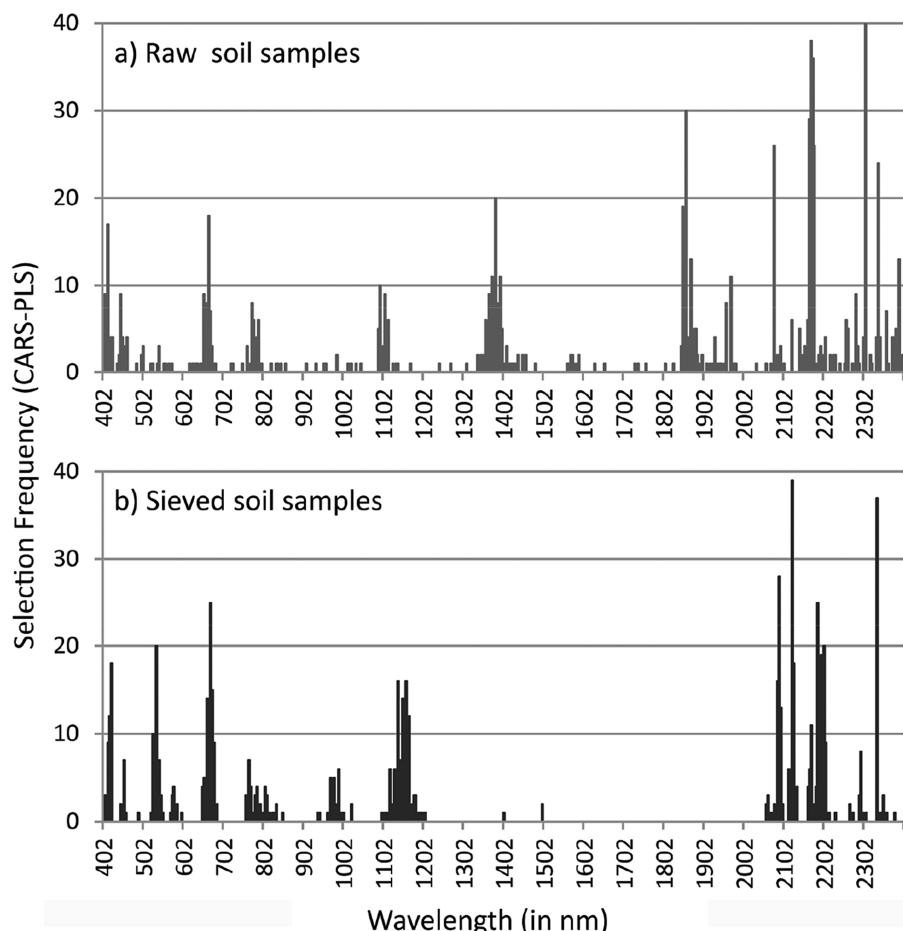


Fig. 5: Selection frequencies (raw (a) and sieved (b) samples) for spectral variables in the full range from 402 nm to 2398 nm (realised in 50 runs of CARS-PLS with OC as target soil constituent).

studies to be relevant for assessing OC with spectroscopy (e.g. MOUAZEN et al. 2007, VIS-CARRA ROSEL & BEHRENS 2010, VOHLAND et al. 2014). BELLON-MAUREL & McBRATNEY (2011) quote the 1600 nm – 2500 nm range to be the most relevant for measuring OC. CÉCILLON et al. (2009) present a compilation of important NIR wavelengths for OC and also N that are all beyond 1100 nm.

As most of these essential wavelength regions were not included in the pruned ASD spectra and the UHD data, a drop of accuracies was a priori to be expected for the multivariate calibrations with these datasets. The obtained results were, de facto, inferior to those with full range spectra (Tab. 3), but especially for OC these differences were small when using grinded samples and the CARS-PLS method; for both datasets (pruned ASD and averaged UHD Spectra) the cross-validation resulted in “good” estimates. In addition, very similar results were obtained for OC from sieved samples using full and pruned ASD spectra and also for HWE-C from grinded samples with full range ASD and UHD data (Tab. 3).

Differences of accuracy between the three instrumental settings were most pronounced when raw samples were measured and used for the calibration with CARS-PLS; in this case, the general order for all soil variables was ASD (full spectra) >> ASD (pruned spectra) >> UHD data. The CARS variable selection procedure obviously highlighted these differences, as accuracies obtained with PLS

from raw samples were on a similar level at least for pruned ASD and UHD data (Tab. 3). As the UHD spectra were obtained by averaging all pixel values over the complete image, it is not entirely clear why these data performed generally worse than the ASD readings. The differences were probably due to the irregular surface roughness of the raw samples which caused multidirectional light scattering effects and strong contrasts between illuminated and shadowed image regions (Fig. 3). Soil surface roughness is known as one main disturbing factor for e.g. SOC estimates from proximally sensed VNIR data, which may be compensated, in case of larger samples sets, by stratified models specified for different surface roughness classes (RODIONOV et al. 2014). Thus, for future in-field tests of the UHD hyperspectral frame camera its potential to assess soil roughness from the images (e.g. by analysing the extent of shadowed image portions; GARCÍA MORENO et al. 2008) should be fully exploited.

3.2 Spatial Analysis: How Much Variability is in One Image?

We selected three samples with different levels of mean OC contents to analyse the variability in the hyperspectral images (Tab. 4). Within each image, 500 randomly determined pixels were extracted and then used to obtain pixel-wise estimates for OC. For this estima-

Tab. 4: Statistics for OC estimates from image data obtained with CARS-PLS (each sample and preparation level: 500 randomly selected pixels).

	Raw			Sieved			Grinded		
	Mean ²	Std	Min Max	Mean ²	Std	Min Max	Mean ²	Std	Min Max
Sample #1 ¹	1.62	0.77	-1.21 3.77	1.72	0.61	-0.06 3.56	1.95	1.88	-4.05 6.18
Sample #2 ¹	2.28	0.66	0.51 6.40	2.21	0.85	-0.24 4.69	2.53	1.91	-4.04 8.20
Sample #3 ¹	1.10	0.41	0.17 2.37	0.98	0.82	-1.44 3.51	1.26	2.09	-5.58 6.93

¹ Wet-chemical reference values (OC): #1: 1.90, #2: 2.70, #3: 0.62

² Previous estimates from averaged images (see 3.1):

Sample #1: raw: 1.83, sieved: 1.81, grinded: 1.90; Sample #2: raw: 2.34, sieved: 2.20, grinded: 2.33; Sample #3: raw: 1.28, sieved: 1.28, grinded: 1.09

tion, the already available models calibrated before (for $n = 40$ reference values) were applied.

The results we obtained were similar for all three images. In all cases, the estimates followed the normal distribution. As an example, the Q-Q (quantile-quantile) plot is illustrated for sample #1 (grinded) in Fig. 6. Mean values calculated from the 500 image pixels provided useful estimates close to the measured reference values (Tab. 4). The range of estimates indicated, on the one hand, highly variable OC contents; on the other hand, however, we often received inconsistently low and high values, i.e. negative values and obvious overestimates (OC contents of more than 6%, for example; see boxplots in Fig. 6 and Tab. 4). Evidently, the calibration set was not sufficient to represent all situations (including illumination differences) contained in the image data; this may be due to the small number of calibration samples and the way the calibration set was compiled, as only averaged and thus “smoothed” image spectra were used.

4 Summary and Conclusions

We tested two multivariate calibration methods; in all cases, PLS combined with CARS outperformed full spectrum-PLS (without

variable selection). CARS was found to be an effective selection method that improved accuracies at least in the cross-validation; however, it should be tested with an independent validation set. The majority of CARS-selected wavelengths were physically meaningful, as they were related – in the case of organic carbon – to water absorption bands, the hydroxyl band at 2200 nm or C-H absorption bands in the region beyond 2300 nm.

In soil spectroscopy, the SWIR domain is of high relevance. Although the tested hyperspectral camera (UHD 285) does not cover this region, obtained values indicated, at least in part, good estimates. These results were restricted to crushed (grinded) samples; accuracies dropped distinctly for raw samples (which represent the normal in-field situation with rough soil surfaces). Thus, for in-field studies, the full potential of the image data should be used, which is to estimate soil roughness directly from the images to define stratified models or to eliminate shadowed pixels which have very restricted information content.

The image data that we analysed in detail showed a great variability of the contained (spectral) information. These fine-scale variations are relevant for chemometric approaches, as they require a careful definition of calibration sets that have to cover these variations adequately.

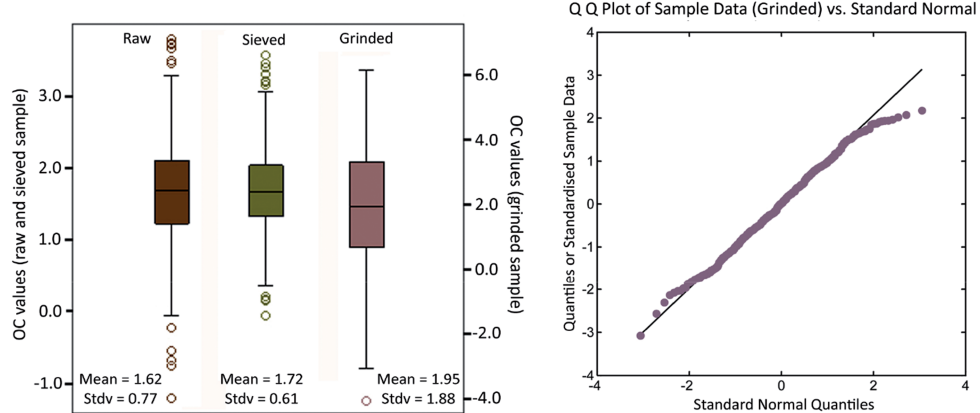


Fig. 6: Statistics for OC estimates (in %) obtained from 500 randomly selected pixels for one sample (#1) and its different preparation levels (for clarification, boxplot for grinded sample is scaled differently).

Acknowledgements

Our special thanks go to Cubert GmbH that made it possible to use and test the hyperspectral frame camera, by name to RAINER GRASER and Dr. RENÉ MICHELS. We would like to thank the Soil Science Department at University of Trier, headed by SÖREN THIELE-BRÜHN, for carrying out chemical analyses. CARS calculations were carried out using the freely available CARS package (Copyright HONGDONG Li, 2011; <https://code.google.com/p/carspls/>). The project was supported by a grant of the German Research Foundation (DFG, VO 1509/3-1).

References

- ABDI, V., 2003: Partial least squares (PLS) regression. – LEWIS-BECK, M., BRYMAN, A. & FUTING, T. (eds.): Encyclopedia for research methods for the social sciences: 772–795, Sage Publications, Thousand Oaks, CA, USA.
- BELLON-MAUREL, V. & McBRATNEY, A., 2011: Near-infrared (NIR) and mid-infrared (MIR) spectroscopic techniques for assessing the amount of carbon stock in soils – Critical review and research perspectives. – *Soil Biology and Biochemistry* **43** (7): 1398–1410.
- BEN-DOR, E. & BANIN, A., 1995: Near-infrared analysis as a rapid method to simultaneously evaluate several soil properties. – *Soil Science Society of America Journal* **59** (2): 364–372.
- BOWERS, S.A. & HANKS, R.J., 1965: Reflection of radiant energy from soils. – *Soil Science* **100** (2): 130–138.
- CÉCILLON, L., BARTHÈS, B.G., GOMEZ, C., ERTLEN, D., GENOT, V., HEDDE, M., STEVENS, A. & BRUN, J.J., 2009: Assessment and monitoring of soil quality using near-infrared reflectance spectroscopy (NIRS). – *European Journal of Soil Science* **60** (5): 770–784.
- E DIN ISO 11277:1994-06, 1994: Bodenbeschaffenheit – Bestimmung der Partikelgrößenverteilung in Mineralböden – Verfahren durch Sieben und Sedimentation nach Entfernen der löslichen Salze, der organischen Substanz und der Carbonate. – Beuth-Verlag, Berlin.
- FAO (Food and Agriculture Organization of the United Nations), 2006: Guidelines for soil description. – 4th ed., 97 pp., Rome, Italy.
- GARCÍA MORENO, R., SAA REQUEJO, A., TARQUIS ALONSO, A.M., BARRINGTON, S. & DÍAZ, M.C., 2008: A shadow analysis method to measure soil surface roughness. – *Geoderma* **146** (1–2): 201–208.
- HILL, J., UDELHOVEN, T., VOHLAND, M. & STEVENS, A., 2010: The Use of Laboratory Spectroscopy and Optical Remote Sensing for Estimating Soil properties. – OERKE, E.C., GERHARDS, R., MENZ, G. & SIKORA, R.A. (eds.): Precision crop protection – the challenge and use of heterogeneity: 67–86. – 441 pp., Springer Science, Dordrecht, The Netherlands.
- JUNG, A., VOHLAND, M., HEINRICH, J., MICHELS, R. & GRASER, R., 2013: Soil analysis with hyperspectral data – an experiment with a hyperspectral frame camera and VIS-NIR spectrometers. – 8th EARSeL SIG Imaging Spectroscopy Workshop, Nantes, France, in press.
- KOOISTRA, L., WANDERS, J., EPEMA, G.F., LEUVEN, R.S.E.W., WEHRENS, R. & BUYDENS, L.M.C., 2003: The potential of field spectroscopy for the assessment of sediment properties in river floodplains. – *Analytica Chimica Acta* **484** (2): 189–200.
- KÖRSCHENS, M., WEIGEL, A. & SCHULZ, E. 1998: Turnover of Soil Organic Matter (SOM) and Long-Term Balances – Tools for Evaluating Sustainable Productivity of Soils. – *Zeitschrift für Pflanzenernährung und Bodenkunde* **161** (4): 409–424.
- KURZ, T.H., BUCKLEY, S.J. & HOWELL, J.A., 2013: Close-range hyperspectral imaging for geological field studies: workflow and methods. – *International Journal of Remote Sensing* **34** (5): 1798–1822.
- LI, H., LIANG, Y., XU, Q. & CAO, D., 2009: Key wavelengths screening using competitive adaptive reweighted sampling method for multivariate calibration. – *Analytica Chimica Acta* **648** (1): 77–84.
- MAGNAN, P., 2003: Detection of visible photons in CCD and CMOS: A comparative view. – *Nuclear Instruments and Methods in Physics Research Section A: Accelerators, Spectrometers, Detectors and Associated Equipment* **504** (1): 199–212.
- MOUAZEN, A.M., MALEKI, M.R., DE BAERDEMAEKER, J. & RAMON, H., 2007: On-line measurement of some selected soil properties using a VIS-NIR sensor. – *Soil and Tillage Research* **93** (1): 13–27.
- RODIONOV, A., PATZOLD, S., WELP, G., PALLARES, R.C., DAMEROW, L. & AMELUNG, W., 2014: Sensing of soil organic carbon using VIS-NIR spectroscopy at variable moisture and surface roughness. – *Soil Science Society of America Journal* **78** (3): 949–957.
- SAEYS, W., MOUAZEN, A.M. & RAMON, H., 2005: Potential for onsite and online analysis of pig ma-

- nure using visible and near infrared spectroscopy. – *Biosystems Engineering* **91** (4): 393–402.
- STEFFENS, M. & BUDDENBAUM, H., 2013: Laboratory imaging spectroscopy of a stagnic Luvisol profile – High resolution soil characterisation, classification and mapping of elemental concentrations. – *Geoderma* **195**: 122–132.
- STEVENS, A., VAN WESEMAEL, B., BARTHOLOMEUS, H., ROSILLON, D., TYCHON, B. & BEN-DOR, E., 2008: Laboratory, field and airborne spectroscopy for monitoring organic carbon content in agricultural soils. – *Geoderma* **144** (1–2): 395–404.
- STEVENS, A., UDELHOVEN, T., DENIS, A., TYCHON, B., LIOY, R., HOFFMANN, L. & VAN WESEMAEL, B., 2010: Measuring soil organic carbon in croplands at regional scale using airborne imaging spectroscopy. – *Geoderma* **158** (1–2): 32–45.
- SUDDUTH, K.A., HUMMEL, J.W. & FUNK, R.C., 1989: NIR soil organic matter sensor. – *ASAE-Paper 89-1035*.
- UDELHOVEN, T., EMMERLING, C. & JARMER, T., 2003: Quantitative analysis of soil chemical properties with diffuse reflectance spectrometry and partial-least-square regression: A feasibility study. – *Plant and Soil* **251** (2): 319–329.
- VIGNEAU, N., ECARNO, M., RABATEL, G. & ROUMET, P., 2011: Potential of field hyperspectral imaging as a non destructive method to assess leaf nitrogen content in wheat. – *Field Crops Research* **122** (1): 25–31.
- VISCARRA ROSSEL, R.A. & BEHRENS, T., 2010: Using data mining to model and interpret soil diffuse reflectance spectra. – *Geoderma* **158** (1–2): 46–54.
- VISCARRA ROSSEL, R.A. & McBRATNEY, A.B., 1998: Laboratory evaluation of a proximal sensing technique for simultaneous measurement of soil clay and water content. – *Geoderma* **85** (1–2): 19–39.
- VOHLAND, M., HARBICH, M., SCHMIDT, O., JARMER, T., EMMERLING, C. & THIELE-BRÜHN, S., 2011: Use of imaging spectroscopy to assess different organic carbon fractions of agricultural soils. – NEALE, C.M.U. & MALTESE, A. (eds.): *Remote Sensing for Agriculture, Ecosystems, and Hydrology XIII*. – Proceedings of SPIE 8174, Bellingham, WA, USA.
- VOHLAND, M., LUDWIG, M., THIELE-BRÜHN, S. & LUDWIG, B., 2014: Determination of soil properties with visible to near- and mid-infrared spectroscopy: effects of spectral variable selection. – *Geoderma* **223–225**: 88–96.
- WOLD, S., SJÖSTRÖM, M. & ERIKSSON, L., 2001: PLS-regression: a basic tool of chemometrics. – *Chemometrics and Intelligent Laboratory Systems* **58** (2): 109–130.
- XIAOBO, Z., JIEWEN, Z., POVEY, M.J., HOLMES, M. & HANPIN, M., 2010: Variables selection methods in near-infrared spectroscopy. – *Analytica Chimica Acta* **667** (1–2): 14–32.
- YE, X., SAKAI, K., OKAMOTO, H. & GARCIANO, L.O., 2008: A ground-based hyperspectral imaging system for characterizing vegetation spectral features. – *Computers and Electronics in Agriculture* **63** (1): 13–21.

Address of the Authors:

Dr. ANDRÁS JUNG & Prof. Dr. MICHAEL VOHLAND,
Institute for Geography, University of Leipzig,
Geoinformatics and Remote Sensing, Johannisallee 19a, D-04103 Leipzig, Tel.: +49-341-97-32785,
Fax: +49-341-97-32799, e-mail: {andras.jung},
{michael.vohland}@uni-leipzig.de

Manuskript eingereicht: Juni 2014

Angenommen: September 2014



An Enhanced Classification Approach using Hyperspectral Image Data in Combination with *in situ* Spectral Measurements for the Mapping of Vegetation Communities

BASTIAN SIEGMANN, Osnabrück, CORNELIA GLÄSSER, Halle, SIBYLLE ITZEROTT & CARSTEN NEUMANN, Potsdam

Keywords: hyperspectral, aisaEAGLE, spectral field measurements, dry grass vegetation, heathland vegetation, support vector machine classification, random forest classification

Summary: This paper shows the potential of a method using field spectral measurements as independent training data for the classification of airborne hyperspectral imagery of a natural preserve in Germany, using two different machine learning algorithms. The spectral reflectance of different *dry grass-* and *heathland* vegetation communities was measured with field spectrometers (350 nm – 2500 nm) in August 2009. Additionally, hyperspectral imagery was acquired by the airborne scanner aisaEAGLE (390 nm – 970 nm). The developed normalization technique was proven to be a suitable method to make image and field spectra comparable for classification. A support vector machine (SVM) and random forest (RF) classifier trained with normalized field spectra were applied to normalized image data to classify *dry grass-* and *heathland* communities in different levels of detail. SVM (overall accuracy (OAA) 89.13%) provided significantly better classification results compared to RF (OAA 71.74%) in the second level of detail. Consequently, only SVM was used for classification in the highest level of detail (third level), which also led to high classification accuracy (OAA 77.27%). The results indicate the potential of the developed approach classifying airborne hyperspectral image data with field spectral measurements for the spatial assessment and separation of *dry grass-* and *heathland* communities.

Zusammenfassung: Ein kombinierter Ansatz zur Klassifizierung hyperspektraler Bilddaten mit im Gelände erfassten spektralen Punktmessungen zur räumlichen Erfassung von Vegetationsgesellschaften. Im vorliegenden Beitrag wurde das Potenzial einer Methode untersucht, bei der spektrale Punktmessungen eines Feldspektrometers als unabhängige Trainingsdaten zur Klassifizierung hyperspektraler Flugzeugscanneraufnahmen verwendet wurden. Dabei kamen zwei Algorithmen des maschinellen Lernens zum Einsatz, deren Performanz unter Betrachtung verschiedener Genauigkeitslevels getestet wurde. Im August 2009 wurden spektrale Signaturen von Trockengras- und Heidekrautgesellschaften mit einem Geländespektrometer (350 nm – 2500 nm) erfasst. Zusätzlich fand eine flächendeckende Befliegung des Untersuchungsgebietes mit dem hyperspektralen Flugzeugscanner aisaEAGLE (390 nm – 970 nm) statt. Um eine Vergleichbarkeit beider Datensätze herzustellen, wurde eine Methode zur Normalisierung der Gelände- und Bilddaten entwickelt. Die Klassifizierung der Trockengras- und Heidekrautgesellschaften erfolgte mit den Algorithmen Support Vector Machine (SVM) und Random Forest (RF). Beide Algorithmen wurden mit den normalisierten Geländespektren trainiert und dann die Klassifizierung der normalisierten Bilddaten durchgeführt. SVM (Gesamtgrenauigkeit (OAA) 89,13%) lieferte im Vergleich zu RF (OAA 71,74%) das bessere Klassifizierungsergebnis im zweiten Genauigkeitslevel. Aus diesem Grund erfolgte die Klassifizierung des höchsten Genauigkeitslevels (drittes Genauigkeitslevel) ausschließlich mit dem Algorithmus SVM, wobei erneut eine hohe Klassifizierungsgüte (OAA 77,27%) erzielt wurde. Als Ergebnis konnte eine genaue räumliche Erfassung und Trennung von

Trockengras- und Heidekrautgesellschaften erzielt werden, wodurch das Potenzial der entwickelten Methode zur Klassifizierung hyperspektraler Bild-

daten mit spektralen Geländemessungen verdeutlicht wurde.

1 Introduction

One of the main applications of remote sensing is the classification of different land cover types. In general, classification of airborne or satellite images is conducted by training a classification algorithm with spectral data directly extracted from the same image. Subsequently, the trained model is applied to the image data. However, there is often no information about the location of suitable training areas for the classification algorithm, which leads to inaccurate classification results. The rising number of libraries containing field or laboratory spectral measurements of different land cover classes can be used as an alternative to train classification algorithms without extracting spectral information directly from the image data. At present only a few studies using spectral data collected in the field or the laboratory exist as independent training data for the classification of airborne hyperspectral images for mapping minerals (e.g. KOKALY et al. 2008, SWAYZE et al. 2009), soils (e.g. BROWN 2007) and especially vegetation (e.g. BIRGER et al. 1998, NIDAMANURI et al. 2007, NIDAMANURI & ZBELL 2011, ZOMER et al. 2009).

Detection of occurring plant species and mapping of different vegetation communities in the field is very time consuming and expensive. In this context, airborne and spaceborne hyperspectral remote sensing data with its high spectral information content increases the possibility for a highly accurate detection of different types of vegetation (FAUVEL et al. 2013). Especially for hyperspectral data many classification methods have been developed and refined in recent years (Camps-Valls et al. 2014, LUNGA et al. 2014). Therefore, hyperspectral data provides an alternative for fast and area-wide classification of different vegetation communities and species in order to locate and protect areas with endangered species which have to be preserved, e.g. in the context of the European habitats directive (EUROPEAN UNION 1992).

Several studies have shown the potential of hyperspectral remote sensing data for separating vegetation communities or even single species (ARTIGAS & YANG 2006, CHAN & PAELINCKX 2008, COCHRANE 2000, SCHMIDT & SKIDMORE 2003). The high information content of hyperspectral data is well suited for a data basis for area-wide mapping of vegetation habitats and for vegetation monitoring over long time periods. However, acquisition of appropriate spectral reflectance signatures directly from hyperspectral image data for each class as representative training data for the classification of natural vegetation is still a challenge because of the heterogeneous character of the plant communities and their patchy stand density. In this context, field reflectance spectra of areas where species composition was botanically determined can serve as an alternative to generate suitable training data of an area wide image classification.

The main objective of this paper is the classification of dry land vegetation communities at different levels of detail from airborne hyperspectral images using field spectral measurements as representative reference data for the different classes. The classification was also conducted comparatively using the two classification algorithms support vector machine (SVM) and random forest (RF).

2 Study Area and Data

2.1 Study Area

The study area ($52^{\circ}30' \text{ N}$, 13° E) was the natural preserve Döberitzer Heide, located in the federal state of Brandenburg, west of the German capital Berlin (Fig. 1). From the early 18th century till 1994 the area was used as a military training area. After this long period of military usage large parts were protected by the German Federal Nature Conservation Act in 1996. The Döberitzer Heide has a size of about 5000 ha and is characterized by wet

biotopes in the western and dry biotopes in the middle and eastern parts (RUTSCHKE 1997). The study area is situated in the transition area between maritime and continental climates. For that reason the region has a mean annual precipitation of 590 mm and 8.8 °C mean annual temperature (HENDL 1996). Over 50% of the Döberitzer Heide is covered by deciduous and coniferous forest, while other parts are characterized by heathland, sandy grassland, mesophile grassland, seminatural humid meadows, wetland and wasteland.

The four test sites are located in the northwest (test site A), the northeast (test site B), the east (test site C) and the south (test site D) of the study area (Fig. 1). The test sites are dominated by dry vegetation communities, especially different types of *dry grassland*, *heathland*, *broom*, *sand pioneer corridors* and *browse bristle*.

2.2 Data

Hyperspectral data of the airborne imaging system aisaEAGLE (Specim Ltd.) was used for classification of *dry grass*- and *heathland* vegetation. The aisaEAGLE imagery of the study area was acquired on August, 19, 2009 with a geometric resolution of 2 m in 252 spectral bands covering the wavelength range 390 nm – 970 nm. Thirteen flight stripes – alternately scanned in north-south and south-north directions – were recorded during flyover. The ROME de-striping algorithm was used to reduce the sensor mis-calibration effects of defi-

cient lines along tracks in the images (ROGASS et al. 2011). Atmospheric correction was performed using software developed at the University of Valencia (GUANTER et al. 2009). Additionally, empirical line correction was applied including spectral ground measurements of different dark and bright targets collected in the test site during aisaEAGLE overpass (SMITH & MILTON 1999). aisaEAGLE data geometric correction was realized with the software CaliGeo and orthorectification was performed with the software ENVI.

Furthermore, 46 vegetation plots (1 m^2 size each) in areas with homogenous plant populations were defined in the study area. Colour infrared airborne data of previous years was evaluated for identifying suitable locations of the plots in field and for allowing a representative sampling of the investigated vegetation communities (NEUMANN et al. 2013). Spectral reflectance measurements of all plots were collected in the study area between August, 15 and 24, 2009 by different ASD FieldSpec Pro spectroradiometers recording spectral reflectance in 2151 spectral bands in the wavelength range 350 nm – 2500 nm. For each plot, 25 spectral measurements were taken. In addition, the height of vegetation was measured, photos were taken for documentation and plot positions were located by a handheld GPS.

2.3 Vegetation Mapping

During vegetation mapping, open land habitats with low vegetation growth were de-



Fig. 1: Location of the study area and the test sites within the study area (left) and test site B in detail (right).

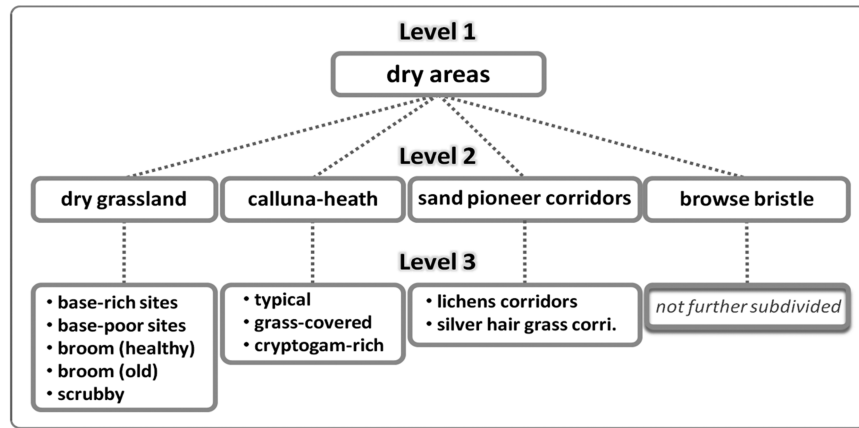


Fig. 2: Division of dry grass- and heathland habitats in different level for classification.

termined in detail. Wooden areas and shrub lands were not the focus of the investigations except broom heath, which was mapped and classified, too. The vegetation mapping scheme was finally structured in a hierarchical division of open land habitats with different levels (Fig. 2).

3 Methods

3.1 Spectral Pre-Processing

At the beginning of spectral pre-processing the inner fence (IF) was calculated for the 25 spectral field measurements of each plot. The IF is a statistical method to find outliers in a dataset. First, the inter-quartile range (IQR) has to be computed (1), and then the upper (IF_{upper}) and lower inner fence (IF_{lower}) is determined (2) (TUKEY 1977). Q_{0.25} and Q_{0.75} represent the first and the third quantile.

$$\text{IQR} = Q_{0.75} - Q_{0.25} \quad (1)$$

$$\begin{aligned} \text{IF}_{\text{upper}} &= (Q_{0.75} + 1.5 * \text{IQR}) \text{ and} \\ \text{IF}_{\text{lower}} &= (Q_{0.25} - 1.5 * \text{IQR}) \end{aligned} \quad (2)$$

In this study, for every spectral band the upper and lower IF was calculated from the 25 spectral field measurements of each plot. As a result, an inner fence range (IFR) was created limited by two artificially generated spectral signatures. Consequently, all spectral meas-

urements of a plot outside the IFR were excluded from further processing and from final classification (Fig. 3). For classification of the aisaEAGLE image data with all selected spectral measurements of each plot, the data had to be spectrally prepared because spectral attributes of the training (ASD field measurements) and classification datasets (aisaEAGLE image data) showed significant spectral differences. Therefore, field spectra were resampled to aisaEAGLE spectral resolution and spectral range, making both datasets comparable.

Data adjustment of aisaEAGLE data and selected field spectra was achieved by normalization of both datasets, dividing reflectance values of the single bands (ref_n) by the maximum reflectance value of the spectral curve (ref_{\max}). This procedure was adapted to all spectral signatures in both datasets.

$$\text{ref}_{\text{norm}} = \frac{\text{ref}_n}{\text{ref}_{\max}} \quad (3)$$

As a result, all spectral reflectance signatures were scaled to a maximum value of 1. Fig. 4 shows the spectral curves of an aisaEAGLE pixel with corresponding ASD field measurements before and after normalization.

The result clearly indicates a better match of the spectral reflection curves after the normalization procedure. Furthermore, in total 122 spectral bands at the beginning and end of the datasets (390 nm – 500 nm, 800 nm – 970 nm) were deleted because of noise, leav-

ing 130 spectral bands in the range 500 nm – 800 nm for the classification (Fig. 4, right). Subsequently, normalized aisaEAGLE data and selected, resampled and finally normalized field measurements were applied for classification of *dry grass*- and *heathland* vegetation.

3.2 Machine Learning Classification

A requirement for classification with SVM and RF is the availability of training sam-

ples for each dataset class (Muñoz-Mari et al. 2007). In this study only *dry grass*- and *heathland* areas were in the focus of the investigations, so that all the other classes had to be masked before starting with the machine learning classification. First, subsets with the spatial extension of the four test sites were extracted from aisaEAGLE image data. Afterwards, wooded areas, areas without vegetation and shadows were classified by applying an unsupervised K-means classification algorithm. Subsequently, a mask was created from the three classes and used to reduce the aisa-

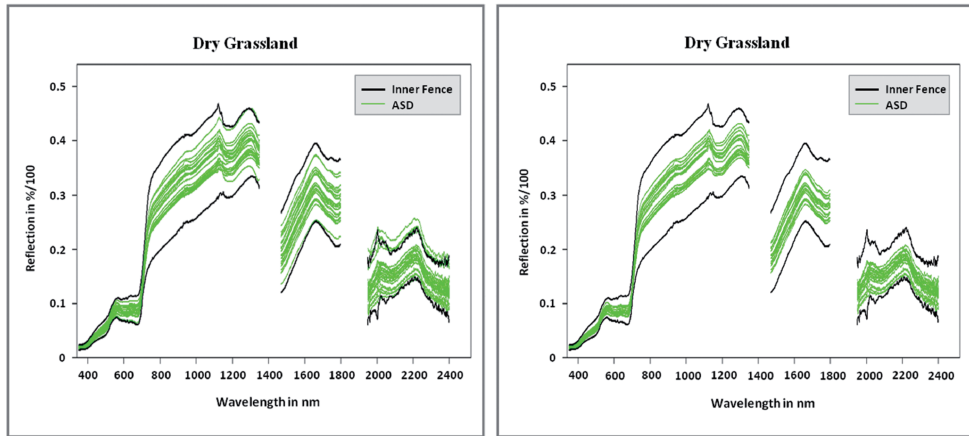


Fig. 3: Left: Spectral field measurements of a dry grassland plot before selection by inner fence. Right: Spectral field measurements of a dry grassland plot after selection by inner fence.

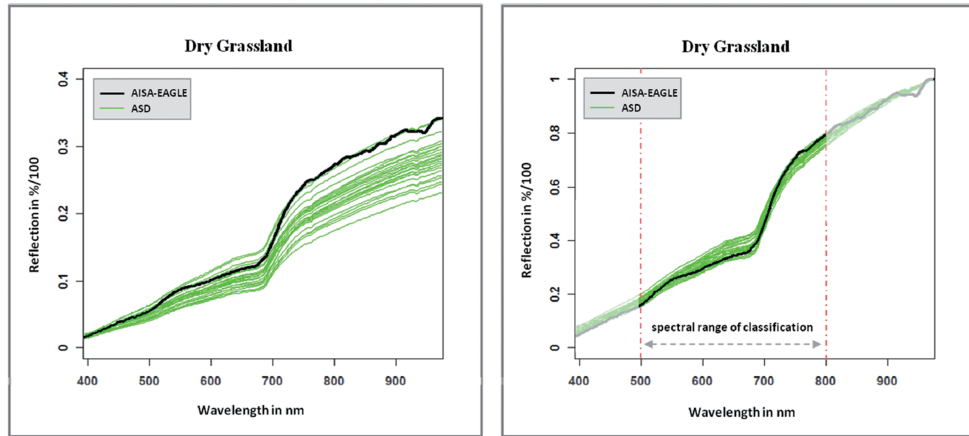


Fig. 4: Spectral reflection comparison of a dry grassland plot between the sensors aisaEAGLE and ASD FieldSpec. Left: Before normalization. Right: After normalization with the spectral range used for classification.

EAGLE data of the different test sites only to areas with *dry grass-* and *heathland*.

SVMs and RFs trace back to statistical learning theory, and some years ago they were adapted to solve classification and regression problems in the field of remote sensing. The advantage of SVMs and RFs compared with other classification algorithms, e.g. maximum likelihood and spectral angle mapper, is their capability to deal with high dimensional data. For that reason, SVMs (BRAUN et al. 2010, FOODY & MATHUR 2004, HUANG et al. 2002, PAL & MATHER 2006) and RFs (CHAN & CANTERS 2007, CRAWFORD et al. 2003, LAWRENCE et al. 2006) have often been used for classification of hyperspectral data in recent years.

SVM classification of dry grassland communities was realized with the software "ImageSVM" (RABE et al. 2010), which is freely available as a part of the EnMAP-Box (www.enmap.org). In this context, a Gaussian radial basis function (RBF) kernel was used to build the SVM classification models. In order to find the optimal parameter values for C (regularization parameter) and g (Gaussian RBF kernel parameter), imageSVM uses a grid search technique based on an implementation in "libsvm" (CHANG & LIN 2001). For RF classification, the free programming language R for statistical computing and graphics was used in combination with the additional R-package "randomForest", which provides a direct implementation of BREIMAN's RF algorithm (BREIMAN 2001). For classification of the vegetation communities, each RFR model was made up of 500 individual trees. Each tree was built with two thirds of the training data randomly selected (bootstrap samples), while the remaining third (out-of-bag samples) was used for a model internal validation. At each node of a tree, only a small number of features (square root of all features) were randomly selected for decision making.

The procedure to train the classification model and apply it to aisaEAGLE image data from the test sites was the same for both classification algorithms. First, the algorithms were trained with field spectra. Then, derived models were applied to the image data to classify *dry grass-* and *heathland*. Accuracy assessment was conducted by simply verifying whether a pixel corresponding to a measured

plot in the field was classified in the right or in a wrong class. This approach of accuracy assessment could be performed because training data and classification data were independent datasets, so that a division between training and validation data was not necessary.

4 Results and Discussion

In level 1 the objective was to separate *dry grass-* and *heathland* vegetation from all other land cover classes. Just one of the 46 field plots was incorrectly masked in level 1 (overall accuracy (OAA) = 97.83%). This plot represented *healthy broom*, which at this growing stage had a very similar spectral reflectance compared to young trees. The subsequent classification of level 2 was conducted with the 45 remaining plots. For classification in level 2 the machine learning algorithms SVM and RF were used. The validation procedure was similar to level 1, except that at this point the classes of level 2 were intended to serve as reference for validation. While SVM classified 41 of the 46 plots (89.13%) correctly, with RF just 33 of the 46 plots (71.74%) were assigned to the correct class.

Tab. 1 shows results for SVM classification for the different classes at level 2. The *calluna heath* (CH) and *browse bristle* (BB) plots were all classified in the correct classes. The incorrect classified plot in the class *dry grassland* (DGL) was the *healthy broom* plot, which was already masked at level 1 and is consequently incorrect at level 2, too. The classification of the *sand pioneer corridor* (SPC) plots was more problematic compared to the other classes. Four of the 16 plots were assigned to wrong classes, mostly in the class CH.

Based on the substantially better results at level 2 for SVM compared to RF, at level 3 classification was only continued with SVM. At level 3, 34 of the 44 plots (77.27%) were classified to their corresponding classes. In this context, it has to be noted that the class *browse bristle* was not further subdivided at level 3, reducing the total number of plots to 44.

Classification accuracies at level 3 are listed in Tab. 2. The class *caluna-heath* provided the best classification result at level 3 with 11 of 13

Tab. 1: Classification results for the different classes of level 2 with SVM (DGL = dry grassland, CH = calluna-heath, SPC = sand pioneer corridor, BB = broom bristle).

Classes (level 2)	DGL	CH	SPC	BB
Result	14/15	13/13	12/16	2/2
Accuracy	93.33%	100%	75%	100%
Overall accuracy	41/46 (89.13%)			

Tab. 2: Classification results for the different classes of level 3 with SVM.

Classes (level 3)	DGL	CH	SPC
Correct/incorrect	12/15	11/13	11/16
Accuracy	80.00%	84.62%	68.75%
Overall accuracy	34/44 (77.27%)		

correctly classified plots (84.62%). *Dry grassland* also had high accuracy, at 80%, and 12 of 16 correctly assigned plots. The accuracy for the class *sand pioneer corridors* is relatively low compared to the other classes, with only 11 of 16 plots (68.75%) correctly classified.

The presented results underline that a detailed classification of *dry grass-* and *heathland* vegetation communities with hyperspectral airborne- and field data within the study area was possible. At level 1 the masking proved to be an appropriate procedure to reduce the aisaEAGLE data to *dry grass-* and *heathland* areas, which were the focus of this study. The incorrect masking of the pixel corresponding to the *healthy broom* plot could possibly be prevented if the area were classified again with data acquired at another time in the growing season, for example during the blossoming of *broom*. Under these conditions the spectral curve of *broom* should be different from young trees because of the dominance of the yellow blossoms.

The classification at level 2 showed that SVMs are more suitable than RFs for the classification of *dry grass-* and *heathland* in the study area. The reason for this could be the small number of training spectra for some classes. Foody et al. (2006) demonstrated that SVMs can handle classification problems with a small amount of training data very well because the algorithm only needs samples from the edges of the classes, the so-called “support vectors”. In contrast, RFs appear to have more

problems with the small number of training samples in the presented study. A higher number of training samples could possibly solve this problem: PAL & MATHER (2006) showed that the classification of hyperspectral data with more than 250 training samples per class provided nearly the same classification accuracies for SVM and RF. Furthermore, the out-of-bag error, which is an indicator for the robustness of a RF, was also very high, at 15.49%. This fact indicates that the algorithm RF already had problems to separate the processed ASD field spectra, and therefore no satisfactory results were expected before classification.

SVM results for level 2 underline the capability of the classification algorithm to separate different dry and heathland classes. There was only a problem with the classification of the *sand pioneer corridors*. This class was unique because it had numerous variations of nearly uncovered soils, from areas slightly covered with lichen to areas with increasing grass cover, which can be seen as a transitional stage to the class *dry grassland*. Especially here, mixed pixels in the aisaEAGLE data had a major impact on the classification accuracy. For future work, classification approaches including spectral unmixing techniques and gradient mapping could help to overcome the problem; data should also be used with a spatial resolution higher than 2 m ground sampling distance. At level 3, classification accuracy for the different classes of *dry grassland*

and *caluna-heath* was lower by more than 10% compared to level 2, whereas the accuracy for the *sand pioneer corridors* was lower only by 7%. At this level mixed pixels also became problematic for the separation of different *dry grassland* and *calluna-heath* classes, but with 80.00% and 84.62% correct classified plots accuracy was still high. Finally, Fig. 5 illustrates the classification results for an aisaEAGLE image data subset of test site B at all three levels. At level 3, no more accuracy improvement seems to be possible.

The already-mentioned spectral unmixing or new ordination techniques for vegetation mapping in a floristic continuum are promising approaches to map plants in even higher levels of detail. Especially the latter approach has already provided detailed mapping results for different types of natural vegetation (FEILHAUER et al. 2011, SCHMIDTLEIN et al. 2007,

SCHMIDTLEIN & SASSIN 2004). NEUMANN et al. (2011, 2012, 2013) also used continuous vegetation gradients in combination with multivariate regression analysis to map heterogeneous dry vegetation communities of the Döberitzer Heide, demonstrating the potential of the method with very promising results.

5 Conclusions

In the presented study, *dry grass-* and *heathland* communities of a dryland nature preserve in Germany were classified in different levels of detail on the basis of hyperspectral aisaEAGLE image data in combination with spectral field measurements. The normalization of image and field spectra before classification was proven to be a suitable method to make both datasets spectrally compara-

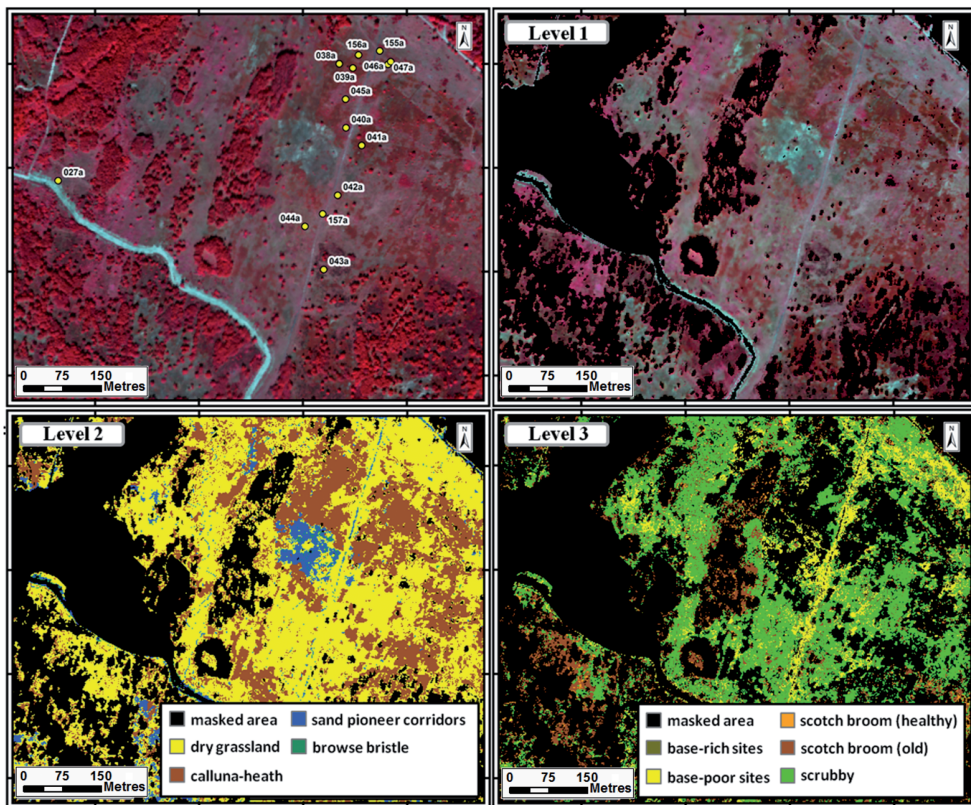


Fig. 5: Classification procedure for a subset of test site B. Top left: aisaEAGLE input image with the locations of several field plots. Top right: Masked aisaEAGLE data – level 1. Bottom left: SVM classification result – level 2. Bottom right: SVM classification result for dry grassland – level 3.

ble. The subsequent classification with the machine learning algorithms SVM (89.13% – level 2) and RF (71.74% – level 2) provided results with significantly differing classification accuracies, because SVMs can obviously deal better with training data which was not from the same source than the classification data. Therefore, the classification of the highest level of detail (level 3) was only performed with the algorithm SVM, also providing a result with relatively high classification accuracy (77.27%).

The acquired field spectral measurements of dry vegetation communities used in this study were stored in a spectral library system for the first time (*SPECTATION* www-app2.gfz-potsdam.de/spectation). This and many other spectral libraries offer open access to spectral reflectance measurements of numerous plants, soils and minerals and can be used as reference data for future classification studies in remote sensing. However, it is important that these libraries provide additional meta information about the reflectance measurements, e.g. day of acquisition, measurement conditions, for verifying their suitability for a certain classification problem. By the use of reference data from spectral libraries cost- and time intensive field campaigns to measure spectral reference data in field would no longer be necessary for every classification application.

The presented classification approach showed the potential of using field spectral reflectance measurements for the classification of hyperspectral image data with high accuracy. Furthermore, the classification procedure can easily be transferred to other classification problems where image data with high spatial resolution and suitable field reflectance measurements (possible from spectral libraries) are available.

Acknowledgements

This work was funded by the Deutsche Bundesstiftung Umwelt - DBU [26257]. We would like to thank LUP GmbH and ecostrat GmbH for providing field spectra and species composition data. The authors would especially like to thank THERES KÜSTER and KARL SEGL,

who generously supported data preprocessing. Additional thanks go to RANDOLF KLINKE und DANIEL STICH, who assisted in data collection.

References

- ARTIGAS, F.J. & YANG, J., 2006: Spectral discrimination of marsh vegetation types in the New Jersey meadowlands. – *Wetlands* **26** (1): 271–277.
- BIRGER, J., GLÄSSER, C., HERRMANN, B. & TISCHEW, S., 1998: Multisensoral and multitemporal remote sensing of ecological damage caused by open-cast lignite mining in Central Germany. – ISPRS Commission VII Symposium on Resource and Environmental Monitoring. International Archives of Photogrammetry and Remote Sensing **XXXII** (7), Budapest, Hungary.
- BRAUN, A.C., HINZ, S. & WEIDNER, U., 2010: Support Vector Machines for Vegetation Classification – A Revision. – PFG – Photogrammetrie, Fernerkundung, Geoinformation **2010** (4): 273–281.
- BREIMAN, L., 2001: Random forests. – *Machine Learning* **45** (1): 5–32.
- BROWN, D.J., 2007: Using a global VNIR soil-spectral library for local soil characterization and landscape modeling in a 2nd-order Uganda watershed. – *Geoderma* **140** (4): 444–453.
- CAMPS-VALLS, G., TUIA, D., BRUZZONE, L. & BENEDIKTSSON, J.A., 2014: Advances in Hyperspectral Image Classification: Earth monitoring with statistical learning methods. – *IEEE Signal Processing Magazine* **31** (1): 45–54.
- CHAN, J.C.W. & PAELINCKX, D., 2008: Evaluation of Random Forest and Adaboost treebased ensemble classification and spectral band selection for ecotope mapping using airborne hyperspectral imagery. – *Remote Sensing of Environment* **112** (6): 2999–3011.
- CHAN, J.C.W. & CANTERS, F., 2007: Ensemble Classifiers for Hyperspectral Classification. – 5th EARSEL Workshop on Imaging Spectroscopy, Bruges, Belgium.
- CHANG, C.C. & LIN, C.J., 2011: LIBSVM: A library for support vector machines. – *ACM Transactions on Intelligent Systems and Technology* **2** (3): 1–27.
- CRAWFORD, M.M., HAM, J., CHEN, Y. & GHOSH, J., 2003: Random forest of binary hierarchical classifiers for analysis of hyperspectral data. – IEEE Workshop on Advances in Techniques for Analysis of Remotely Sensed Data, Greenbelt, MD, USA.
- COCHRANE, M.A., 2000: Using vegetation reflectance variability for species level classification

- of hyperspectral data. – *International Journal of Remote Sensing* **21** (10): 2075–2087.
- EUROPEAN UNION, 1992: Council Directive 92/43/EEC of 21 May 1992 on the conservation of natural habitats and of wild fauna and flora. – http://ec.europa.eu/environment/nature/legislation/habitatsdirective/index_en.htm (31.3.2014).
- FAUVEL, M., TARABALKA, Y., BENEDIKTSSON, J.A., CHANUSSET, J. & TILTON, J.C., 2013: Advances in Spectral-Spatial Classification of Hyperspectral Images. – *IEEE* **101** (3): 652–675.
- FEILHAUER, H., FAUDE, U. & SCHMIDTLEIN, S., 2011: Combining Isomap ordination and imaging spectroscopy to map continuous floristic gradients in a heterogeneous landscape. – *Remote Sensing of Environment* **115** (10): 2513–2524.
- FOODY, G.M. & MATHUR, A. 2004: A relative evaluation of multiclass image classification by support vector machines. – *IEEE Transactions on Geoscience on Remote Sensing* **42** (6): 1335–1343.
- FOODY, G.M., MATHUR, A., SANCHEZ-HERNANDEZ, C. & BOYD, D.S., 2006: Training set size requirements for the classification of a specific class. – *Remote Sensing of Environment* **104** (1): 1–14.
- GUANTER, L., SEGL, K., SANG, B., ALONSO, L., KAUFMANN, H. & MORENO, J., 2009: Scene-based spectral calibration of high spectral resolution imaging spectrometers. – *Optics Express* **17** (14): 11594–11606.
- HENDL, M., 1996: Grundzüge des Klimas des Landes Brandenburg. – Berichte zur deutschen Landeskunde **70**: 435–477.
- HUANG, C., DAVIS, L.S. & TOWNSHEND, J.R.G., 2002: An assessment of support vector machines for land cover classification. – *International Journal of Remote Sensing* **23** (4): 725–749.
- KOKALY, R.F., KING, T.V.V. & LIVO, K.E., 2008: Airborne hyperspectral survey of Afghanistan 2007: flight line planning and HyMAP data collection. – USGS Afghanistan Project Product No. 186, US Geological Survey, Reston, VA, USA.
- LAWRENCE, R.L., WOOD, S.D. & SHELEY, R.L., 2006: Mapping invasive plants using hyperspectral imagery and Breiman Cutler Classifications (RandomForest). – *Remote Sensing of Environment* **100** (3): 356–362.
- LUNGA, D., PRASAD, S., CRAWFORD, M.M. & ERSOY, O., 2014: Manifold-Learning-Based Feature Extraction for Classification of Hyperspectral Data: A review of advances in manifold learning. – *IEEE Signal Processing Magazine* **31** (1): 55–66.
- MUÑOZ-MARÍ, J., BRUZZONE, L. & CAMPS-VALLS, G., 2007: A Support Vector Domain Description Approach to Supervised Classification of Remote Sensing Images. – *IEEE Transactions on Geosciences and Remote Sensing* **45** (8): 2683–2692.
- NEUMANN, C., FÖRSTER, S. & ITZEROTT, S., 2011: From field spectra to an area-wide monitoring – A case study in a dryland nature reserve in Germany. – *ESA Hyperspectral Workshop 2010*, Frascati, Italy.
- NEUMANN, C., ITZEROTT, S. & WEISS, G., 2012: The importance of spatial, spectral and temporal constraints for a hyperspectral modeling of vegetational continuum and habitat assessment parameter. – *IEEE International Geoscience and Remote Sensing Symposium, IGARSS, Munich*.
- NEUMANN, C., WEISS, G., ITZEROTT, S., KÜHLING, M., FÜRSTENOW, J., LUFT, L. & NITSCHKE, P., 2013: Entwicklung und Erprobung eines innovativen, naturschutzfachlichen Monitoringverfahrens auf der Basis von Fernerkundungsdaten am Beispiel der Döberitzer Heide, Brandenburg. – *Scientific Technical Report 13/02, Deutsches GeoForschungsZentrum GFZ*, 238.
- NIDAMANURI, R.R., GARG, P.K. & GHOSH, S.K., 2007: Development of an agricultural crops spectral library and classification of crops at cultivar level using hyperspectral data. – *Precision Agriculture* **8** (4–5): 173–185.
- NIDAMANURI, R.R. & ZBELL, B., 2011: Use of field reflectance data for crop mapping using airborne hyperspectral image. – *ISPRS Journal of Photogrammetry and Remote Sensing* **66** (5): 683–691.
- PAL, M. & MATHER, P.M., 2006: Some issues in the classification of DAIS hyperspectral data. – *International Journal of Remote Sensing* **27** (14): 2895–2916.
- RABE, A., VAN DER LINDEN, S. & HOSTERT, P., 2010: Simplifying Support Vector Machines for classification of hyperspectral imagery and selection of relevant features. – *2nd Workshop on Hyperspectral Image and Signal Processing: Evolution in Remote Sensing (WHISPERS)*, Reykjavik, Iceland.
- ROGASS, C., SPENGLER, D., BOCHOW, M., SEGL, K., LAUSCH, A., DOKTOR, D., ROESSNER, S., BEHLING, R., WETZEL, H.U. & KAUFMANN, H., 2011: Reduction of Radiometric Miscalibration-Application to Pushbroom Sensors. – *Sensors* **11** (6): 6370–6395.
- RUTSCHKE, E., 1997: Döberitzer Heide. Konzeptionen für die Bewahrung und Entwicklung eines Naturerbes in Brandenburg. – Potsdam.
- SCHMIDT, K.S. & SKIDMORE, A.K., 2003: Spectral discrimination of vegetation types in a coastal wetland. – *Remote Sensing of Environment* **85** (1): 92–108.

- SCHMIDLEIN, S. & SASSIN, J., 2004: Mapping of continuous floristic gradients in grasslands using hyperspectral imagery. – *Remote Sensing of Environment* **92** (1): 126–138.
- SCHMIDLEIN, S., ZIMMERMANN, P., SCHÜPFERLING, R. & WEISS, C., 2007: Mapping the floristic continuum: Ordination space position estimated from imaging spectroscopy. – *Journal of Vegetation Science* **18** (1): 131–140.
- SMITH, G.M. & MILTON, E.J., 1999: The use of the empirical line method to calibrate remotely sensed data to reflectance. – *International Journal of Remote Sensing* **20** (13): 2653–2662.
- SWAYZE, G.A., KOKALY, R.F., HIGGINS, C.T., CLINKENBEARD, J.P., CLARK, R.N., LOWERS, H.A. & SUTLEY, S.J., 2009: Mapping potentially asbestos-bearing rocks using imaging spectroscopy. – *Geology* **37** (8): 763–766.
- TUKEY, J.W., 1977: *Exploratory Data Analysis*. – 688 p., Addison Wesley, Reading, MA, USA.
- ZOMER, R.J., TRABUCCO, A. & USTIN, S.L., 2009: Building spectral libraries for wetlands land cover classification and hyperspectral remote sensing. – *Journal of Environmental Management* **90** (7): 2170–2177.

Addresses of the Authors:

Dipl. Geographer BASTIAN SIEGMANN, University of Osnabrück, Institute for Geoinformatics and Remote Sensing, Barbarastraße 22b, D-49076, Osnabrück, Tel.: +49-541-969-3930, e-mail: bsiegmann@igf.uos.de

Prof. Dr. CORNELIA GLÄSSER, Martin-Luther-University Halle-Wittenberg, Institute for Geosciences, Von-Seckendorff-Platz 4, D-06120 Halle (Saale), e-mail: cornelia.glaesser@geo.uni-halle.de

Dr. SIBYLLE ITZEROTT & Dipl. Geoecologist CARSTEN NEUMANN, Helmholtz Centre Potsdam, German Research Centre for Geosciences GFZ, Section 1.4 – Remote Sensing, Telegrafenberg, D-14473 Potsdam, e-mail: {sibylle.itzerott} {carsten.neumann}@gfz-potsdam.de

Manuskript eingereicht: April 2014

Angenommen: September 2014





Spatiotemporally Varying Relationships between Urban Growth Patterns and Driving Factors in Xuzhou City, China

CHENG LI, NGUYEN XUAN THINH & JIE ZHAO, Dortmund

Keywords: remote sensing, urban growth patterns, spatial metrics, geographically weighted regression, spatiotemporal heterogeneity

Summary: Urban spatial patterns are usually affected by different factors in urbanization processes. Scientific interpretations of the effects of underlying determinants of spatial patterns are important for a better understanding of urban developments. However, only few studies have quantitatively examined the spatiotemporal relationships between spatial patterns and driving factors. This study explores the use of remote sensing (RS), spatial metrics and geographically weighted regression (GWR), with a case study in Xuzhou city, China, to analyse the spatial patterns of urban growth as well as their spatiotemporally varying relationships with three driving factors (1) slope, (2) distance to major urban centres, and (3) distance to major roads. The historical urban growth from 1990 to 2010 was derived from multi-temporal remote sensing images. Spatial metrics were used to quantify the urban growth patterns for different periods. The effects of the factors on urban growth patterns were further investigated using GWR. The results indicate that the spatial patterns of Xuzhou have significantly changed along the urbanization process. GWR performs better than ordinary least squares (OLS) in interpreting the relationships indicated by higher adjusted R^2 , lower corrected Akaike information criterion (AICc) values and reduced spatial autocorrelations of residuals. The parameters of the driving factors obtained from GWR indicate that their effects on spatial patterns are spatiotemporally varying. The findings help in better understanding the effects of the considered factors on spatial patterns, as well as to provide support for urban planning and management.

Zusammenfassung: Raumzeitliche Beziehungen zwischen Einflussfaktoren und Stadtwachstum in Xuzhou City, China. Unterschiedliche Faktoren beeinflussen städtische Flächennutzungsmuster im Urbanisierungsprozess. Gesicherte Erkenntnisse über Einflussfaktoren der Flächeninanspruchnahme sind wichtig für die Stadtentwicklungsplanung. Unser Beitrag beschreibt die Klassifizierung der Flächennutzung der chinesischen Stadt Xuzhou in fünf Flächennutzungarten anhand der Landsat-Bilder für die drei Zeitpunkte 1990, 2001 und 2010, die anschließende Berechnung von raumstrukturellen Indizes (Class Area, Number of Patches, Mean Shape Index, Largest Patch Index, Area Weighted Mean Euclidean Nearest Neighbour Distance, Edge Density) und die Untersuchung der raumzeitlichen Beziehungen zwischen den drei ersten Kennzahlen und drei treibenden Faktoren der Flächennutzungsänderungen: (1) Steigung, (2) Entfernung zu urbanen Zentren, und (3) Entfernung zu Hauptstraßen. Die Herausarbeitung der raumzeitlichen Beziehungen erfolgt unter Einsatz der geografisch gewichteten Regression (Geographically Weighted Regression, GWR) und der Methode der kleinsten Quadrate (Ordinary Least Squares, OLS), wobei GWR die Zusammenhänge zwischen den genannten Faktoren und Indizes besser erklärt als OLS. Die GWR-Ergebnisse belegen, dass der Einfluss der Faktoren auf das Raummuster räumlich und zeitlich variiert. Dies gilt es bei künftigen Stadtentwicklungen zu beachten.

1 Introduction

Urbanization has been a universal and important social and economic phenomenon taking place all around the world (DENG et al. 2009). During the past decades, urban growth has been accelerating with the significant increase in urban population, and this process is expected to continue to be one of the crucial issues of global change in the future, especially in less developed regions (SUI & ZENG 2001). Urbanization alters the spatial structure of land use within a region (JENERETTE & WU 2001), which has resulted in a series of environmental problems such as the loss of natural vegetation, loss of open spaces, appearance of heat island effect, and general decline in the spatial extent and connectivity of wetlands and wildlife habitat, which threaten sustainable urban development (GAO & LIU 2010).

Recently, the efforts to understand spatial patterns and mechanisms, and the effects of urbanization have been highlighted. Here the analysis of spatial patterns can help to better understand the urban growth process and to make policy decisions (DIETZEL 2005, SCHWARZ 2010, THINH et al. 2002). Studies on the qualitative relationships between urbanization and spatial growth patterns have demonstrated that human induced factors play an important role in urban growth patterns (DENG et al. 2009, KONG & NAKAGOSHI 2006, WENG 2007). Most of them, however, only focused on describing the characteristics of spatial patterns and their relationships with underlying determinants for the whole study area, and failed to address the spatial heterogeneities in the effects of driving factors on spatial patterns in response to urbanization. In addition, analyzing the change of spatial patterns for one period would overlook the fact that an area experiencing the most intense urbanization is not necessarily static, but could shift its location within the urbanization process, so that the characteristics of urbanization process cannot be fully captured. In order to address these gaps in previous studies and to effectively capture and analyze the urbanization process, it is necessary to explore the quantitative relationships between urban growth patterns and driving factors while taking into

account the spatiotemporal dynamics of driving factors.

Satellite imagery is the most common data source for detection, quantification and mapping of land cover change patterns (YUAN et al. 2005). It provides a cost and time effective tool for obtaining great amounts of multi-temporal information on the geographic distribution of land cover (DEWAN & YAMAGUCHI 2009). Spatial metrics are widely used to quantify the pattern of an urban area by computing them directly from thematic maps (HEROLD et al. 2005). The temporal variations of spatial metrics have a potential to improve the levels of interpretation and assessment of urbanization processes and thus to contribute to a better understanding of spatial pattern changes, as well as of potential impacts on the environment and ecosystem (DIETZEL et al. 2005).

Geographically weighted regression (GWR) has been developed and widely used to explore spatially varying relationships (BRUNSDON et al. 1996, FOTHERINGHAM et al. 2001). Local rather than global parameters can be estimated for analyzing the spatial dynamics of effects of driving factors on urban patterns.

This study aims at enhancing the understanding of urban growth patterns and the spatiotemporally varying effects of the driving factors on urban growth patterns through the integration of remote sensing, spatial metrics, and GWR, with a case study of Xuzhou city in China. For this purpose multi-temporal land cover data is derived from remote sensing images. A set of selected spatial metrics is computed for the detailed analysis of urban growth patterns and to improve the representation of urban spatial characteristics. GWR methods have been developed to investigate spatiotemporally varying relationships between urban growth patterns and their related factors.

2 Material and Methods

2.1 Study Area and Data

Xuzhou city in China is located in eastern part of China (Fig. 1), in the plains of Yellow River and Huaihe River, with an administrative area of 11,258 km². It is regarded as a medium-sized metropolitan area in comparison to oth-

er cities in China. Xuzhou city is composed of five districts (Quanshan, Gulou, Yunlong, Jiawang and Tongshan), in which the first three districts are viewed as the city core. Main land cover types are built-up land, farmland, vegetation, and water body. The study area covers the main urban area of Xuzhou city and suburban fringe, with the area of around 2,897 km² and the population of over 3 million inhabitants in 2010.

In this research Landsat images for 1990, 2001 and 2010 were obtained from the U.S. Geological Survey (USGS) and used for land cover classification. It is widely acknowledged that spatial pattern analysis is sensitive to the spatial resolution of the image data used for mapping (WENG 2007, WU 2004). In this study, small urban patches (smaller than 900 m²) could not be recognized in Landsat data with the spatial resolution of 30 m. This leads to the underestimation of the amount of urban patches and total areas. In addition, the mixed pixel problem, caused by medium resolution, contributes to the low accuracy of the classification results, hereby, affecting the spatial metrics values. However, the settlements in urban fringes of Xuzhou city are typically small-sized but numerous. These settlements are not important to study, but could cause

noises in analyzing the urban spatial patterns. By employing the medium resolution Landsat data, this noise can be avoided. Therefore, the spatial resolution of Landsat data seems quite suitable to analyze the urban spatial patterns in this study.

Before the classification process, an atmospheric correction technique called cosine of the sun zenith angle (COST) was applied (CHAVEZ 1988). After the atmospheric correction, all images were georeferenced using well distributed ground control points (GCPs) and topographic maps. A second order polynomial was applied, resulting in root-mean-square errors (RMSE) less than 0.75 pixels. The images were resampled to a pixel size of 30 m × 30 m using the nearest neighbour algorithm to maintain the radiometric properties of the original data. The image processing was performed using ERDAS IMAGINE 2011 software.

A digital elevation model (DEM) at a spatial resolution of 30 m, acquired from the global land cover facility (GLCF), was used to represent topography. Slope gradients were derived from the elevation surface. The major road networks (1990, 2000, and 2010) were collected from Xuzhou Urban Planning Bureau for the further analysis.

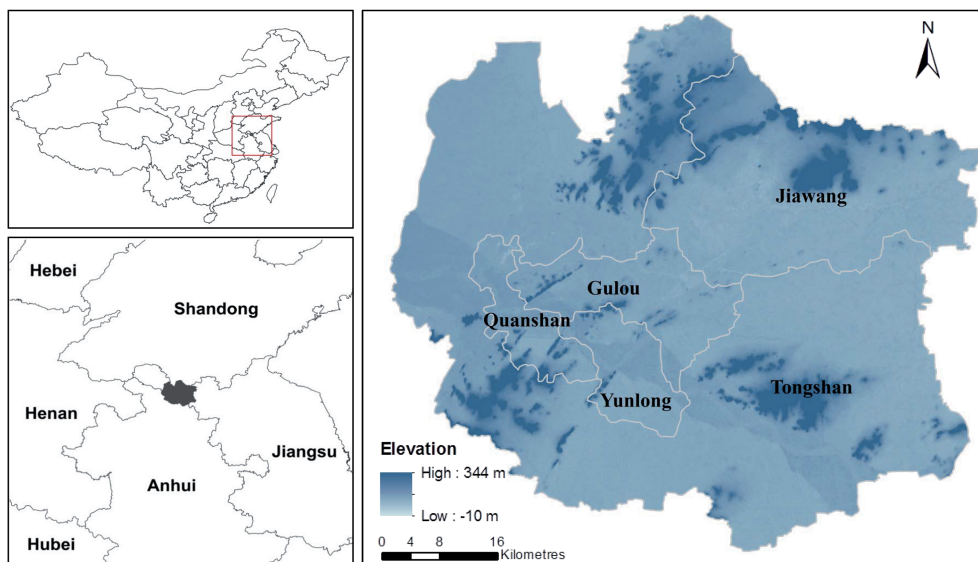


Fig. 1: The study area.

2.2 Land Cover Classification

A maximum likelihood classifier (MLC) was selected to classify the Landsat images into four categories: built-up land, farmland, vegetation and water body. Post classification refinement was used to improve the accuracy of the classification. For this study, farmland was not expected to be found in areas with slopes higher than 10 degree. Therefore, the farmland pixels with slopes higher than 10 degree were reclassified as vegetation. The tasseled cap transformation (TCT) is a conversion of the original bands of an image into a new set of bands with defined interpretations that are useful for vegetation mapping (DYMOND et al. 2002, LI & THINH 2013). The built-up and bare soil areas have higher values compared with other classes in the brightness band. In the greenness band the built-up land has lower values, whereas the areas covered by green vegetation have higher values. In the wetness band the water bodies have higher values. Therefore, we defined specific thresholds to distinguish different classes in each band

generated by TCT. In addition, a 3×3 majority filter was applied to remove salt and pepper appearances in the images.

In order to check whether the results are suitable for the spatial pattern analysis, an error matrix was calculated to assess the accuracy of the classification. The set of necessary reference data included topographic maps and field survey data. A total of 300 random points generated by stratified random sampling method were adopted to assess classification accuracy. Finally, the classified data and reference data were compared and statistically represented in the error matrix.

2.3 Spatial Patterns Analysis

Tab. 1 provides a description of the spatial metrics used in the study. The selection of the metrics was based on the research objective and their values in representing specific spatial characteristics as explored in previous studies on urban areas (HEROLD et al. 2005, LUCK & WU 2002, SCHWARZ 2010). SHAPE_AM was

Tab. 1: Description of the spatial metrics used in this study (McGARIGAL et al. 2012).

Spatial metrics	Abbreviation	Description
Class area	CA	The sum area (m^2) of all urban land use patches, divided by 10,000.
Number of patches	NP	Total number of urban patches.
Largest patch index	LPI	The percentage of the area of the largest urban patch to the total area of the investigation.
Edge density	ED	The ratio of total edge of urban patches to total landscape area.
Shape index (Area weighted mean shape index/Mean shape index)	SHAPE (SHAPE_AM/ SHAPE_MN)	The index describes the complexity of the patch shape. It uses patch area as a weighting factor. It equals 1 if the patch has a square shape and increases as the irregularity of the shape increases. SHAPE_AM averages the shape index of the patches by weighting patch area so that larger patches weigh more than smaller patches. SHAPE_MN equals the sum of shape index of the patches divided by the number of patches of the same type.
Euclidean nearest-neighbour distance (Area weighted mean Euclidean nearest-neighbour distance)	ENN (ENN_AM)	ENN equals the distance (m) to the nearest neighbouring patch of the same type, based on shortest edge-edge distance. ENN_AM averages the ENN index of the patches by weighting with the patch area size.

used for the general description of the urbanization pattern in order to improve the measure of class patch fragmentation as the structure of smaller patches is often determined more by the image pixel size than by characteristics of natural or manmade features found in the landscape (MILNE 1991). The higher the value of the ENN (Euclidean nearest neighbour), the greater is the isolation of the patches. In order to consider the different influence of patches according to the areas, ENN_AM is calculated by incorporating patch area size weighting. Since the study focuses on urban growth, the land cover maps were reclassified into two classes: urban and non-urban. Built-up was defined as urban land, while farmland, vegetation and water body were reclassified into non-urban land. The spatial metrics associated with sustainability were calculated using Fragstats 4 (McGARIGAL et al. 2012).

2.4 Variables Calculation

Investigation of the relationships between urban growth patterns and their related factors were performed on a block basis. The square block, the most commonly used shape for spatial pattern analysis (LUCK & WU 2002, WENG 2007), was applied in this study. A preliminary test of the effects of block size on spatial pattern analysis was carried out considering sizes of 1 km, 2 km, 3 km and 5 km. A block size of 2 km was chosen because it retains more details of the spatial pattern than a larger block size does. A block size of 1 km could lead to the situation that no urban patch or only a few urban patches exist in some blocks, which generates noise in the spatial pattern analysis. Therefore, the study area was firstly divided into several square blocks of $2\text{ km} \times 2\text{ km}$. The selected metrics (CA, NP, SHAPE_MN in Tab. 1) being suitable at local level, were then calculated for each block to measure the urbanization intensity, fragmentation and irregularity of urban area. After obtaining metrics values for the 1990, 2001 and 2010 data, the changes of metrics were calculated for each block.

Urban growth patterns are the result of the complex interaction of physical, environmental and socioeconomic factors. Slope has been

considered as a major factor in several studies on land use change (ASPINALL 2004, DUBOVYK et al. 2011, HE et al. 2006, HU & LO 2007, LI et al. 2013, SUI & ZENG 2001). Slope can speed up or slow down the process of urban development as the costs of land development can increase as the slope increases (ASPINALL 2004). Socioeconomic development is one of the most important driving factor of urban growth patterns and can best be characterized by the access that a location has to important facilities (HE et al. 2006, LI et al. 2013, VERBURG et al. 2004). The significant effects of distance to major urban centres on urban growth patterns have been confirmed by several studies (ASPINALL 2004, BATISANI & YARNAL, 2009, CHENG & MASSER 2003, DUBOVYK et al. 2011, HU & LO 2007, LI et al. 2013, LONG et al. 2012, REILLY et al. 2009, SUI & ZENG 2001, VERBURG et al. 2004). Transportation plays an indispensable part in urban patterns because a good transportation increases the accessibility of land and decreases the cost of construction (REILLY et al. 2009). Therefore, distance to major roads has been used as a driving factor by many researchers (CHENG & MASSER 2003, DUBOVYK et al. 2011, HE et al. 2006, HU & LO 2007, LI et al. 2013, LONG et al. 2012, REILLY et al. 2009, SUI & ZENG 2001, VERBURG et al. 2004). In this study, distance to major urban centres (abbreviation: Dis2urban) and distance to major roads (abbreviation: Dis2road) were used to represent socioeconomic factors. The gross domestic product (GDP) and population were not considered as their spatial resolutions are much coarser than that of other variables used in this study.

Coefficients could be misleading, if the underlying variables are measured in different units. For comparing the impacts of different variables on the urban spatial patterns, a linear membership function method was adopted to implement the standardization. The variable with the highest value was assigned 1, and the lowest value was assigned 0.

2.5 Geographically Weighted Regression

GWR is an extension of global regression method such as OLS (ordinary least squares),

and can be used to explore the spatially varying relationships between explanatory variables and spatial patterns by generating a set of local-specific coefficients (BRUNSDON et al. 1996, FOTHERINGHAM et al. 1996, FOTHERINGHAM et al. 2001). In contrast to traditional regression method, GWR is conducted using localized points within geographic space. Thus, instead of producing a single average parameter for each relationship, GWR has a potential to produce a set of local parameters that can be mapped to get insight into hidden possible causes of this pattern.

The GWR model can be expressed as:

$$y_i = a_0(\mu_i, v_i) + \sum_k a_k(\mu_i, v_i)x_{ik} + \varepsilon_i \quad (1)$$

Where (μ_i, v_i) represents the coordinate location of the i^{th} point. $a_0(\mu_i, v_i)$ and $a_k(\mu_i, v_i)$ express the intercept and local parameter estimate for an independent variable x_{ik} at location i , respectively. ε_i is the random error term for location i .

In GWR, the parameters for each observation at location i can be estimated by weighting all observations around a specific point i according to their spatial proximity, which is calculated by the Euclidean distance in this study. The observations which are spatially closer to the location i will have a greater impact on the local parameters for the location than those which originate at more distant points. Gaussian distance decay can be used to express the weighting function:

$$w_{ij} = \exp\left(-\frac{d_{ij}^2}{h^2}\right) \quad (2)$$

Where w_{ij} represents the weight of observation j for location i . d_{ij} is the Euclidean distance between points i and j . h is a kernel bandwidth that affects the distance-decay of the weighting function. There are three choices of the bandwidth method: corrected Akaike information criterion (AICc), cross validation (CV) and bandwidth parameter. If the bandwidth is known a priori, bandwidth parameter could be applied. If it is unknown, the first two types allow for using an automatic method to find the optimum bandwidth. In this study, the AICc method was used for the GWR model. The AICc method finds the bandwidth which

minimises the AICc value: the model with lowest AICc values suggests a stronger ability of a regression model in reflecting reality.

For the comparison purpose, we also employed OLS models to investigate the relationships between spatial patterns and explanatory factors. Three statistical parameters were used to compare the performance between GWR and OLS: adjusted R^2 , AICc, and Moran's I. Adjusted R^2 and AICc measures provide some indications of the goodness of fit of the corresponding model. Higher adjusted R^2 values indicate that more variances can be explained for dependent variables. Moran's I is widely used as an indicator of spatial autocorrelation (range: -1 to 1). Large absolute values of Moran's I indicate that spatial autocorrelation is more significant. Residuals are the differences between observed and predicted values. We employed Moran's I value to examine spatial autocorrelation in the residuals.

3 Results

3.1 Spatial Patterns Analysis

The overall accuracies calculated for 1990, 2001, and 2010 were 86.4%, 87.7%, and 88.3%, respectively (Tab. 2). Urban landscape is a complex combination of different land covers. In this study, mixed pixel problems were found between built-up land and vegetation categories. In addition, some farmlands without crop were misclassified as built-up due to their spectral similarities. The producer's and user's accuracy of built-up land cover are consistently high, ranging from 85.0% to 88.7% and meet the minimum USGS total accuracy set out by ANDERSON et al. (1976). Hence, the classified results are considered suitable as data source for spatial pattern analysis. The multi-temporal land cover classification maps for Xuzhou city are shown in Fig. 2.

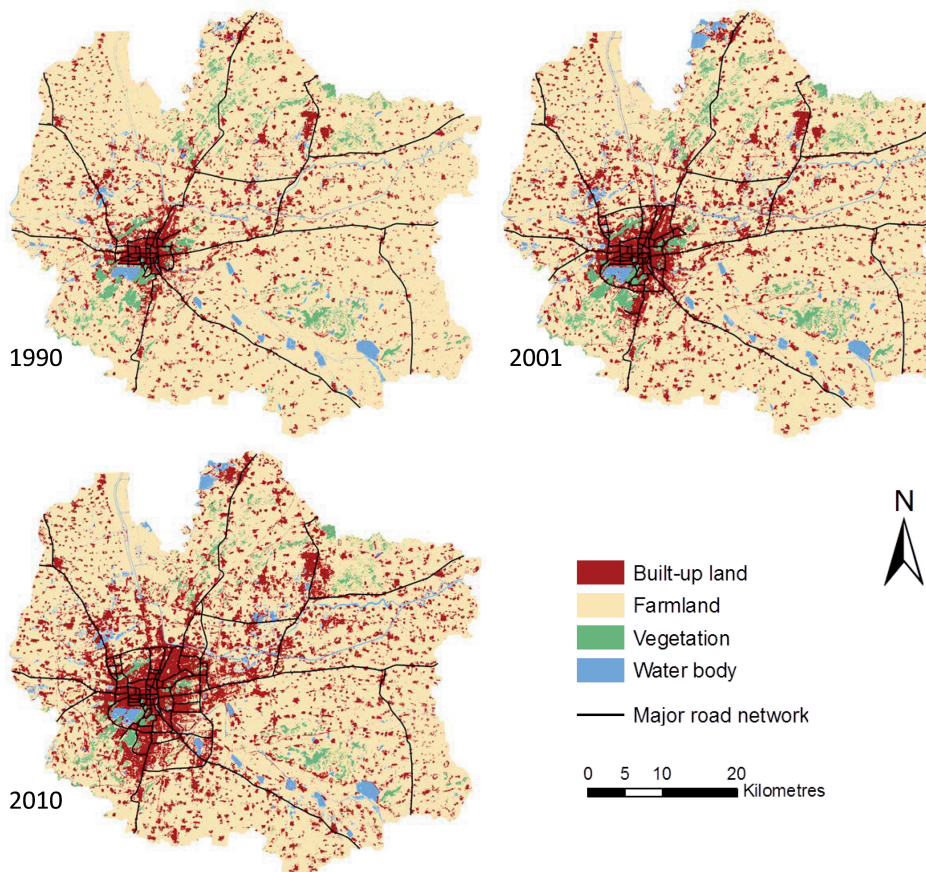
Tab. 3 presents spatial metrics values from 1990 to 2010. The CA value of Xuzhou city shows a rapid urbanization process between 1990 and 2010 (see also Fig. 2). The allocation of urban area included both the developing outward from the original city core and the growth of new individual urban patches, which is illustrated by the increases in both

Tab. 2: Summary of Landsat classification accuracies (%) for 1990, 2001, and 2010.

Land cover class	1990		2001		2010	
	Producer's	User's	Producer's	User's	Producer's	User's
Built-up	85.0	87.9	87.1	85.7	88.7	87.5
Farmland	89.0	85.8	90.2	87.5	89.1	89.8
Vegetation	79.2	82.4	81.8	88.2	81.1	86.0
Water body	88.2	90.0	88.2	90.0	93.6	88.0
Overall accuracy	86.4		87.7		88.3	

Tab. 3: Spatial metrics derived from the land cover classification maps.

Date	CA	NP	LPI	ED	SHAPE_AM	ENN_AM
1990	27636	2345	1.8253	12.7665	3.4157	297.0055
2001	38559	2412	3.7846	15.4546	5.2129	275.0119
2010	54938	2509	7.0688	19.5735	8.4627	246.3587

**Fig. 2:** Multiple temporal land cover classification maps.

metrics: LPI and NP. The development of new individual urban patches created more edges, which leads to the increase in ED value. Some individual urban patches continued to grow together to form larger patches, the connection of individual urban patches increased, according to the decreasing ENN_AM value. It also implies the significant loss of open space

between urban patches. As the increasing rapid urbanization process, Xuzhou's irregular and fragmented growth is illustrated by the continuous increasing of SHAPE_AM, NP, and ED.

Changes of spatial metrics across the study area are shown in Fig. 3. The variations of spatial metrics show spatiotemporal heterogenei-

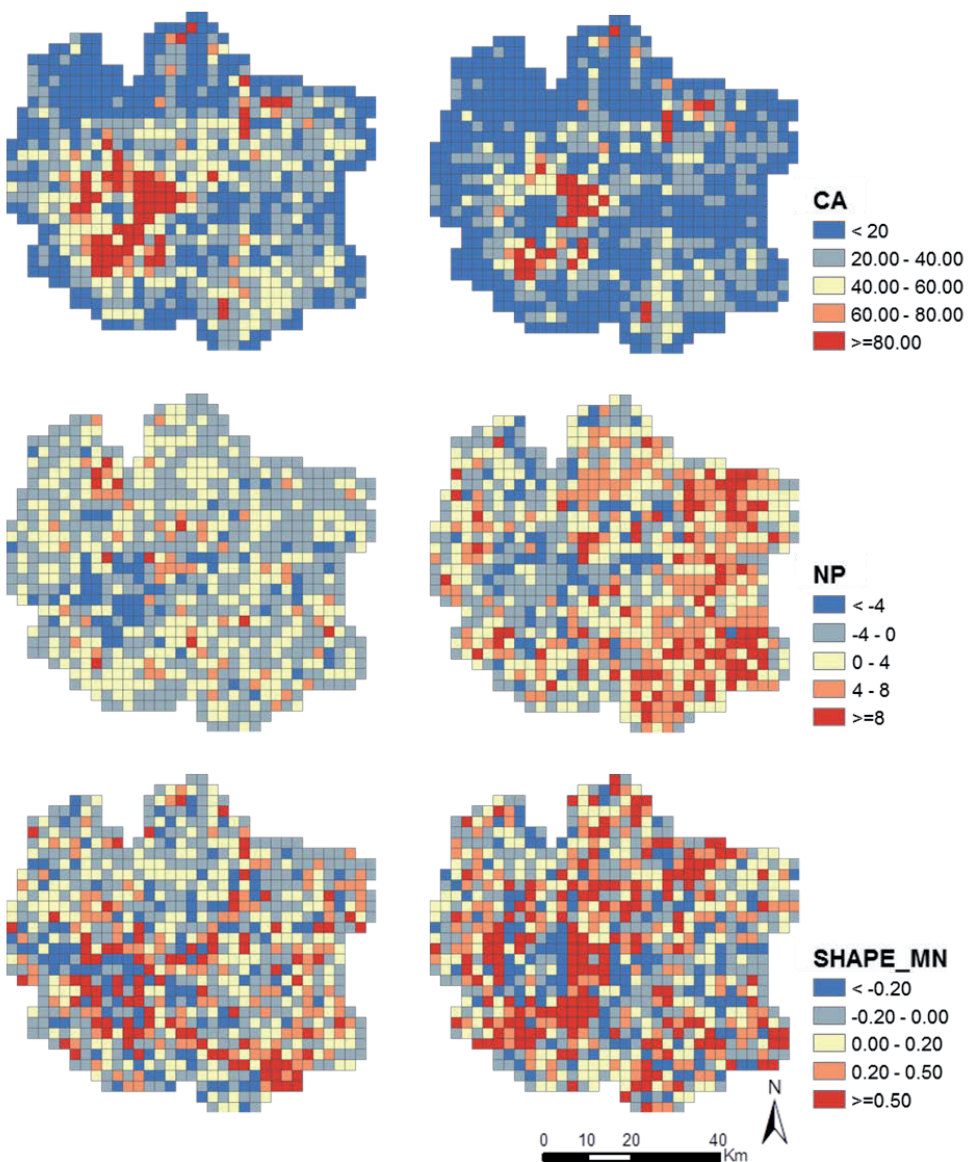


Fig. 3: Changes of spatial metrics selected in this study for 1990 – 2001 (left column) and 2001 – 2010 (right column) (CA = class area, NP = number of patches, SHAPE_MN = mean shape index).

ties. Moreover, the variations of spatial patterns can, in considerable parts, be explained by selected factors. For example, most of the blocks with significant growth of CA values are found around the city core, and the significant decrease of NP values are also observed around the city core.

3.2 Comparison between OLS and GWR Models

OLS models only provide one statistical average parameter for the whole study area, whereas the GWR results show variables changes throughout the study area. The adjusted R² and AICc values generated by GWR and

Tab. 4: Comparison of adjusted R² between GWR and OLS for two periods.

		1990 – 2001			2001 – 2010		
		CA	NP	SHAPE_MN	CA	NP	SHAPE_MN
Dis2urban	Adjusted R ² G	0.523	0.443	0.470	0.474	0.466	0.449
	Adjusted R ² O	0.136	0.175	0.101	0.119	0.079	0.047
Dis2road	Adjusted R ² G	0.560	0.566	0.525	0.463	0.444	0.427
	Adjusted R ² O	0.099	0.057	0.075	0.002	0.007	0.001
slope	Adjusted R ² G	0.509	0.349	0.581	0.461	0.474	0.423
	Adjusted R ² O	0.114	0.017	0.107	0.050	0.012	0.025

R²G is the R² for GWR model; R²O is the R² for OLS model.

Tab. 5: Comparison of AICc between GWR and OLS for two periods.

		1990 – 2001			2001 – 2010		
		CA	NP	SHAPE_MN	CA	NP	SHAPE_MN
Dis2urban	AICcG	6182.2	3957.6	4735.5	7388.5	5128.9	6003.2
	AICcO	6590.6	4064.8	4888.0	7804.5	5541.6	6317.0
Dis2road	AICcG	6170.3	3949.2	4771.1	7403.9	5144.4	6022.2
	AICcO	6622.5	4051.4	4901.5	7804.0	5536.4	6360.5
slope	AICcG	6256.6	3981.7	4812.9	7408.5	5124.5	6030.0
	AICcO	6703.4	4089.5	4901.7	7802.0	5532.3	6340.3

AICcG is the AICc for GWR model; AICcO is the AICc for OLS model.

Tab. 6: Comparison of Moran's I of residuals between GWR and OLS for two periods.

		1990 – 2001			2001 – 2010		
		CA	NP	SHAPE_MN	CA	NP	SHAPE_MN
Dis2urban	Moran's IG	0.175	0.071	0.189	0.054	0.044	0.012
	Moran's IO	0.402	0.258	0.396	0.517	0.550	0.436
Dis2road	Moran's IG	0.095	0.012	0.119	0.069	0.081	0.013
	Moran's IO	0.578	0.390	0.560	0.518	0.544	0.435
slope	Moran's IG	0.120	0.147	0.048	0.073	0.053	0.027
	Moran's IO	0.611	0.421	0.589	0.505	0.547	0.435

Moran's IG is the Moran's I for GWR model; Moran's IO is the Moran's I for OLS model.

OLS models for different periods are shown in Tabs. 4 and 5. For all cases in the different periods, the GWR results are characterized by higher R^2 and lower AICc values compared to the corresponding OLS models. The comparison of these two indicators suggests that GWR models perform better than OLS models in investigating the relationships between urban spatial patterns and related factors. The results obtained from GWR indicate that the variations of selected spatial metrics are significantly associated with the explanatory factors.

Moreover, Tab. 6 summarizes the Moran's I statistics on the models residuals from GWR and OLS. Significant positive spatial autocorrelations are found in all OLS models, which are characterized by higher Moran's I values ranging from 0.258 to 0.611. In contrast, the Moran's I values of GWR models range from 0.012 to 0.189. This indicates that GWR models can improve the expressiveness of relationships by effectively reducing spatial autocorrelations in residuals.

3.3 Spatiotemporal Heterogeneity of Relationships between Spatial Patterns and Driving Factors

The GWR model generated a set of parameters for the blocks for each period, which can be used to analyse the spatiotemporally varying effects of the driving factors on urban growth patterns (Figs. 4–6).

Clear relationships between the variations of CA values and three driving factors can be identified (Fig. 4). Dis2urban and Dis2road showed significant negative correlations with the variations of CA near the city core and roads for the period of 1990–2001. It suggests that greater urbanization intensity was strongly related to shorter distance to major urban centres and roads within a certain extent, with stronger explanatory power indicated by local R^2 . However, the effects of these factors decreased or transformed to positive influence when extending to a certain distance. Slope is also an important factor that can explain more than 30% of the variations of CA outside the city core, whilst it explained less in the city core. Compared to the former period, Dis2ur-

ban and Dis2road had positive effects on CA values in a larger area in 2001–2010. Furthermore, significant positive influence was found in the area around the city core and roads. This indicates that the rise in distance to centres and roads up to a certain extent can cause

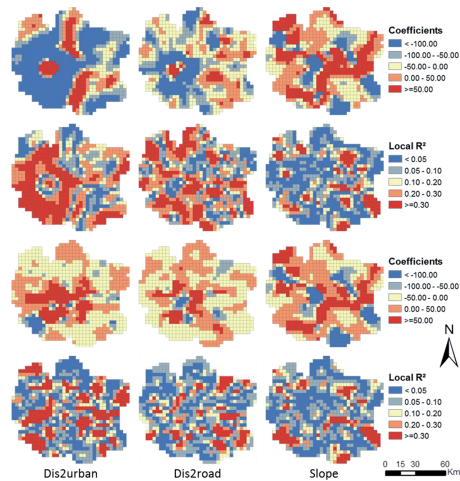


Fig. 4: Spatial distributions of the coefficients and local R^2 for CA. Figures in the two upper rows show the results for 1990–2001 and figures in the two lower rows show the results for 2001–2010 (CA = class area, NP = number of patches, SHAPE_MN = mean shape index).

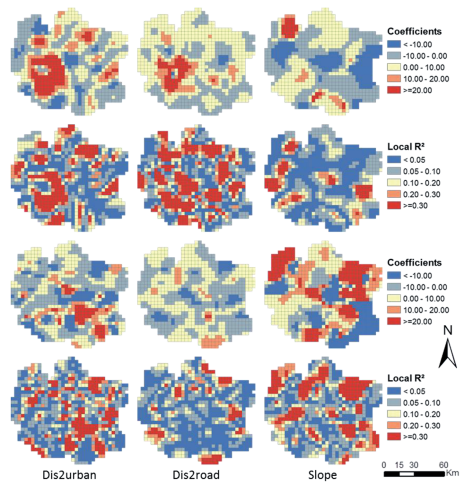


Fig. 5: Spatial distributions of the coefficients and local R^2 for NP. Figures in the two upper rows show the results for 1990–2001 and figures in the two lower rows show the results for 2001–2010.

a considerable increase in urbanization intensity. The effects of slope on the variations of CA were similar to the former period.

Fig. 5 exhibits both, the positive and negative correlation between the variations of NP and the explanatory factors. In 1990 – 2001, stronger effects of Dis2urban on the variations of NP as well as higher local R^2 were located around the city core, while negative and weaker relationships and lower local R^2 values were found outside the city core. Dis2road had a similar effect on the variations of NP values. The results indicate that the increase in distance to urban centres and roads can lead to more fragmented pattern. Compared to other factors, slope had less significant influence on the fragmentation (lower adjusted R^2 and local R^2 , Tab. 2). For the period 2001 – 2010, an increase in distance to the new urban centre had a direct influence on the variations in NP values, whilst weaker correlations with Dis2urban were found around the former city core in 2001 – 2010. Dis2road had a weaker impact on the variations in NP values, according to the coefficients and local R^2 . In contrast to the weaker effect of slope in the former period, both significant positive and negative effects were observed in 2001 – 2010. The variations of NP in areas with higher slope received more

significant impact from the factor of slope, where the effects of road and urban centres could almost be neglected.

The spatially varying relationships between the SHAPE_MN values and the three explanatory factors were identified through the GWR model (Fig. 6). A more significant effect of Dis2urban on the variations of SHAPE_MN value concentrated on the city core during 1990 – 2001. The influence varied significantly from positive to negative, if distance to urban centres increases. The roads around the city core also had a significant positive effect on the variations of SHAPE_MN and higher local R^2 . This implies that the irregularity pattern received more significant impacts from these two factors in highly urbanized areas than in less-urbanized areas. Relatively weak correlation with slope and higher local R^2 values can be observed in areas far from the city core, which suggests that the irregularity was more strongly influenced by slope outside of the city core. Compared to the previous period, the relationships between explanatory factors and the variations of SHAPE_MN value varied in 2001 – 2010. In particular, Dis2urban had a stronger influence in suburban areas than in the city core. The distance to major roads presented a significant negative effect on the variations of SHAPE_MN value in the eastern part of the city core with higher local R^2 . The decrease in distance to major roads in this area could cause more irregular patterns. The effects of slope in 2001 – 2010 also varied from positive to negative across space.

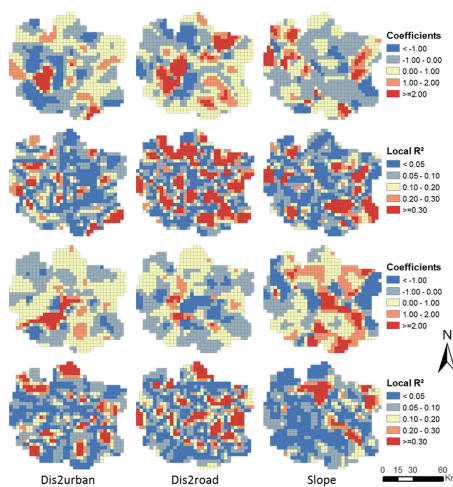


Fig. 6: Spatial distributions of the coefficients and local R^2 for SHAPE_MN. Figures in the two upper rows show the results for 1990 – 2001 and figures in the two lower rows show the results for 2001 – 2010.

4 Discussion and Conclusion

4.1 Spatiotemporally Varying Relationships between Urban Growth Patterns and Explanatory Factors

The study suggests that the historical urban growth patterns in Xuzhou city can, in considerable parts, be affected by distance to urban centres, distance to major roads and slope with relatively high levels of explanation of the spatial variability. This corresponds with the findings in literature related to other cities in the world (BRAIMOH & ONISHI 2007, CLARKE

et al. 1997, WENG 2007). Our research extends these previous studies by investigating spatiotemporally varying effects of related factors instead of global effects.

Overall, significant correlations were found around the city core and around major roads. This can be linked with the attraction due to locations closer to the urban centres or roads offering more opportunities to access socio-economic resources. In the city core, the landscape is dominated by a well-connected matrix of built-up land, whereas the expanded built-up areas on the edge of town are always highly fragmented and complex in shape (SOLON 2009, WENG 2007). Some unexpected local relationships were also identified by GWR. For example, significant positive influence of slope on urban growth was observed around highly urbanized areas. This can be explained by the shortage of land for development around existing highly urbanized areas.

Furthermore, temporal changes of the effects of driving factors were also assessed in this study. The effects of Dis2urban on the variations of CA varied from negative to positive over the study period, which can be explained by the socioeconomic processes and the consequence of urban development policy. In the first period, urbanization mainly occurred in the city core. Due to the lack of space for further development in the city core, the edges of the town were those places where rapid urbanization occurred in 2001 – 2010. As a result, the influences of related factors on fragmentation and irregularity also varied significantly over time in the city core, because the degree of landscape fragmentation and irregularity gradually decreased when urban use became dominant in city core. In addition, the urban growth was focused more on the development of new urban centres to form a polycentric development pattern in the period of 2001 – 2010.

4.2 Methodological Implications

One of the crucial findings in the study is the use of GWR model, which enables to analyse the spatial variability of results. Urban growth patterns and the effects of their causal factors are usually location-dependent and

auto-correlated (GAO & LI 2011). Therefore, the way of how causal factors affect the urban growth patterns differently across space should be addressed. However, many studies examined pattern-process relationships using the global relationship estimated over the entire study area (WENG 2007, BATISANI & YARNAL 2009). Consequently, spatially varying effects of driving factors on spatial patterns are lost. The use of GWR model includes a spatial component in its specifications. This indicates that the coefficients estimated for this regression vary according to the geographical location. The results show that GWR models can provide detailed information about the different roles of related factors in different parts of the study area, rather than generating an average coefficient for the entire area.

4.3 Implications for Urban Planning and Management

The temporal analysis of spatial metrics in Xuzhou city throughout the study period revealed that urbanization not only dramatically increased the size of the built-up areas, but that the urban area became also fragmented and irregular. Fragmented and irregular development patterns are associated with ecological and environmental problems, which threaten the sustainable development (JENKS et al. 1996). Therefore, some related plans and measures should be implemented to facilitate connectivity between built-up fragments instead of random development. Furthermore, the positive effect of slope on urban expansion which has been found in some areas, suggests an increasing pressure for development in the mountainous areas which in turn are regarded as ecologically valuable zones. Therefore, the implementation of policies for protecting such ecologically valuable zones is required.

4.4 Outlook

Although some successful results have been obtained, challenges lie ahead. Firstly, different block shape and size can result in different explanatory ability of models. Notwithstanding preliminary tests were conducted, further

studies need to be carried out to consider the different block shape and size in order to obtain insight into their effects on spatial pattern analysis. Secondly, three spatial variables were incorporated to analyse the effects of driving factors in this study. The GWR model did not include other possible variables that may affect urban growth patterns, as it lacked input data. Although a good agreement between model results and actual maps was observed, it is recommended to include further potential variables into future studies.

Acknowledgements

This study was supported by the National Natural Science Foundation of China (Grant No. 41201166) and China Scholarship Council (No. 2010642012). The authors would like to thank the editor and anonymous reviewers for their valuable comments and suggestions that improve this article. We also thank SZILVIA KOLLÁR for helpful suggestions.

References

- ANDERSON, J.R., HARDY, E.E., ROACH, J.T. & WITMER, R.E., 1976: A land use and land cover classification system for use with remote sensor data. – <http://landcover.usgs.gov/pdf/anderson.pdf> (15.5.2014).
- ASPINALL, R., 2004: Modelling land use change with generalized linear models – a multi-model analysis of change between 1860 and 2000 in Gallatin Valley, Montana. – *Journal of Environmental Management* **72** (1–2): 91–103.
- BATISANI, N. & YARNAL, B., 2009: Urban expansion in Centre County, Pennsylvania: spatial dynamics and landscape transformations. – *Applied Geography* **29** (2): 235–249.
- BRAIMOH, A.K. & ONISHI, T., 2007: Spatial determinants of urban land use change in Lagos, Nigeria. – *Land Use Policy* **24** (2): 502–515.
- BRUNSDON, C., FOTHERINGHAM, A.S. & CHARLTON, M., 1996: Geographically weighted regression: a method for exploring non-stationarity. – *Geographical Analysis* **28** (4): 281–298.
- CHAVEZ, P.S., 1988: An improved dark-object subtraction technique for atmospheric scattering correction of multispectral data. – *Remote Sensing of Environment* **24** (3): 459–479.
- CHENG, J.Q. & MASSER, I., 2003: Urban growth pattern modeling: a case study of Wuhan city, PR China. – *Landscape and Urban Planning* **62** (4): 199–217.
- CLARKE, K.C., HOPPEN, S. & GAYDOS, L., 1997: A self-modifying cellular automaton model of historical urbanization in the San Francisco Bay area. – *Environment and Planning B: Planning and Design* **24** (2): 247–261.
- DENG, J.S., WANG, K., HONG, Y. & QI, J.G., 2009: Spatio-temporal dynamics and evolution of land use change and landscape pattern in response to rapid urbanization. – *Landscape and Urban Planning* **92** (3–4): 187–198.
- DEWAN, A.M. & YAMAGUCHI, Y., 2009: Land use and land cover change in Greater Dhaka, Bangladesh: Using remote sensing to promote sustainable urbanization. – *Applied Geography* **29** (3): 390–401.
- DIETZEL, C., HEROLD, M., HEMPHILL, J.J. & CLARKE, K.C., 2005: Spatio-temporal dynamics in California's Central Valley. – *International Journal of Geographical Information Science* **19** (2): 175–195.
- DUBOVYK, O., SLIUZAS, R. & FLACKE, J., 2011: Spatio-temporal modelling of informal settlement development in Sancaktepe district, Istanbul, Turkey. – *ISPRS Journal of Photogrammetry and Remote Sensing* **66** (2): 235–246.
- DYMOND, C.C., MLADENOFF, D.J. & RADELOFF, V.C., 2002: Phenological differences in Tasseled Cap indices improve deciduous forest classification. – *Remote Sensing of Environment* **80** (3): 460–472.
- FOTHERINGHAM, A.S., CHARLTON, M.E. & BRUNSDON, C., 1996: The geography of parameter space: an investigation of spatial non-stationarity. – *International Journal of Geographical Information System* **10** (5): 605–627.
- FOTHERINGHAM, A.S., CHARLTON, M.E. & BRUNSDON, C., 2001: Spatial variations in school performance: a local analysis using geographically weighted regression. – *Geographical and Environmental Modelling* **5** (1): 43–66.
- GAO, J. & LI, S., 2011: Detecting spatially non-stationary and scale-dependent relationships between urban landscape fragmentation and related factors using Geographically Weighted Regression. – *Applied Geography* **31** (1): 292–302.
- GAO, J. & LIU, Y., 2010: Determination of land degradation causes in Tongyu County, Northeast China via land cover change detection. – *International Journal of Applied Earth Observation and Geoinformation* **12** (1): 9–16.
- HE, C., OKADA, N., ZHANG, Q., SHI, P. & ZHANG, J., 2006: Modeling urban expansion scenarios by coupling cellular automata model and system dynamic model in Beijing, China. – *Applied Geography* **26** (3–4): 323–345.

- HEROLD, M., COUCLELIS, H. & CLARKE, K.C., 2005: The role of spatial metrics in the analysis and modeling of urban land use change. – Computer, Environment and Urban Systems **29** (4): 369–399.
- HU, Z. & LO, C.P., 2007: Modeling urban growth in Atlanta using logistic regression. – Computers, Environment and Urban Systems **31** (6): 667–688.
- JENERETTE, G.D. & WU, J., 2001: Analysis and simulation of land-use change in the central Arizona-Phoenix region, USA. – Landscape Ecology **16** (7): 611–626.
- JENKS, M., BURTON, E. & WILLIAMS, K., 1996: Compact cities and sustainability: an introduction. – JENKS, M., BURTON, E. & WILLIAMS, K. (eds.): The Compact City: A Sustainable Urban Form? – E&FN SPON, London, UK.
- KONG, F. & NAKAGOSHI, N., 2006: Spatial-temporal gradient analysis of urban green spaces in Jinan, China. – Landscape and Urban Planning **78** (3): 147–164.
- LI, C. & THINH, N.X., 2013: Investigation and comparison of land-cover change patterns in Xuzhou city, China, and Dortmund city region, Germany, using multitemporal Landsat images. – Journal of Applied Remote Sensing **7** (1): 073458.
- LI, X., ZHOU, W. & OUYANG, Z., 2013: Forty years of urban expansion in Beijing: What is the relative importance of physical, socioeconomic, and neighborhood factors? – Applied Geography **38**: 1–10.
- LONG, Y., GU, Y.Z. & HAN, H.Y., 2012: Spatiotemporal heterogeneity of urban planning implementation effectiveness: Evidence from five urban master plans of Beijing. – Landscape and Urban Planning **108** (2–4): 103–111.
- LUCK, M. & WU, J., 2002: A gradient analysis of urban landscape pattern: a case study from the Phoenix metropolitan region, Arizona, USA. – Landscape Ecology **17** (4): 327–339.
- MCGARIGAL, K., CUSHMAN, S.A. & ENE, E., 2012: Fragstats v4: Spatial pattern analysis program for Categorical and Continuous Maps, <http://www.umass.edu/landeco/research/fragstats/fragstats.html/> (6.6.2013).
- MILNE, B.T., 1991: Lessons from applying fractal models to landscape patterns. – TURNER, M.G. & GARDNER, R.H. (eds.): Quantitative methods in landscape ecology: the analysis and interpretation of landscape heterogeneity. – Springer Verlag, New York, NY, USA.
- REILLY, M.K., O'MARA, M.P. & SETO, K.C., 2009: From Bangalore to the bay area: comparing transportation and activity accessibility as drivers of urban growth. – Landscape and Urban Planning **92** (1): 24–33.
- SCHWARZ, N., 2010: Urban form revisited-Selecting indicators for characterising European cities. – Landscape and Urban Planning **96** (1): 29–47.
- SOLON, J., 2009: Spatial context or urbanization: landscape pattern and changes between 1950 and 1990 in the Warsaw metropolitan area, Poland. – Landscape and Urban Planning **93** (3–4): 250–261.
- SUI, D.Z. & ZENG, H., 2001: Modeling the dynamics of landscape structure in Asia's emerging desakota regions: a case study in Shenzhen. – Landscape and Urban Planning **53** (1–4): 37–52.
- THINH, N.X., ARLT, G., HEBER, B., HENNERSDORF, J. & LEHMANN, I., 2002: Evaluation of urban land-use structures with a view to sustainable development. – Environmental Impact Assessment Review **22** (5): 475–492.
- VERBURG, P.H., RITSEMA, VAN ECK, J.R.R., DE NIJS, T.C.M., DIJST, M.J. & SCHOT, P., 2004: Determinants of land use change patterns in the Netherlands. – Environment and Planning B: Planning and Design **31** (1): 125–150.
- WENG, Y.C., 2007: Spatiotemporal changes of landscape pattern in response to urbanization. – Landscape and Urban Planning **81** (4–5): 341–353.
- WU, J., 2004: Effects of changing scale on landscape pattern analysis: scaling relations. – Landscape Ecology **19** (2): 125–138.
- YUAN, F., SAWAYA, K.E., LOEFFELHOLZ, B.C. & BAUER, M.E., 2005: Land cover classification and change analysis of the Twin Cities (Minnesota) Metropolitan Area by multi-temporal Landsat remote sensing. – Remote Sensing of Environment **98** (2–3): 317–328.

Address of the Authors:

M.Sc. CHENG LI, Prof. Dr. rer. nat. habil. NGUYEN XUAN THINH & M.Sc. JIE ZHAO, TU Dortmund University, Faculty of Spatial Planning, Department of Spatial Information Management and Modelling, August-Schmidt-Straße 10, D-44227 Dortmund, Tel.: +49-231-755-2247, Fax: +49-231-755-2508, e-mail: {cheng.li} {nguyen.thinh} {jie2.zhao}@tu-dortmund.de

Manuskript eingereicht: Dezember 2013
Angenommen: Juli 2014

Berichte von Veranstaltungen

13. Internationales 3D-Forum, 6.–7. Mai 2014, Lindau

Das 13. Internationale 3D-Forum Lindau fand am 6. und 7. Mai 2014 im Kongresszentrum Inselhalle Lindau statt und erreichte erstmals die 200-Teilnehmernsgrenze. Zudem wurde mit 30 ausstellenden Firmen auch hier ein neuer Höchststand erreicht. Die Teilnehmer kamen aus 7 Ländern, vornehmlich aus Europa.

Die Veranstalter Dipl.-Ing. CLAUS BIHL (Stadt Lindau) und Dr.-Ing. ACHIM HELLMEIER (Ingenieurbüro Real.IT, Aalen) hatten unter den Schwerpunktthemen *Mobile Mapping und UAVs – Effiziente Erfassung von 3D-Daten*, *3D-Stadtmodelle in Architektur und Stadtplanung* und *Open Data – Neue Möglichkeiten durch freien Zugang zu raumbezogenen Daten* wieder ein sehr aktuelles Programm erstellt, das von Referenten aus Wirtschaft, Wissenschaft und Verwaltung ausgefüllt wurde. Partner der Veranstaltung waren die Gesellschaft für Geodäsie, Geoinformation und Landmanagement (DVW), die Deutsche Gesellschaft für Photogrammetrie, Fernerkundung und Geoinformation (DGPF) und das Virtual Dimension Center (VDC) Stuttgart/Fellbach. Hauptsponsor der Veranstaltung war die Firma Esri Deutschland GmbH.

Wie in den Vorjahren wurde die Veranstaltung in einen Vortragsteil am ersten Tag und in Vertiefungsthemen und Workshops am zweiten Tag aufgeteilt. Dr. GERHARD ECKER, Oberbürgermeister der Stadt Lindau, eröffnete die Veranstaltung. Er hob in seiner Begrüßungsrede u.a. hervor, dass die Stadt Lindau in den kommenden Jahren zwei große Bauprojekte durchführen wird, bei denen bereits in der Planungsphase 3D-Modelle eine wichtige Rolle spielen und auch in den weiteren Ausführungsschritten von Bedeutung sein werden.

Nach der Eröffnung übernahm ACHIM HELLMEIER die Moderation der Veranstaltung und führte den ersten Vortragenden, DIETER FRITSCH von der Universität Stuttgart, ein. FRITSCH gab mit seinem Eröffnungsvortrag *Von der Punktwolke zum Augmented Reality*

3D Modell einen umfassenden Überblick über die Entwicklungen im 3D-Bereich der letzten Jahre. Anschließend berichtete WALTER SIEH von der Freien und Hansestadt Hamburg über *Zehn Jahre 3D-Stadtmodell im Vertrieb*. Dieser Beitrag zeigte eindrucksvoll, wie wichtig es ist, die richtigen Vermarktungsstrategien zu finden, um ein 3D-Stadtmodell für potentielle Anwender attraktiv zu machen.

Den zweiten Vortragsblock eröffnete FRANK ENGEL vom Landesamt für Vermessung und Geoinformation Thüringen in Erfurt. In seiner Präsentation mit dem Titel *3D-Geobasisdaten in Thüringen – Stand und Ausblick* zeigte ENGEL sehr klar, wie Thüringen Schritt für Schritt LOD2 realisiert und welche Rolle diese 3D-Daten innerhalb der Geobasisdaten Thüringens spielen. Der letzte Vortrag im Vormittagsprogramm kam von der Stadt Kempten. THOMAS VOLKWEIN und WILHELM FEHR stellten unter dem Titel *Mobile Mapping – Wirtschaftliche Erfassung von Gebäuden und Straßen im kommunalen Bereich* vor, wie bei der Stadt Kempten 3D-Daten aus einer Mobile-Mapping-Befahrung vielfältig und erfolgreich eingesetzt werden.

Um den Tagungsteilnehmern ein gezieltes Zugehen auf die ausstellenden Firmen zu erleichtern, stellten die Veranstalter vor der Mittagspause die beteiligten Firmen in Kurzporträts vor.

Das Nachmittagsprogramm eröffnete STEFAN OVERMANN von der Stadt Aalen. Er berichtete unter der Überschrift *Die Kombination von GIS und 3D-Stadtmodell – Basis für vielfältige Anwendungen* über sehr interessante Projekte im kommunalen Bereich. Danach zeigte ULRICH SCHWARZ vom Architekturbüro 21_ARCH Architekten (Calw) auf, wie *3D-Stadtmodelle aus Sicht des Architekten und Stadtplaners* bewertet werden. Im letzten Vortragsblock am Dienstag gab STEPHAN NEBIKER von der Hochschule für Bau und Architektur der FHNW aus Muttenz/Schweiz einen sehr informativen Überblick über *UAVs im Einsatz für die Erfassung von 3D Geo- und Gebäudemodellen*.

Mit einem geselligen Beisammensein auf der Insel Lindau im Gasthaus Sünfzen, das aus einer mittelalterlichen Trinkstube der Patrizier hervorgegangen ist, klang der erste Veranstaltungstag aus. Dieser Abend ist traditionell fester Bestandteil des 3D-Forums Lindau und führte bei guter Stimmung wieder einmal zu einem angeregten Gedankenaustausch zwischen den Teilnehmern.

Das Vormittagsprogramm des zweiten Veranstaltungstags begann mit drei Vertiefungsthemen, am Nachmittag folgten dann Workshops. Das erste Vertiefungsthema *3D-Stadtmodelle und kommunale Energiekonzepte* wurde von VOLKER COORS von der Hochschule für Technik, Stuttgart, präsentiert. Mit den Unterpunkten Erzeuger, Verbraucher, Netze und Wärmebedarfsatlas zeigte COORS eindrucksvoll auf, welche Rolle 3D-Stadtmodelle in diesen Themen spielen und vor allem, zukünftig noch spielen werden. Im zweiten Vertiefungsthema referierte Ministerialrat TOBIAS KUNST vom Bayerischen Staatsministerium der Finanzen, für Landentwicklung und Heimat über *Open Government / Open Data – mehr Transparenz durch Geoanwendungen*.

Ein überaus aufschlussreicher Beitrag, der

verdeutlichte, welche Entwicklungen sich hier in den nächsten Jahren auftun werden. In der letzten Präsentation dieses Blockes stellte GÜNTER POMASKA von der Fachhochschule Bielefeld Verfahren zur Effizienten *3D-Objektfassung kleiner und mittlerer Gebiete* für Denkmalpflege, Deponien etc. vor. Dabei ging POMASKA u.a. auch auf UAVs für die Datenerfassung und Open Source Lösungen für die Modellberechnung ein.

Nach Abschluss des eigentlichen Vortragssprogramms folgten dann am Nachmittag Workshops. Neben vier Firmenworkshops fand zum vierten Mal der CityGML Workshop mit Experten aus der SIG3D und der Standard Working Group des OGC statt. Hier wurde neben Anwendungen im kommunalen Bereich auch über den aktuellen Stand und die weiteren Planungen von CityGML berichtet. Die Firmenworkshops wurden von Esri, VirtualCitySystems (VCS), UVM Systems und Leica abgehalten. Esri berichtete über den 3D-City-Workflow, VCS über webbasiertes Verwalten, Verteilen und Veröffentlichen von 3D-Geodaten. UVM stellte die automatische Texturierung von 3D-Stadtmodellen und Leica das neu zur Leica Geosystems gehörende



Abb.: Eröffnung durch den Oberbürgermeister der Stadt Lindau Dr. Gerhard Ecker

Softwaresystem Tridicon für die automatische Erstellung von 3D-Stadtmodellen vor.

Die Workshops bildeten den Abschluss der Veranstaltung, die gegen 17 Uhr zu Ende ging. Zusammenfassend lässt sich festhalten, dass das 13. Internationale 3D-Forum Lindau nicht nur wegen der hohen Teilnehmer- und Ausstellerzahl als voller Erfolg gewertet werden kann, sondern vor allem auch wegen der eindrucksvollen Vorträge und der interessanten Präsentationen der teilnehmenden Firmen.

Zudem wurden auch zwei weitere wichtige Ziele der Veranstaltung erreicht: das Präsentieren von praxisnahen Beispielen mit den dazugehörigen Diskussionen sowie das Herstellen und die Pflege persönlicher Kontakte und der Erfahrungsaustausch zwischen den Teilnehmern.

Das nächste Internationale 3D-Forum Lindau findet am 5. und 6. Mai 2015 statt (www.3d-forum.li).

UWE LOHR, Salem

Hochschulnachrichten

Karlsruher Institut für Technologie

Dissertation von Nawras Shatnawi

Herr M.Sc. NAWRAS SHATNAWI promovierte am 13. Februar 2014 an der Fakultät für Bauingenieur-, Geo- und Umweltwissenschaften des Karlsruher Instituts für Technologie mit der Arbeit *Assessment of Ground Water Potential Zones in the Lower Jordan Valley Using Remote Sensing Approaches* zum Dr.-Ing.

1. Gutachter: Prof. Dr.-Ing. habil. STEFAN HINZ, Karlsruher Institut für Technologie (KIT).
2. Gutachter: Prof. Dr. rer.nat. HEINZ HÖTZL, Karlsruher Institut für Technologie.
3. Gutachter: Prof. Dr. ABDULLAH AL-ZOUBI, Al-Balqa Applied University, Jordanien.

Zusammenfassung:

Jordanien liegt in einer ariden bis semi-ariden Region und ist eines der an Wasserressourcen ärmsten Ländern der Welt. Das Jordantal ist ein wichtiges Gebiet für die landwirtschaftliche Nutzung, leidet aber an der zunehmenden Wasserknappheit. Diese Arbeit leistet einen Beitrag zu Grundwassererkundung und -management im jordanischen Teil des unteren Jordantals. Hauptziel ist dabei eine verbesserte Entdeckung potentieller Grundwasservorkommen durch die Kombination von Fernerkundungs-, GIS- und terrestrischen Methoden.

Als Ausgangspunkt der Arbeit wird die Landschaft entsprechend ihrem Grundwas-

serpotential, welches als Potential zur Grundwasserneubildung definiert ist, in verschiedene Klassen unterteilt. Dies geschieht auf Basis unterschiedlicher Kontrollparameter, die durch die Oberflächenbeschaffenheit und die Versickerung von Niederschlagswasser in den tieferen Untergrund beeinflusst werden. Zur Evaluierung und Gewichtung der relevanten Parameter wurden zwei Methoden weiterentwickelt und angewandt: Der Analytische Hierarchieprozess (AHP) sowie die Fuzzylogik. Hierbei ergaben sich für die Erzeugung einer Karte der Grundwasserpotentialzonen (GWPZ) insgesamt neun Parameter wie z.B. die topographische Höhe, morphologische Klasse, Neigung, Entwässerungslineamente bzw. -netze, Landnutzung/-bedeckung und allgemeine Lineamentdichte.

Die entsprechenden Werte der Parameter wurden unter Verwendung von Fernerkundungsdaten und Photogrammetrie- bzw. Bildverarbeitungsmethoden erzeugt. Zusätzlich standen Daten über Geologie/Lithologie, Erdreich und jährlichen Niederschlag aus verschiedenen Quellen zur Verfügung. Als Grundlage der Erzeugung einer thematischen Karte über die Landnutzung/-bedeckung wurden LANDSAT-5 und LANDSAT-7 Bilder der Winter- und Sommersaison von 2010 und 2011 kombiniert, was in einer Klassifikationsgenauigkeit von über 90% bei einem Kappa Koeffizienten von 0,95 resultierte. Außerdem wurden durch Bildanalysemethoden angewandt auf CARTOSAT-1 Bilder Lineament-

karten und statistische Parameter über deren Verteilung und Orientierung erzeugt. Die restlichen topographischen Parameter wurden mithilfe eines hochauflösten DGM – ebenfalls erzeugt aus CARTOSAT-1 Stereobildpaaren – abgeleitet. Zur Bewertung der DGM-Genauigkeit wurden unterschiedliche Kamera- und Orientierungsmodelle genutzt und gegenübergestellt, die in Abhängigkeit der verwendeten Passpunktdata Genauigkeiten im Bereich von zwei bis fünf Metern liefern.

Die verwendeten Methoden zur Erzeugung der GPWZ Karten – AHP und Fuzzylogik – zeigten relativ ähnliche Ergebnisse. Diesen entsprechend wurde das Untersuchungsgebiet in fünf Zonen aufgeteilt und stichprobenartig mit Karten des jordanischen Ministeriums für Wasser und Bewässerung (WAI) verglichen.

Dabei zeigte sich in einer ersten Analyse, dass die verwendeten Daten keinen offensichtlichen Zusammenhang zwischen Ergiebigkeit der Brunnen und den GWPZ aufweisen, was auf die unterschiedlichen Tiefen der Grundwasserzonen und Brunntiefen zurückzuführen ist. Für eine vertiefte und zusätzliche Kontrolle wurden daher die Ergebnisse mit Daten aus geophysikalischen Messungen mit Bodenradar, kernmagnetischer Resonanz und vertikalem Echolot verglichen. Diese zeigten schließlich, dass die mittels Fuzzy-Logik erzeugte GPWZ Karte eine höhere Signifikanz aufweist als die AHP-basierte Karte.

Abschließend wurde eine Sensitivitätsanalyse der Parameter durchgeführt, die vor allem unterstrich, dass die generierten GPWZ-Karten empfindlich gegenüber Parametern aus Geologie, Morphologie und Lineamentdichte sind, wohingegen die anderen Parameter weniger sensitiv sind.

Die Arbeit ist in der KIT-Bibliothek unter <http://digibib.ubka.uni-karlsruhe.de/volltexte/1000041841> veröffentlicht.

Technische Universität München

Dissertation von Michael Schmitt

Herr Dipl.-Ing. MICHAEL SCHMITT promovierte am 28. Juli 2014 an der Ingenieurfakultät Bau Geo Umwelt (Fachgebiet Photogrammetrie

und Fernerkundung) der Technischen Universität München mit der Arbeit *Reconstruction of urban surface models from multi-aspect and multi-baseline interferometric SAR* zum Dr.-Ing.

1. Gutachter: Prof. Dr.-Ing. UWE STILLA, Technische Universität München (TUM).
2. Gutachter: Prof. Dr.-Ing. JOACHIM ENDER, Universität Siegen.
3. Gutachter: Prof. Dr.-Ing. UWE SÖRGEL, Technische Universität Darmstadt.

Zusammenfassung:

Schon seit vielen Jahren wird Synthetik Apertur Radar-Interferometrie dazu verwendet, die dreidimensionale Topographie der Erdoberfläche unabhängig von Wolkenbedeckung oder Tageszeit zu erfassen. Sie gilt deshalb als wertvolles Werkzeug für schnelle Datenerfassung vor allem in zeitkritischen Szenarien. Die seitwärtsblickende SAR-Abbildungsgeometrie führt jedoch zu den störenden Effekten Überlagerung und Radarschatten. Mit dem Ziel, diese Nachteile aufzulösen, untersucht die vorliegende Arbeit innovative InSAR-Prozessierungsstrategien zur Rekonstruktion urbaner Oberflächenmodelle unter Verwendung von Daten mehrerer Aspekte sowie Basislinien. Da nur Flugzeuge die Möglichkeit bieten, hochkohärente Single-Pass-Daten von beinahe beliebigen Aspektwinkeln aufzunehmen, liegt der Fokus der Arbeit dabei auf der Verwendung von flugzeuggetragenem SAR.

Der erste Schritt in einer Mehrfachbasislinien-InSAR-Prozesskette ist normalerweise die Schätzung der komplexen Kovarianzmatrizen aller Pixel im Stapel der koregistrierten Bilder, da diese Matrizen die vollständige interferometrische Information der zugehörigen Auflösungszelle beinhalten. Deshalb ist der erste Beitrag dieser Arbeit die Vorstellung zweier neuer adaptiver Verfahren zur Kovarianzmatrix-Schätzung, die speziell für Single-Pass-InSAR-Stapel mit nur wenigen Aufnahmen entworfen wurden.

Als zweites wird ein neuartiger Algorithmus zur SAR-Tomographie beschrieben, der darauf abstellt, überlagerte Streuer zu trennen und die Fokussierung dünnbesetzter dreidimensionaler SAR-Bilder zu ermöglichen. Im Gegensatz zu den meisten bislang vorgeschla-

genen TomoSAR-Ansätze ist er nicht auf Repeat-Pass-Datenstapel, die sich durch eine große Gesamtbasislinie und eine hohe Zahl an Beobachtungen ausweisen, angewiesen, um eine ausreichende Elevationsauflösung bereitzustellen.

Ergänzend dazu wird als dritter Beitrag die Fusion von Multi-Aspekt-InSAR-Daten untersucht. Dabei ist das Ziel, Informationen dort aufzufüllen, wo sie in einzelnen Aspekten von Radarschatten verdeckt wurden. Zu diesem Zweck wird ein radargrammetrischer Registrierungsansatz, der als Vorprozessierungsschritt für weitere Fusionsoperationen verwendet wird, beschrieben. Auf dieser Voraussetzung aufbauend wird ein neues Maximum-Likelihood-Schätzverfahren entwickelt, das verwendet wird, um InSAR-Daten mehrerer Aspekte und Basislinien simultan zu fusionieren, um ein flächendeckendes 2,5D-Höhenmodell zu generieren. Analog dazu wird eine Voxelraum-basierte Fusion von 3D-Punktwolken, welche durch SAR-Tomographie gewonnen wurden, vorgeschlagen.

Alle in der Arbeit beschriebenen Methoden werden mit Hilfe von experimentellen SAR-Daten des flugzeuggetragenen Millimeterwellen-Sensors MEMPHIS untersucht. Sie bestehen aus Single-Pass-Mehrfachbasislinien-InSAR-Stapeln, die vier koregistrierte Aufnahmen enthalten. Der Testdatensatz zeigt die Innenstadt von München und dient als Beispiel für komplexe urbane Szenen. Er ist zusammengesetzt aus dichten Gebäudeblocks, isolierten großen Gebäuden, Straßen und vielen Stadtbäumen.

Zuerst wird in den Experimenten sowohl die Effizienz als auch die Adaptivität der Kovarianzschätzungsmethoden mit Hilfe von Bildverarbeitungstechniken evaluiert. Anschließend wird die Fähigkeit, Überlagerungen aufzulösen, des TomoSAR-Algorithmus untersucht, bevor die Rekonstruktionsergebnisse, die mit der simultanen Fusion von Multi-Aspekt- und Mehrfachbasislinien-Daten erreicht werden, analysiert werden. Zuletzt werden diese Rekonstruktionsergebnisse mit den 3D-Daten, die durch eine Fusion von Multi-Aspekt-TomoSAR-Punktwolken erhalten werden, verglichen. Indem die beiden Rekonstruktionsergebnisse mit einer dichten Laser-Punktwolke abgeglichen werden, kann ge-

zeigt werden, dass eine flächendeckende Rekonstruktion von 2,5D-Höhenkarten und 3D-Punktwolken mit Genauigkeiten im Meterbereich mit flugzeuggetragenen Single-Pass-InSAR-Daten möglich ist.

Technische Universität Dresden

Dissertation von Stefan Hahmann

Mr. Dipl.-Ing. (FH) STEFAN HAHMANN, completed his doctorate (Dr.-Ing.) at the faculty of Environmental Sciences of the Technische Universität Dresden, Institute of Cartography, on June 12, 2014, with the work *On the relationship of space and content of volunteered geographic information*.

1. Reviewer: Prof. Dr. DIRK BURGHARDT, TU Dresden.
2. Reviewer: Prof. Dr. (em.) Dr. BERND TEICHERT, TU Dresden.
3. Reviewer: Prof. Dr. ROSS PURVES, Universität Zürich.

Summary:

In the past ten years, there has been a significant progress of the World Wide Web, which evolved to become the so-called “Web 2.0”. The most important feature of this new quality of the WWW is the participation of the users in generating contents. This trend facilitates the formation of user communities, which collaborate on diverse projects, where they collect and publish information. Prominent examples of such projects are the online encyclopedia “Wikipedia”, the microblogging-platform “Twitter”, the photo-platform “Flickr” and the database of topographic information “OpenStreetMap”.

User-generated content, which is directly or indirectly geospatially referenced, is often termed more specifically as “volunteered geographic information”. The geospatial reference of this information is constituted either directly by coordinates given as meta-information or indirectly through georeferencing of toponyms or addresses that are contained in this information.

Volunteered geographic information is particularly suited for research, as it can be ac-

cessed with low or even at no costs at all. Furthermore, it reflects a variety of human decisions, which are linked to geographic space. In this thesis, the relationship of space and content of volunteered geographic information is investigated from two different perspectives.

The first part of this thesis addresses the question for which share of information there exists a relationship between space and content of the information, such that the information is locatable in geo-space. In this context, the assumption of about 80% of all information having a reference to space is well known in the community of GIS users. Since the 1980s it has served as a marketing tool within the whole geo-information sector, although there has not been any empirical evidence. This thesis contributes to fill this research gap.

For the validation of the “80%-hypothesis” two approaches are presented. The first approach is based on a corpus of information that is as representative as possible for world knowledge. For this purpose, the German language edition of Wikipedia has been selected. This corpus is modeled as a network of information where the articles are considered the nodes and the cross references are considered the edges of a directed graph. With the help of this network a graduated definition of geospatial references is possible. It is implemented by computing the distance of each article to its closest article within the network that is assigned with spatial coordinates. Parallel to this, a survey-based approach is developed where participants have the task to assign pieces of information to one of the categories “direct geospatial reference”, “indirect geospatial reference” and “no geospatial reference”. A synthesis of both approaches leads to an empirically justified figure for the “80%-assertion”. The result of the investigation is that for the corpus of Wikipedia 27% of the information may be categorized as directly geospatially referenced and 30% of the information may be categorized as indirectly geospatially referenced.

In the second part of the thesis the question is investigated in how far volunteered geographic information that is produced on mobile devices is related to the locations where it is published. For this purpose, a collection of

microblogging-texts produced on mobile devices serve as research corpus. Microblogging-texts are short texts that are published via the World Wide Web. For this type of information the relationship between the content of the information and their position is less obvious than e.g. for topographic information or photo descriptions. The analysis of microblogging-texts offers new possibilities for market and opinion research, the monitoring of natural events and human activities as well as for decision support in disaster management. The spatial analysis of the texts may add extra value. In fact, for some of the applications, the spatial analysis is a necessary condition. For this reason, the investigation of the relationship of the published contents with the locations where they are generated is of interest.

Within this thesis, methods are described that support the investigation of this relationship. In the presented approach, classified Points of Interest serve as a model for the environment. For the purpose of the investigation of the correlation between these points and the microblogging-texts, manual classification and natural language processing are used in order to classify these texts according to their relevance in regard to the respective feature classes. Subsequently, it is tested whether the share of relevant texts in the proximity of objects of the tested classes is above average. The results of the investigation show that the strength of the location-content-correlation depends on the tested feature class. While for the feature classes ‘train station’, ‘airport’ and ‘restaurant’ a significant dependency of the share of relevant texts on the distance to the respective objects may be observed, this is not confirmed for objects of other feature classes, such as ‘cinema’ and ‘supermarket’. However, as prior research that describes investigations on small cartographic scale has detected correlations between space and content of microblogging-texts, it can be concluded that the strength of the correlation between space and content of microblogging texts depends on scale and topic.

Dissertation von Thomas Schulz

Mr. Dipl.-Ing. (FH) THOMAS SCHULZ, President of SGK, completed his doctorate (Dr.-Ing.) at

the faculty of Environmental Sciences of the Technische Universität Dresden on June 26, 2014, with the work *The Statistical Atlas – studies on classificatory, conceptual, formal, technical and communication aspects (Der Statistische Atlas – Untersuchungen zu klassifikatorischen, inhaltlichen, gestalterischen, technischen und kommunikativen Aspekten)*.

1. Reviewer: Prof. Dr. (em.) Dr. WOLF GÜNTHER KOCH, TU Dresden.
2. Reviewer: Prof. (em.) Dr. WOLFGANG DENK, Hochschule Karlsruhe.
3. Reviewer: Prof. Dr. MANFRED BUCHROITHNER, TU Dresden.

Summary:

For more than 150 years statistical institutions have been issuing large thematic atlases that portray social and economic facts about countries, regions or cities. Currently, about 2500 statistical atlases can be found in respective bibliographies. However, all those works have almost never played a role in scientific studies, be it in statistics or in cartography. Extensive research on this atlas type is lacking until today. It is the expressed objective of this thesis to fill this gap, especially in the field of thematic and atlas cartography, by closely analysing the character, the historical development and current features of the *Statistical Atlas* using various theoretical and empirical methods.

Within the special framework of rules and regularities of public statistics, that influence the atlases from the publisher's side, and general classificatory features for atlases, four essential parameters could be identified, which single out the *Statistical Atlas* from the existing plethora of other atlases: contents, topicality, source and publisher. Based upon these parameters, a fundamental clarification of the term «Statistical Atlas» could be reached for the first time, followed by a new and general definition. Such atlases were then dissociated from other atlas types, such as national, regional or planning atlases. In the last consequence and based upon these results, a new atlas classification could be set up, which comprises the *Statistical Atlas*.

In the context of this work, also a bibliography of statistical atlases with app. 800 titles was established. Together with inputs from the

history of statistics and cartography, it helped to explain the historical and societal background as well as motivations on the institutional side to publish such atlases at certain times. Altogether, eight historical periods could be identified, that characterise the evolution of this atlas type since the first issue around 1818.

Twenty statistical atlases with more than 6000 individual maps were representatively selected for a more detailed quantitative analysis. In respect of contents, a unique system in the topical structure of all atlases could be discovered, to which occasional changes occurred over time, but almost never between regions. In a comparison to the overall content structures of public statistics it could be shown, that only half of all general statistical topics also appear in statistical atlases. Reasons are mainly to be found in the data acquisition methods for each topic. Through their access to primary data statistical atlases in general reach a degree of topicality unlike any other atlas type. Relative and absolute data in the form of simple key figures (98% share) are dominating the atlases.

The overwhelming availability of elementary analytical data in the public statistical domain clearly correlates to the cartographic representation methods applied in these products. Three methods (also 98% share) dominate statistical atlases: area cartograms, symbol cartograms and combinations of both. Other methods remain at the margin. The choice and application of appropriate reference areas have always been of crucial and timeless importance for the composition and quality of statistical maps. Therefore, one chapter deals explicitly with this complex. For the first time also a structural scheme of the about twenty known and available area types was developed. In spite of this theoretical abundance of reference areas, official statistics, due to their methods and for political reasons, are generally unable to go beyond the representation of administrative boundaries. 96.2% of all maps still refer to this area type. Existing and innovative possibilities for optimising these representations were studied and assessed.

Statistical atlases usually apply the technological means and standards of their time.

Nevertheless, in lack of existing solutions for some current needs on the cartographic market, the statistics itself has stimulated the development of new mapping methods during three periods, which eventually contributed to the enhancement and efficiency of thematic map production in general. This was the case in the early phase of thematic cartography during the 19th century, later on during the introduction of computer maps via an automated production, and currently in the field of semi-automated atlas platforms and Content Management Systems. Finally, in the scope of the evolution of the modern information society and her impact on all of us, the reception and acceptance of many official publications depend today (again) largely on the good presentation of their contents, especially by means of visually edited information modules. Thus, maps and atlases for the last two decades have experienced a true revival in statistics. They are able to address a broad user audience from all professions and classes in society.

Technische Universität Berlin

Dissertation von Ronny Hänsch

Mr. Dipl.-Inform. RONNY HÄNSCH completed his doctorate (Dr.-Ing.) at the faculty of Electrical Engineering and Computer Science of the Technische Universität Berlin (TUB) on January 22, 2014, with the work *Generic Object Categorization in PolSAR images – and beyond*.

1. Reviewer: Prof. Dr.-Ing. OLAF HELLWICH, Technische Universität Berlin.
2. Reviewer: Prof. Dr.-Ing. STEFAN HINZ, Karlsruher Institut für Technologie.
3. Reviewer: Prof. Dr.-Ing. CHRISTIAN HEIPKE, Leibniz Universität Hannover.

Summary:

The automatic understanding of digital images is still a difficult task despite decades of research. The analysis of remotely sensed images is particularly challenging due to usually larger image size, less reference data, as well as high intra-class and low inter-class variability if compared to close-range digital pho-

tography. Over the years many expert systems have been developed which are designed to perform specific classification or detection tasks in specific types of image data, e.g. forest detection in SAR images, land-use classification in hyperspectral images, building detection in optical images, etc. Although these expert systems are to some degree successful in their domain, they can seldom be applied to other classification tasks.

The objective of this work is to develop a framework, which is not specifically designed to solve one single, specific task, but can be applied to any image-based classification problem and shows a good performance on average. In the context of this thesis “generic object categorization” refers to the task of detecting instances of object classes within images. However, unlike other works, this thesis assumes that the final categorization problem, i.e. objects of which specific classes are searched for in the images, is not known during the design of the framework. Consequently, any kind of category-specific optimization such as sophisticated feature design or manual selection, top-down processing, or task-specific choice of the classifier is not possible. Although the main focus of this work is on polarimetric synthetic aperture radar (PolSAR) images, it is by no means limited to it. The generic framework of the developed system provides a certain independence of the specific classification task as well as of the given data type.

The proposed system is based on a two-stage framework. The first stage consists of a feature extraction module (FEM) and a subsequent classification module. The FEM contains a large set of general low-level feature operators that capture mainly radiometric and textural properties of PolSAR, SAR, colour, grayscale, as well as binary images. A given PolSAR image is projected to all of these image types before the corresponding operators are applied. Images of a lower data level are projected to the corresponding subset of these image types. A colour image for example only leads to colour, grayscale, and binary images, but not to SAR or PolSAR images. In the case of PolSAR data nearly 400 different features are extracted. A newly proposed variant of random forests (Projection-based random for-

ests, ProB-RF) is used to estimate a first probabilistic label based on these features. RF in general are able to handle high-dimensional input spaces, while ProB-RF exploit local contextual information which is inherent in structured data like images. The second stage starts with a semantic segmentation of the image, which is not only based on the radiometric or texture information of the image itself, but also on the classification result of the first stage. For each segment several high-level features are computed, which represent geometric, radiometric, textural, as well as semantic information. A second ProB-RF classifier estimates the final category posterior distribution in a fully probabilistic manner.

In contrast to many other classifiers, the proposed framework is not a black-box system. On the one hand, it provides meaningful internal measurements to understand and interpret the achieved classification performance and to give cues how to adapt system parameters to improve accuracy and/or speed. On the other hand, it provides not only a probabilistic classification output, but also which of the used features are especially relevant/irrelevant for the given classification task.

Random forests are known to be not only robust and accurate, but also very efficient classifiers. Many processing steps of the proposed system are independent of each other and can be carried out in parallel, which leads to relatively fast processing times, even for

large input images. The system allows additional trade-offs between accuracy and speed, depending on what is of more importance to the user. It can be easily extended and specialized if necessary, e.g. by extending the feature extraction module.

Although no task-specific expert knowledge is used during the design of the classifier, it is possible to incorporate this information into the system if it is available. The end user is for example able to include his knowledge of which features are relevant for his specific classification task.

The exhaustive experimental study of the thesis not only investigates the basic characteristics of the newly proposed extension of the random forest classifier. It also applies the developed framework to a vast amount of image data, including PolSAR data, remotely sensed optical images, and close-range photographs with various categorization tasks ranging from land cover classification, over building detection, to the localization of cars. Not a single system parameter is adapted to the problem at hand. The whole framework is evaluated, i.e. trained and applied, without further optimization. Nevertheless, reasonable classification accuracies are achieved, which partly even compare favourably with state-of-the-art expert systems.

The dissertation is available under: <http://opus4.kobv.de/opus4-tuberlin/frontdoor/index/index/docId/4933>

Veranstaltungskalender

2014

9.–12. Dezember: **ISPRS Technical Commission VIII Symposium 2014** in **Hyderabad**, Indien. nrsc.gov.in/technicalcommission8.html

14.–17. Dezember: **ICDM – IEEE Conference on Data Mining 2014** in **Shenzhen**, China. icdm2014.sfu.ca/

2015

25.–27. Februar: **CIPA + 3D-ARCH'2015** in **Avila**, Spanien. 3d-arch.org

16.–18. März: **35. Jahrestagung der DGPF** in **Köln**, dgpf.de/con/jt2015.html

23.–27. März: **ESA FRINGE Workshop** in **Frascati**, Italien. seom.esa.int/fringe2015

25.–27. März: **PIA15 + HRIGI: Joint Conference of Photogrammetric Image Analysis and High Resolution Earth Imaging for Geospatial Information 2015** in **München**. pf.bgu.tum.de/isprs/pia15/index.html

30. März – 1. April: **JURSE - IEEE Joint Urban Remote Sensing Event 2015** in **Lausanne**, Schweiz. jurse2015.org

11.–15. Mai: **ISRSE36 – International Symposium on Remote Sensing of the Earth in Berlin**. isrse36.org

7.–12. Juni: **CVPR 2015 – Conference on Computer Vision and Pattern Recognition 2015** in **Boston**, USA. pamitc.org/cvpr15/

26.–31. Juli: **IGARSS 2015 – International Geoscience and Remote Sensing Symposium 2015** in **Mailand**, Italien. igarss2015.org

23.–28. August: **ICC – International Cartographic Conference** in **Rio de Janeiro**, Brasilien. icc2015.org

30. August – 2. September: **UAV-g: Unmanned Aerial Vehicles in Geomatics** in **Toronto**, Kanada. uav-g2015.org

6.–9. Oktober: **GCPR (DAGM): German Conference on Pattern Recognition** in **Aachen**.

7.–13. Dezember: **ICCV 2015 – International Conference for Computer Vision 2015** in **Santiago**, Chile.

Weitere Konferenzen und Workshops finden sich beispielsweise unter:
isprs.org/calendar
conferences.visionbib.com

Korporative Mitglieder

Firmen

AEROWEST GmbH
AICON 3D Systems GmbH
aphos Leipzig AG
Bernhard Harzer Verlag GmbH
Black Bridge AG
Blom Deutschland GmbH
Brockmann Consult GmbH
bsf swissphoto GmbH
Büro Immekus
CGI Systems GmbH
DB Netz AG
DELPHI IMM GmbH
Deutsches Bergbau-Museum
EFTAS Fernerkundung Technologietransfer
GmbH
ESG Elektroniksystem- und Logistik-GmbH
Esri Deutschland GmbH
EUROPEAN SPACE IMAGING
Eurosense GmbH
Exelis Visual Information Solution GmbH
fokus GmbH
g.on experience gmbh
GAF GmbH
GeoCart Herten GmbH
Geoinform. & Photogr. Engin. Dr. Kruck & Co.
GbR
geoplana Ingenieurgesellschaft mbH
GEOSYSTEMS GmbH
GGS – Büro für Geotechnik, Geoinformatik,
Service
Hansa Luftbild AG
Herbert Wichmann, VDE Verlag GmbH
IAGB mbH
IGI – Ingenieur-Gesellschaft für Interfaces mbH
ILV Ingenieurbüro für Luftbildauswertung und
Vermessung
Infoterra GmbH
INVERS – Industrievermessung & Systeme
J. Linsinger ZT-GmbH
Leica Geosystems GmbH
Luftbilddatenbank-Würzburg
Messbildstelle GmbH
Microsoft Photogrammetry
MILAN Geoservice GmbH
M.O.S.S. Computer Grafik Systeme GmbH
PHOENICS GmbH
PMS – Photo Mess Systeme AG
RIEGL Laser Measurement Systems GmbH
RWE Power AG, Geobasisdaten/Markscheidewe-
sen
technet GmbH

Terra-Messflug GmbH

topometric GmbH

TRIGIS Vermessung + Geoinformatik GmbH

Trimble Germany GmbH

trimetric 3D Service GmbH

Z/I Imaging Ltd.

Behörden

Amt für Geoinformationswesen der Bundeswehr
Bayerische Landesanstalt für Wald und Forstwirt-
schaft
Bundesamt für Kartographie und Geodäsie
Bundesministerium für Ernährung, Landwirt-
schaft und Verbraucherschutz
Hessisches LA für Bodenmanagement und
Geoinformation
Innenministerium NRW, Gruppe Vermessungswe-
sen
Institut für Umwelt- und Zukunftsforschung
LA für Geoinformation und Landentwicklung,
BW
LA für Vermessung und Geoinformation, Bayern
LA für Vermessung und Geoinformation,
Schleswig-Holstein
LB Geoinformation und Vermessung, Hamburg
LB für Küstenschutz, Nationalpark und Meeres-
schutz, SH
Landeshauptstadt Düsseldorf, Vermessungs- und
Liegenschaftsamt
Landesvermessung und Geobasisinformation
Niedersachsen
Märkischer Kreis, Vermessungs- und Katasteramt
Regierungspräsident Tübingen, Abt. 8 Forstdirek-
tion
Regionalverband Ruhr
Staatsbetrieb Sachsenforst
Stadt Bocholt, Fachbereich 31
Stadt Köln, Amt für Liegenschaften, Vermessung
und Kataster
Stadt Wuppertal, Vermessung, Katasteramt und
Geodaten
Thüringer LA für Vermessung und Geoinformati-
on

Hochschulen

BTU Cottbus, Lehrstuhl für Vermessungskunde
FH Frankfurt a.M., FB 1, Studiengang Geoinfor-
mation
FH Mainz, Institut für Raumbezogene Informa-
tions- und Messtechnik
Jade Hochschule, Institut für Angewandte
Photogrammetrie und Geoinformatik

- HCU HafenCity Universität Hamburg, Geomatik
HfT Stuttgart, Vermessung und Geoinformatik
HS Bochum, FB Vermessung und Geoinformatik
HS Karlsruhe, Fakultät für Geomatik
HTW Dresden, FB Vermessungswesen/Kartographie
LUH Hannover, Institut für Kartographie und Geoinformatik
LUH Hannover, Institut für Photogrammetrie und Geoinformation
MLU Halle, FG Geofernerkundung
Ruhr-Uni Bochum, Geographisches Institut
RWTH Aachen, Geodätisches Institut
TU Bergakademie Freiberg, Institut für Markscheidewesen und Geodäsie
TU Berlin, Computer Vision & Remote Sensing
TU Berlin, Institut für Geodäsie und Geoinformationstechnik
TU Braunschweig, Institut für Geodäsie und Photogrammetrie
TU Clausthal, Institut für Geotechnik und Markscheidewesen
- TU Darmstadt, Institut für Photogrammetrie und Kartographie
TU Dresden, Institut für Photogrammetrie und Fernerkundung
TU München, FG Photogrammetrie und Fernerkundung
TU Wien, Institut für Photogrammetrie und Fernerkundung
Uni Bonn, Institut für Photogrammetrie
Uni Göttingen, Institut für Waldinventur und Waldwachstum
Uni Heidelberg, IWR Interdisziplinäres Zentrum für Wissenschaftliches Rechnen
Uni Kassel, FB Ökologische Agrarwissenschaften
Uni Kiel, Geographisches Institut
Uni Stuttgart, Institut für Photogrammetrie
Uni Trier, Institut für Umweltfernerkundung und Geoinformatik
Uni Würzburg, Geographisches Institut
Uni zu Köln, Geographisches Institut

Jahresübersicht 2014

Vorstand der DGPF

Präsident

Prof. Dr. rer. nat. THOMAS H. KOLBE
Technische Universität München
Institut für Geodäsie, GIS und Landmanagement
Lehrstuhl für Geoinformatik
Arcisstraße 21, 80333 München
Tel.: 089 / 289-23888
Fax: 089 / 289-22878
e-mail: thomas.kolbe@tum.de

Vizepräsident

Prof. Dr.-Ing. UWE STILLA
Technische Universität München
Fachgebiet Photogrammetrie und Fernerkundung
Arcisstraße 21, 80333 München
Tel.: 089 / 289-22671
Fax: 089 / 289-23202
e-mail: stilla@tum.de

Sekretär

Prof. Dr.-Ing. EBERHARD GÜLCH
Hochschule für Technik Stuttgart
Fakultät Vermessung, Mathematik und Informatik
Schellingstraße 24, 70174 Stuttgart
Tel.: 0711 / 8926-2610
Fax: 0711 / 8926-2556
e-mail: sekretaer@dgpf.de

Schatzmeister

Dr.-Ing. HERBERT KRAUSS
Rodenkirchener Straße 47, 50997 Köln
Tel.: 02233 / 22514
Fax: 032 222 / 427178
e-mail: mh.krauss@t-online.de

Hauptschriftleiter

Prof. Dr.-Ing. WOLFGANG KRESSE
Hochschule Neubrandenburg
Fachbereich Landschaftswissenschaften und Geomatik
Brodaer Straße 2, 17033 Neubrandenburg
Tel.: 0395 / 5693-4106
Fax: 0395 / 5693-4999
e-mail: kresse@hs-nb.de

Beirat

Prof. Dr. CORNELIA GLÄSSER
Martin-Luther-Universität Halle-Wittenberg
Institut für Geographie
Von-Seckendorff-Platz 4, 06120 Halle
Tel.: 0345 / 55-260 20
Fax: 0345 / 55-271 68
e-mail: cornelia.glaesser@geo.uni-halle.de

Beirat

Dr. rer. nat. KLAUS-ULRICH KOMP
EFTAS Fernerkundung
Technologietransfer GmbH
Oststraße 2–18, 48145 Münster
Tel.: 0251 / 1330-70
Fax: 0251 / 1330-733
e-mail: klaus.komp@eftas.com

Beirat

Prof. Dr.-Ing. habil. HANS-GERD MAAS
Technische Universität Dresden
Professur für Photogrammetrie
Helmholtzstraße 10, 01062 Dresden
Tel.: 0351 / 463-32859
Fax: 0351 / 463-37266
e-mail: hans-gerd.maas@tu-dresden.de

Beirat

Prof. Dr.-Ing. habil. MONIKA SESTER
Leibniz Universität Hannover
Institut für Kartographie und Geoinformatik (ikg)
Appelstraße 9a, 30167 Hannover
Tel.: 0511 / 762-3588
Fax: 0511 / 762-2780
e-mail: monika.sester@ikg.uni-hannover.de

Beirat

Dr.-Ing. ECKHARDT SEYFERT
Landesvermessung und Geobasisinformation Brandenburg
Heinrich-Mann-Allee 103, 14473 Potsdam
Tel.: 0331 / 8844-506
Fax: 0331 / 8844-126
e-mail: eckhardt.seyfert@geobasis-bb.de

Ehrenmitglieder der DGPF

Prof. Dr.-Ing. FRIEDRICH ACKERMANN, Stuttgart
 Prof. Dr.-Ing. WOLFGANG FÖRSTNER, Bonn
 Prof. Dr. GERD HILDEBRANDT, Freiburg
 Prof. Dr.-Ing. GOTTFRIED KONECNY, Hannover
 Direktor FRITZ ERICH KRAUSE, Münster
 Dr.-Ing. HERBERT KRAUSS, Köln
 Dipl.-Ing. HORST SCHÖLER, Stadtsteinach
 Prof. Dr.-Ing. KLAUS SZANGOLIES, Jena

Arbeitskreise der DGPF

Aus- und Weiterbildung

Prof. Dr.-Ing. ANSGAR BRUNN
 Hochschule für angewandte Wissenschaften
 Würzburg-Schweinfurt
 Studiengang Vermessung und Geoinformatik
 Röntgenring 8, 97070 Würzburg
 Tel.: 0931 / 3511-8212
 Fax: 0931 / 3511-9510
 e-mail: ansgar.brunn@fhws.de

Dr.-Ing. GÖRRES GRENZDÖRFFER
 Universität Rostock, Agrar- und Umweltwissenschaftliche Fakultät
 Professur Geodäsie und Geoinformatik
 Justus-v.-Liebig-Weg 6, 18051 Rostock
 Tel.: 0381 / 498-3206
 Fax: 0381 / 498-3202
 e-mail: goerres.grenzdoerffer@uni-rostock.de

Auswertung von Fernerkundungsdaten

Prof. Dr. VOLKER HOCHSCHILD
 Universität Tübingen
 Physische Geographie und GIS
 Geographisches Institut
 Rümelinstraße 19–23, 72070 Tübingen
 Tel.: 07071 / 2975316
 Fax: 07071 / 295378
 e-mail: dgpf2013@geographie.uni-tuebingen.de

Prof. Dr. BIRGIT KLEINSCHMIT
 Technische Universität Berlin
 Institut für Landschaftsarchitektur und Umweltplanung
 Straße des 17. Juni 145, 10623 Berlin
 Tel.: 030 / 31472847
 Fax: 030 / 31423507
 e-mail: birgit.kleinschmit@tu-berlin.de

Bildanalyse und Bildverstehen

Dr.-Ing. UWE WEIDNER
 Karlsruher Institut für Technologie
 Institut für Photogrammetrie und Fernerkundung
 Englerstraße 7, 76131 Karlsruhe
 Tel.: 0721 / 608-43945
 Fax: 0721 / 608-48450
 e-mail: uwe.weidner@kit.edu

Prof. Dr.-Ing. EBERHARD GÜLCH
 Hochschule für Technik Stuttgart, Labor für Interpretation und Messung mit bildgebenden Sensoren
 Schellingstraße 24, 70174 Stuttgart
 Tel.: 0711 / 8926 2610
 Fax: 0711 / 8926 2556
 e-mail: eberhard.guelch@hft-stuttgart.de

3D-Stadtmodelle

Dipl.-Ing. BETTINA PETZOLD
 Hessisches Landesamt für Bodenmanagement und Geoinformation
 Schaperstraße 16, 65195 Wiesbaden
 Tel.: 0611 / 535-5372
 Fax: 0611 / 535-5351
 e-mail: bettina.petzold@hvbg.hessen.de
 www.hvbg.hessen.de

Dipl.-Ing. EKKEHARD MATTHIAS
 Freie und Hansestadt Hamburg, Landesbetrieb Geoinformation und Vermessung
 Sachsenkamp 4, 20097 Hamburg
 Tel.: 040 / 428-26-5750
 Fax: 040 / 428-26-5966
 e-mail: ekkehard.matthias@gv.hamburg.de
 www.geinfo.hamburg.de

Fernerkundung in der Geologie

Dr. HANS-ULRICH WETZEL
 GeoForschungsZentrum Potsdam (GFZ)
 PB 1.5, Telegrafenberg, 14473 Potsdam
 Tel.: 0331 / 288-1194
 Fax: 0331 / 288-1192
 e-mail: wetz@gfz-potsdam.de

Geoinformatik

Prof. Dr.-Ing. JAN-HENRIK HAUNERT
 Universität Osnabrück
 Institut für Geoinformatik und Fernerkundung (IGF)
 Barbarastraße 22b, 49076 Osnabrück

Tel.: 0541 / 969-3964
Fax: 0541 / 969-3939
e-mail: janhhaunert@uni-osnabrueck.de

Prof. Dr. BERNHARD HÖFLE
Ruprecht-Karls-Universität Heidelberg
Geographisches Institut, Abt. für Geoinformatik
Berliner Straße 48, 69120 Heidelberg
Tel.: 06221 / 54-5594
Fax: 06221 / 54-4529
e-mail: hoefle@uni-heidelberg.de

Hyperspektrale Fernerkundung

Dr.-Ing. ANDRÁS JUNG
Universität Leipzig
Institut für Geographie, Abt. für Geoinformatik und Fernerkundung
Johannisallee 19a, 04103 Leipzig
Tel.: 0341 / 9732785
Fax: 0341 / 9738619
e-mail: andras.jung@uni-leipzig.de

Dr. JONAS FRANKE
Remote Sensing Solutions GmbH
Wörthstraße 49, 81667 München
Tel.: 089 / 48954765
Fax: 089 / 48954767
e-mail: franke@rssgmbh.de

Optische 3D-Messtechnik

Prof. Dipl.-Ing. THOMAS KERSTEN
HafenCity Universität Hamburg
Labor für Photogrammetrie & Laserscanning
Hebebrandstraße 1, 22297 Hamburg
Tel.: 040 / 428-27-5343
Fax: 040 / 428-27-5359
e-mail: thomas.kersten@hcu-hamburg.de
www.hcu-hamburg.de/geomatik/kersten

Dr.-Ing. DANILO SCHNEIDER
Technische Universität Dresden
Institut für Photogrammetrie und Fernerkundung
Helmholtzstraße 10, 01062 Dresden
Tel.: 0351 / 463 33144
Fax: 0351 / 463 37266
e-mail: danilo.schneider@tu-dresden.de

Radarfernerkundung und Flugzeuglaserscanning

Prof. Dr.-Ing. UWE SÖRGEL

Technische Universität Darmstadt
Institut für Geodäsie
Fachgebiet für Fernerkundung und Bildanalyse
Petersenstraße 13, 64287 Darmstadt
e-mail: soergel@geod.tu-darmstadt.de

Prof. Dr.-Ing. PETER KRZYSTEK
Hochschule für angewandte Wissenschaften, München
Fakultät für Geoinformation
Karlstraße 6, 80333 München
Tel.: 089 / 1265-2617
Fax: 089 / 1265-2698
e-mail: peter.krzystek@hm.edu

Recht und Geodaten

Ansprechpartnerin DGPF: Dipl.-Ing. MARTINA BRAUNE
Landesvermessung und Geobasisinformation Brandenburg
Heinrich-Mann-Allee 103, 14473 Potsdam
Tel.: 0331 / 8844-330
e-mail: martina.braune@geobasis-bb.de

Leiter (DGfK): Dipl.-Ing. DIETRICH DIEZ
Landesamt für Geoinformation und Landentwicklung Baden-Württemberg
Büchselstraße 54, 70174 Stuttgart
Tel.: 0711 / 95980-101
e-mail: dietrich.diez@lgl.bwl.de

Sensoren und Plattformen

Prof. Dr. NORBERT HAALA
Universität Stuttgart
Institut für Photogrammetrie
Geschwister-Scholl-Straße 24d, 70174 Stuttgart
Tel.: 0711 / 685-83383
Fax: 0711 / 685-83297
email: norbert.haala@ifp.uni-stuttgart.de

Standardisierung und Qualitätssicherung

Dipl.-Ing. SVEN BALTRUSCH
Landesamt für Innere Verwaltung Mecklenburg-Vorpommern
Amt für Geoinformation, Vermessung und Katasterwesen
Lübecker Straße 289, 19059 Schwerin
Tel.: 0385 / 588-56322
e-mail: sven.baltrusch@laiv-mv.de

Berichterstatter für ISPRS und CIPA

Kommission I – Image Data Acquisition - Sensors and Platforms

Dr.-Ing. Franz Kurz
82230 Oberpfaffenhofen
e-mail: franz.kurz@dlr.de

Kommission II – Theory and Concepts of Spatial Information Science

Prof. Dr.-Ing. Monika Sester
30167 Hannover
e-mail: monika.sester@ikg.uni-hannover.de

Kommission III – Photogrammetric Computer Vision and Image Analysis

Prof. Dr.-Ing. Stefan Hinz
76128 Karlsruhe
e-mail: stefan.hinz@kit.edu

Kommission IV – Geodatabases and Digital Mapping

Dr.-Ing. Volker Walter
70174 Stuttgart
e-mail: volker.walter@ifp.uni-stuttgart.de

Kommission V – Close-Range Sensing: Analysis and Applications

Dr.-Ing. Danilo Schneider
01062 Dresden
e-mail: danilo.schneider@tu-dresden.de

Kommission VI – Education and Outreach

Dipl.-Inf. Gert König
10623 Berlin
e-mail: gerhard.koenig@tu-berlin.de

Kommission VII – Thematic Processing, Modeling and Analysis of Remotely Sensed Data

Dr.-Ing. Uwe Weidner
76128 Karlsruhe
e-mail: weidner@ipf.uni-karlsruhe.de

Kommission VIII – Remote Sensing Applications and Policies

Prof. Dr. Irmgard Niemeyer
52425 Jülich
e-mail: i.niemeyer@fz-juelich.de

CIPA – Internationales Komitee für Architekturphotogrammetrie

Prof. Dr.-Ing. Michael Scherer
44780 Bochum
e-mail: michael.scherer@ruhr-uni-bochum.de

Gutachter der PFG im Jahr 2014

Fachkundige und kritische Gutachterinnen und Gutachter garantieren die Qualität einer wissenschaftlichen Zeitschrift und sind Voraussetzung für ihre internationale Anerkennung und die Aufnahme in einen Citation Index. Deshalb bedanken sich die Schriftleiter der PFG ganz herzlich bei allen, die 2014 ihre Expertise und ihre Zeit der PFG zur Verfügung gestellt haben. Sie haben neben dem Editorial Board wesentlich zur positiven Entwicklung der PFG beigetragen. Ein ganz herzliches Dankeschön an

- Costas Armenakis, York, ON, Kanada
- Georg Bareth, Köln
- Jan Bartelsen, Neubiberg
- David Belton, Perth, Australien
- Jan Böhm, London, Großbritannien
- Markus Boldt, Ettlingen
- Christian Briese, Wien, Österreich
- Tilman Bucher, Berlin
- Dimitri Bulatov, Ettlingen
- Ismael Colomina, Castelldefels, Spanien
- Douglas Comer, Baltimore, MD, USA
- Christopher Conrad, Würzburg
- Michael Cramer, Stuttgart
- Henri Eisenbeiss, Zürich, Schweiz
- Stefan Erasmi, Göttingen
- Jurgen Everaerts, Mol, Belgien
- Dominik Fechter, Freiburg
- Clive Fraser, Melbourne, Australien
- Othmar Frey, Zürich, Schweiz
- Markus Gerke, Enschede, Niederlande
- Jens Göpfert, Koblenz
- Görres Grenzdörffer, Rostock
- Sebastian Günthert, Heidelberg
- Richard Guercke, Hannover
- Ayman Habib, Calgary, AL, Kanada
- Christian Heipke, Hannover
- Ludwig Högner, München
- Eija Honkavaara, Masala, Finnland

- Karsten Jacobsen, Hannover
- Thomas Jarmer, Osnabrück
- Jarosław Jasiewicz, Poznań, Polen
- Boris Jutzi, Karlsruhe
- Wolfgang Kainz, Wien, Österreich
- Wilfried Karel, Wien, Österreich
- Pierre Karrasch, Dresden
- Thomas Kersten, Hamburg
- Birgit Kleinschmit, Berlin
- Tomasz Kogut, Koszalin, Polen
- Hooman Latifi, Würzburg
- José Luis Lerma Garcia, Valencia, Spanien
- Derek Lichti, Calgary, Kanada
- Fabian Löw, Würzburg
- Marc Löwner, Braunschweig
- Arko Lucieer, Hobart, Australien
- Stephan Mäs, Dresden
- Gunter Menz, Bonn
- Matthias Möller, Berlin
- Stephan Nebiker, Muttenz, Schweiz
- Konstantinos Nikolakopoulos, Patras, Griechenland
- Andreas Nüchter, Bremen
- Paola Passalacqua, Austin, TX, USA
- Pablo Rosso, Berlin
- Michael Ruhnke, Freiburg
- Anke Schickling, Jülich
- Karl Segl, Potsdam
- Camillo Ressl, Wien, Österreich
- Michael Scherer, Bochum
- Jochen Schiewe, Hamburg
- Danilo Schneider, Dresden
- Steffen Schön, Hannover
- Maria v. Schönermark, Wessling
- Karsten Schulz, Ettlingen
- Alexander Schunert, Hannover
- Markus Seifert, München
- Daniel Spengler, Potsdam
- Christoph Stiller, Karlsruhe
- Hans-Peter Thamm, Linz am Rhein
- Daniel Tomowski, Clausthal-Zellerfeld
- Manfred Wiggenhagen, Hannover
- Nils Wolf, Heidelberg
- Andreas Wytzisk, Bochum



PFG – Jahrgang 2014, Heft 1–6

Inhaltsverzeichnis Jahrgang 2014

BILL, R.: Unmanned aerial systems (UAS) – attractive extensions to spatial data collection methods	225
ATZBERGER, C.: Special issue on Geodata processing at the Institute for Surveying, Remote Sensing and Land Information in Vienna.	309

Originalbeiträge, alphabetisch nach Autoren

ASHRAFIANFAR, N., BUSCH, W., DEHGHANI, M., KNOSPE, S. & REZAPOUR TABARI M.M.: DInSAR Time Series of ALOS PALSAR and ENVISAT ASAR Data for Monitoring Hashtgerd Land Subsidence due to Overexploitation of Groundwater	497
BERNHARD, E.-M., TWELE, A. & MARTINIS, S.: The Effect of Vegetation Type and Density on X-Band SAR Backscatter after Forest Fires	275
BRAUCHLE, J., RÜTHER-KINDEL, W. & BERGER, R.: MACS-TumbleCam – A Novel approach for Aerial Oblique Imaging.....	253
BÜTTNER, A. & RÖSER, H.-P.: Hyperspectral Remote Sensing with the UAS “Stuttgarter Adler” – System Setup, Calibration and First Results	265
DROESCHEL, D., HOLZ, D. & BEHNKE, S.: Omnidirectional Perception for Lightweight MAVs using a Continuously Rotating 3D Laser	451
EINZMANN, K., Ng, W.-T., IMMITZER, M., BACHMANN, M., PINNEL, N. & ATZBERGER, C.: Method analysis for collecting and processing in-situ hyperspectral needle reflectance data for monitoring Norway spruce.....	423
ELING, C., KLINGBEIL, L., WIELAND, M. & KUHLMANN, H.: Direct Georeferencing of Micro Aerial Vehicles – System Design, System Calibration and First Evaluation Tests	227
GRIMS, M., ATZBERGER, C., BAUER, T., STRAUSS, P. & MANSBERGER, R.: Low-cost Terrestrial Photogrammetry as a Tool for a Sample-Based Assessment of Soil Roughness	313
HEINE, E., KOGELBAUER, I., PROKOPH, A. & LOISKANDL, W.: Hydrographical Surveying of the Steppe Lake Neusiedl – Mapping the Lake Bed Topography and the Mud Layer	339
HONKAVAARA, E., MARKELIN, L., HAKALA, T. & PELTONIEMI, J.: The Metrology of Directional, Spectral Reflectance Factor Measurements Based on Area Format Imaging by UAVs	175
IMMITZER, M. & ATZBERGER, C.: Early Detection of Bark Beetle Infestation in Norway spruce (<i>Picea abies</i> , L.) using WorldView-2 Data	351
KLISCH, A. & ATZBERGER, C.: Evaluating Phenological Metrics derived from the MODIS Time Series over the European Continent	409
MATTI, E.K. & NEBIKER, S.: Geometry and Colour Based Classification of Urban Point Cloud Scenes Using a Supervised Self-Organizing Map	161

MATTIUZZI, M., BUSSINK, C. & BAUER, T.: Analysing Phenological Characteristics Extracted from Landsat NDVI Time Series to Identify Suitable Image Acquisition Dates for Cannabis Mapping in Afghanistan	383
MÖLLER, M., BIRGER, J. & GLÄSSER, C.: Geometric Accuracy Assessment of Classified Land Use / Land Cover Changes	91
NEUGEBAUER, N. & VUOLO, F.: Crop Water Requirements on Regional Level using Semote Sensing Data – A Case Study in the Marchfeld Region	369
RAMZI, P., SAMADZADEGAN, F. & REINARTZ, P.: An AdaBoost Ensemble Classifier System for Classifying Hyperspectral Data	27
REHAK, M., MABILLARD, R. & SKALOUD, J.: A Micro Aerial Vehicle with Precise Position and Attitude Sensors	239
SCHLICHTING, A., BRENNER, C. & SCHÖN, S.: Bewertung von Inertial/GNSS-Modulen mittels Laserscannern und bekannter Landmarken	5
STERN, O., PASCHMIONKA, B., STOFFELS, J., BUDDENBAUM, H. & HILL, J.: Abbildende und nichtabbildende Geländespektrometrie zur Untersuchung von Stressphänomenen an Buchenpflanzen	17
SUPPAN, F. & FREY-ROOS, F.: Generating Resistance Surfaces for Wildlife Corridor Extraction	435
VUOLO, F. & ATZBERGER, C.: Improving Land Cover Maps in Areas of Disagreement of Existing Products using NDVI Time Series of MODIS – Example for Europe	393
WAWRZASZEK, A., ALEKSANDROWICZ, S., KRUPIŃSKI, M. & DRZEWIECKI, W.: Influence of Image Filtering on Land Cover Classification when using Fractal and Multifractal Features	101
WINDISCH, K., BRONNER, G., MANSBERGER, R. & KOUKAL, T.: Derivation of Dominant Height and Yield Class of Forest Stands by Means of Airborne Remote Sensing Methods	325

Beiträge aus Wissenschaft und Praxis

BAGHERI, H., SADEGHIAN, S. & SADIJAD, S.Y.: The Assessment of using an Intelligent Algorithm for the Interpolation of Elevation in the DTM Generation	197
BOEHM, J.: Accuracy Investigation for Structured-light Based Consumer 3D Sensors	117
CONTE, G., RUDOL, P. & DOHERTY, P.: Evaluation of a Light-weight Lidar and a Photogrammetric System for Unmanned Airborne Mapping Applications	287
JUNG, A. & VOHLAND, M.: Snapshot Hyperspectral Imaging for Soil Diagnostics – Results of a Case Study in the Spectral Laboratory	
511Linck, R., Busche, T. & Buckreuss, S.: Visual Analysis of TerraSAR-X Backscatter Imagery for Archaeological Prospection	55
Li, C., THINH, N.X. & ZHAO, J.: Spatiotemporally Varying Relationships between Urban Growth Patterns and Driving Factors in Xuzhou City, China	535
LINCK, R., BUSCHE, T. & BUCKREUSS, S.: VISUAL ANALYSIS OF TERRASAR-X Backscatter Imagery for Archaeological Prospection	55

SIEGMANN, B., GLÄSSER, C., ITZEROTT, S. & NEUMANN, C.: An Enhanced Classification Approach using Hyperspectral Image Data in Combination with in situ Spectral Measurements for the Mapping of Vegetation Communities	523
SKARLATOS, D., KIPARISSI, S., THEODORIDOU, S. & PANDERMALIS, D.: A Method of Evaluating the Internal Precision of Multi-View Stereo Dense Reconstruction, Applied on Parthenon Frieze	189
THÜRKOW, D., POKLADEK, M., DETTE, D. & GLÄSSER, C.: 3D-Landschaftsvisualisierungen für ein nachhaltiges Management zum Erhalt und zur Pflege des UNESCO Weltkulturerbes Dessau-Wörlitzer Gartenreich	129
VETTER, M. & MANDLBURGER, G.: Modification of High Resolution Airborne Laser Scanning DTMs for Drainage Network Delineation	41

Berichte und Mitteilungen

Deutsche Geodätische Kommission: DGK-Wissenschaftspreis	301
Berichte von Veranstaltungen	
54 th Photogrammetric Week, 9 th – 13 th September 2013, Stuttgart	67
Workshop denkmäler3.de, 16. – 18. Oktober 2013, Dortmund	143
ISPRS Workshops “Laser Scanning”, “ISA13” und “CMRT13”, 11. – 13. November 2013, Antalya, Türkei	144
Workshop 3D-Stadtmodelle, 19. – 20. November 2013, Bonn	146
24th GRSG Annual Meeting – „Status and developments in geological remote sensing“, 9. – 11. Dezember 2013, Berlin	148
13. Oldenburger 3D Tage, 12. – 13. Februar 2014, Oldenburg	209
Gemeinsame Jahrestagung von DGPF, DGfK, GfGI und GiN, 26. – 28. März 2014, Hamburg	465
10. GIS Ausbildungstagung, 12. – 13. Juni 2014, Potsdam	468
13. Internationales 3D-Forum, 6. – 7. Mai 2014, Lindau	549
Berichte der Arbeitskreise der DGPF	
Aus- und Weiterbildung	469
Optische 3D-Messtechnik	471
Bildanalyse und Bildverständen	472
Hyperspektrale Fernerkundung	473
Radarfernerkundung und Flugzeuglaserscanning	474
Sensoren und Plattformen	475
Standardisierung und Qualitätssicherung	476
3D-Stadtmodelle	477
Geoinformatik	478
Gemeinsame Kommission von DGPF, DGfK und DVW „Geodaten und Recht“	478
Preisträger des Karl-Kraus-Nachwuchsförderpreises	484
Mitteilungen	
Unmanned Aerial Systems (UAS), Mitteilung des Bundesministeriums für Verkehr, Bau und Stadtentwicklung	78
Mitteilung aus der Normungsarbeit des DIN	80
Umstellung des Einzugsverfahrens von DGPF-Mitgliedsbeiträgen auf SEPA	219
Persönliches	
Nachruf auf Franz Josef Heimes	77

- Hochschulnachrichten 70, 151, 213, 299, 479, 551
Neuerscheinungen 81, 153, 216, 301
Veranstaltungskalender 81, 154, 216, 302, 489, 558
Korporative Mitglieder 82, 155, 217, 303, 490, 559
Zu den Titelbildern
 Heft 1: Strukturierte 3D-Bewegungsanalyse auf Basis von Bildsequenzen einer
 Tiefenbildkamera
 Heft 2: Detektion von Einzelpersonen und Menschenmassen
 Heft 3: Geometry and Colour Based Classification of Urban Point Cloud Scenes Using a
 Supervised Self-Organizing Map
 Heft 4: Vergleich digitaler Geländemodelle: UAV-Befliegung und terrestrisches
 Laserscanning
 Heft 5: Geodata processing at the University of Natural Resources and Life Sciences, Vienna
 (Universität für Bodenkultur, BOKU), Austria
 Heft 6: xxx

Für den Standort Biberach suchen wir ab sofort eine(n)

Customer Support Specialist (m/w)



Hauptaufgaben:

- Betreuung unserer internationalen Kunden bei technischen Problemen jeder Art
- Support am Telefon, per E-Mail und vor Ort
- Beratung von Kunden hinsichtlich Installation und Konfiguration
- Durchführung von Schulungen vor Ort und online
- Zusammenarbeit mit den Fachbereichen Vertrieb, Entwicklung & Produktion
- Teamleiterfunktion

Anforderungen:

- Abgeschlossenes Studium im Bereich Geoinformatik bzw. Geodäsie oder vergleichbar
- Berufserfahrung mit Lasertechnologien im Bereich Airborne ist von Vorteil
- Fundierte Kenntnisse in Photogrammetrie, Geoinformatik und Bildbearbeitung sind von Vorteil
- Gute Englisch Kenntnisse
- Professionelles Auftreten bei Kundengesprächen und Präsentationen
- Selbständige, strukturierte und lösungsorientierte Arbeitsweise sowie pragmatisches und vernetztes Denken
- Eigenmotivation, Organisations- und Teamfähigkeit
- Hohes Maß an Engagement und Dienstleistungsorientierung
- Reisebereitschaft

Wenn Sie Interesse haben in einem internationalen Team an führender Technologie zu arbeiten, dann senden Sie uns Ihre Bewerbung.

<http://www.trimble.com/careers/emea-jobsearch.aspx>